DISCLAIMER

This report was prepared as an account of work sponsored by an agency of the United States Government. Neither the United States Government nor any agency thereof, nor any of their employees, makes any warranty, express or implied, or assumes any legal liability or responsibility for the accuracy, completeness, or usefulness of any information, apparatus, product, or process disclosed, or represents that its use would not infringe privately owned rights. Reference herein to any specific commercial product, process, or service by trade name, trademark, manufacturer, or otherwise does not necessarily constitute or imply its endorsement, recommendation, or favoring by the United States Government or any agency thereof. The views and opinions of authors expressed herein do not necessarily state or reflect those of the United States Government or any agency thereof. Reference herein to any social initiative (including but not limited to Diversity, Equity, and Inclusion (DEI); Community Benefits Plans (CBP); Justice 40; etc.) is made by the Author independent of any current requirement by the United States Government and does not constitute or imply endorsement, recommendation, or support by the United States Government or any agency thereof.

LLNL-TR-2006187

Lawrence Livermore National Laboratory

Probabilistic Seismic Hazard Analysis for Iraq Based on the Updated Earthquake Catalog (1900-2021) and Ground Motion Characteristics

Wathiq Abdulnaby, Muntadher Al-Kaabi, Tuna Onur, Carlos Herrera, Najah Abd, Majid Albakir, Sinan Al-Dabbagh, Hala Jasim, Raghda Ali, Mustafa Bader, Dhuha Gateaa, Hanan Mahdi, Andrea Chiang, Haydar Al-Shukri

September 2025

Disclaimer

This work performed under the auspices of the U.S. Department of Energy by Lawrence Livermore National Laboratory under Contract DE-AC52-07NA27344.

Probabilistic Seismic Hazard Assessment for Iraq Based on the Updated Earthquake Catalog and Ground Motion Characterization (1900 – 2021)

Wathiq Abdulnaby[1], Muntadher Al-Kaabi[2], Tuna Onur[3,4], Carlos Herrera[3], Najah Abd[5], Majid Albakir[5], Sinan Al-Dabbagh[5], Hala Jasim[5], Raghda Ali[5], Mustafa Bader[1], Dhuha Gateaa[1], Hanan Mahdi[2], Andrea Chiang[6], and Haydar Al-Shukri[2]

[1]University of Basrah, [2]University of Arkansas, Little Rock, [3]Onur Seemann Consulting, Inc., [4]University of Victoria, [5]University of Baghdad, [6]Lawrence Livermore National Laboratory

Abstract

Onur *et al*. (2017) compiled the first comprehensive earthquake catalog for Iraq, covering 1900 to 2009 within 26°–40°N latitude and 36°–51°E longitude. This catalog was utilized in a probabilistic seismic hazard assessment (PSHA) by Abdulnaby *et al*. (2020) to aid in updating Iraq's building code seismic provisions. Recently, we have updated the earthquake catalog for Iraq by adding earthquakes recorded from 2010 to 2021 and directly calculating moment magnitude (Mw) for about 2,800 earthquakes using the coda envelope methodology and waveform data from the Mesopotamian Seismological Network (MPSN) in Iraq. The updated earthquake catalog covers the period from 1900 to the end of 2021 and includes more than 37,000 earthquakes. Ground motion characteristics like Peak Ground Accelerations (PGAs) and Response Spectra (RS) are calculated using data from about 30 strong motion stations in the study area. Based on the epicentral earthquake spatial distribution, locations of seismically active faults, and geological setting, the study area is divided into 20 seismic area zones. The revised earthquake catalog and ground motion characteristics are then used to update the PSHA for Iraq. OpenQuake software is used to do the analyses and to produce the probabilistic seismic hazard maps for Iraq with a 2%

chance of exceedance in 50 years on-site with VS30 at 760 m/s, 500 m/s, and 180 m/s in terms of PGA and spectral accelerations at 0.2, 0.3, 0.5, 1.0, 2.0, and 4.0 s. The highest seismic hazard in Iraq is found to be near the Mandili-Badra-Teeb fault in the east, which has a history of significant ruptures. Northern Iraq also has notable seismic activity, particularly in the Zagros Fold-Thrust belt, evidenced by the Mw7.3 earthquake on November 12, 2017. In contrast, central and western Iraq experience less frequent earthquakes, resulting in lower hazard; however, the possibility remains of a major earthquake occurring anywhere in the country.

1. Introduction

Almost all of Iraq is located within the northeastern part of the Arabian Plate, except a small area in the extreme northeastern part of the country called Shalair Terrane (ST), which belongs to the Eurasian Plate (Figure 1). Different tectonic forces have affected Iraq during the Phanerozoic Era (Numan, 1997). The collision between the Arabian and Eurasian plates controls the recent tectonic setting of Iraq. This collision started during the Early Tertiary and continues to this day. The results of this collision are the genesis of the Taurus and Zagros mountain belts, as well as the formation of the foreland basin within the Arabian plate (the underriding plate) and the hinterland basin within the Iranian plate (the overriding plate) (Abdulnaby, 2019).

Fouad (2015) proposed a tectonic division of Iraq that has been widely accepted among the geology community. In this tectonic division, Iraqi territory is divided into two first-order segments; these are the Arabian Platform and the Shalair Terrane of the Sanandaj-Serjan Zone of the Eurasian plate, which are separated by the Main Zagros Reverse Fault (MZRF), the suture line between the Arabian and Iranian Plates (Berberian, 1995; Al-Qayim *et al*., 2012). The Arabian platform within Iraq is divided into two main tectonic units: the Outer and Inner Arabian Platforms. The Anah Graben Fault (AGF) in the western part of Iraq and the Abu Jir-Euphrates Fault Zone

(AJEFZ) in the southwestern part of the country delineate the contact between the Outer and the Inner Arabian Platforms. The Outer Arabian Platform is unstable and consists of the Zagros Fold-Thrust Belt and the Mesopotamian Foredeep that are separated by a series of anticlines and the Mandili-Badra-Teeb Fault (MBTF). The Inner Arabian Platform is semi-stable and includes the western and southern deserts of Iraq. The Outer Arabian Platform has surface folds at the Zagros Fold-Thrust Belt, and subsurface folds at the Mesopotamian Foredeep, while the Inner Arabian Platform has no anticlines (Abdulnaby, 2019) (Figure 1).

Given the ongoing collision between the Arabian and Eurasian plates, Iraq is prone to seismic activity. Earthquake activity in Iraq varies in magnitude and frequency. While many earthquakes are minor and go unnoticed by people in the Inner Arabian Platform, more significant and destructive earthquakes have occurred in the Outer Arabian Platform (Abdulnaby *et al*., 2016a, b; Abdulnaby *et al*., 2020). The seismic activity of the Inner Arabian Platform in Iraq results from local deformation. In contrast, the seismicity of the Outer Arabian Platform arises from forces generated by the movements of the Arabian plate toward the north and northeast. The forces that created the significant geological structures along the plate boundaries remain active, leading to the accumulation of stress and strain. Overall, the seismicity of Iraq is produced mainly by the Zagros and Taurus systems, with partial neotectonic activation of the upper crust.

Recognizing the need for an up-to-date seismic hazard assessment in Iraq, the team from the Mesopotamian Seismological Network (MPSN) with support from Lawrence Livermore National Laboratory (LLNL) undertook a probabilistic seismic hazard assessment (PSHA) study that incorporates new seismic data recorded locally and recent research conducted since the previous hazard assessment was used in the building code update in 2017. The PSHA framework for this study was designed to help develop a new building code by incorporates a novel characterization

of ground motions that explicitly reflects the period-dependent attenuation for the country based on recorded ground motions, and generate hazard information in a format useful for updating the current building code or developing a new building code for Iraq. The project also aims to provide training and support for local seismologists developing seismic hazard models, performing PSHA, and incorporating in the building code. This study also produced an updated seismic hazard map for Iraq based on an updated earthquake catalog from 1900 to 2021 and ground motion characteristics obtained from seismic stations in the study region.

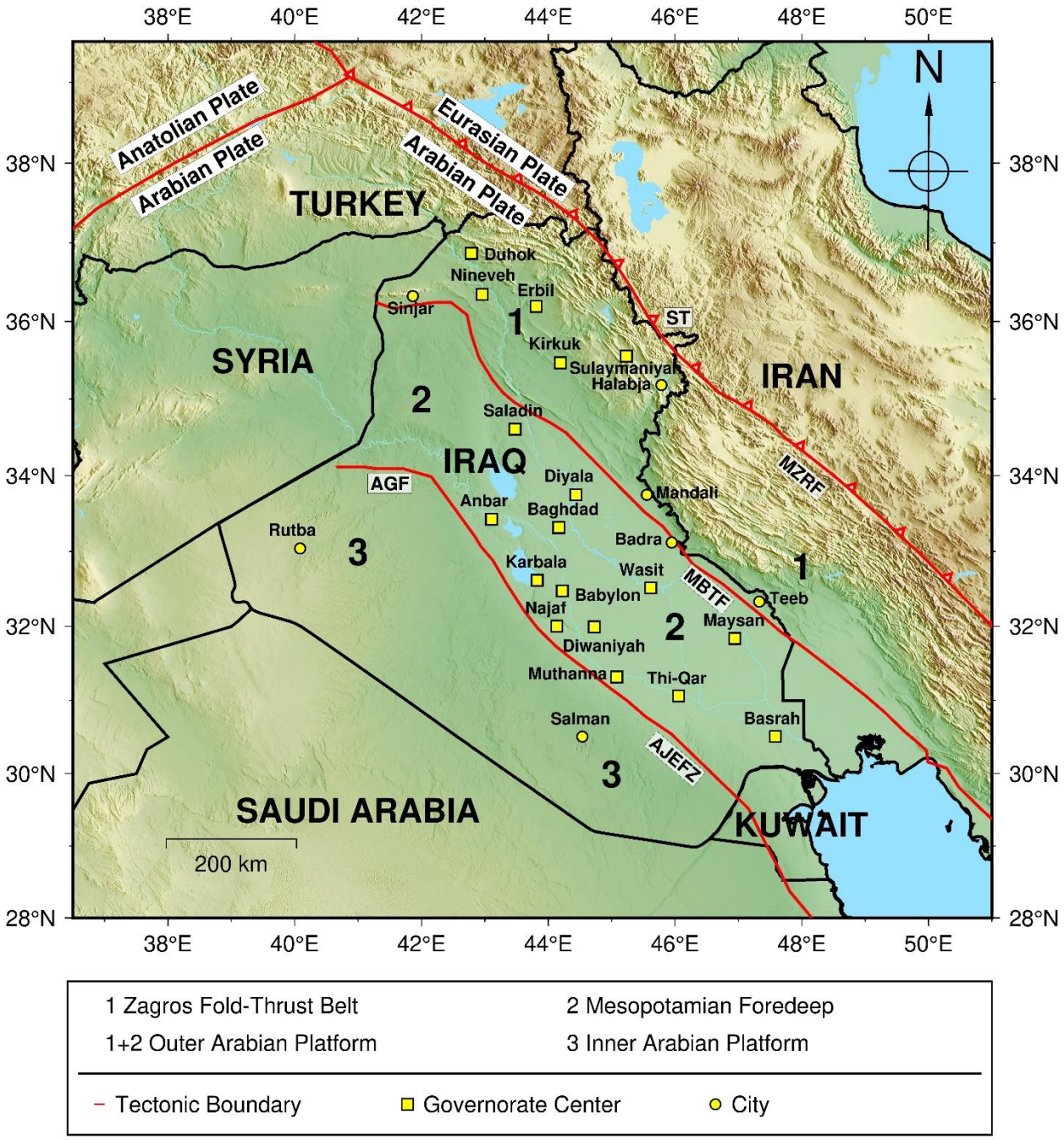

Figure 1*. The tectonic divisions of Iraq based on Fouad (2015). Abbreviations used include the following: AGF= Anah Graben Fault; AJEFZ= Abu Jir-Euphrates Fault Zone; MBTF= Mandili-Badra-Teeb Fault; MZRF= Main Zagros Reverse Fault; and ST= Shalair Terrane.*

2. Updated Earthquake Catalog

2.1. New Bulletin Compilation

Compiling an earthquake catalog is essential for Iraq's national seismic hazard assessment. Onur *et al*. (2017) proposed the first comprehensive earthquake catalog for the country. The catalog covers the geographic region between 36°E and 51°E longitudes and 26°N and 40°N latitudes. Its purpose was to include sources of seismicity that may potentially cause damage within the territory of Iraq. The earthquake catalog included data from the period between 1900 and 2009 and contained approximately 16,000 events with a magnitude of 3.0 or greater, and about 4,000 events with a magnitude of 4.0 or greater. Approximately 90% of the earthquakes in the catalog had a depth ranging from 0 to 35 km. Figure 2 illustrates the seismicity of Iraq and the surrounding regions based on the catalog compiled by Onur *et al*. (2017). Using this catalog, Abdulnaby *et al*. (2020) conducted the PSHA for Iraq.

In this study, we updated the earthquake catalog of Iraq by incorporating data from earthquakes recorded over the past twelve years, from 2010 to 2021. The reviewed earthquake bulletin of the International Seismological Centre (ISC) was used in this effort (Figure 3) in combination with contributions from local, regional and global seismic networks, including MPSN. The resulting earthquake catalog covers the period from 1900 to the end of 2021 and includes more than 36,000 earthquakes (Figure 4).

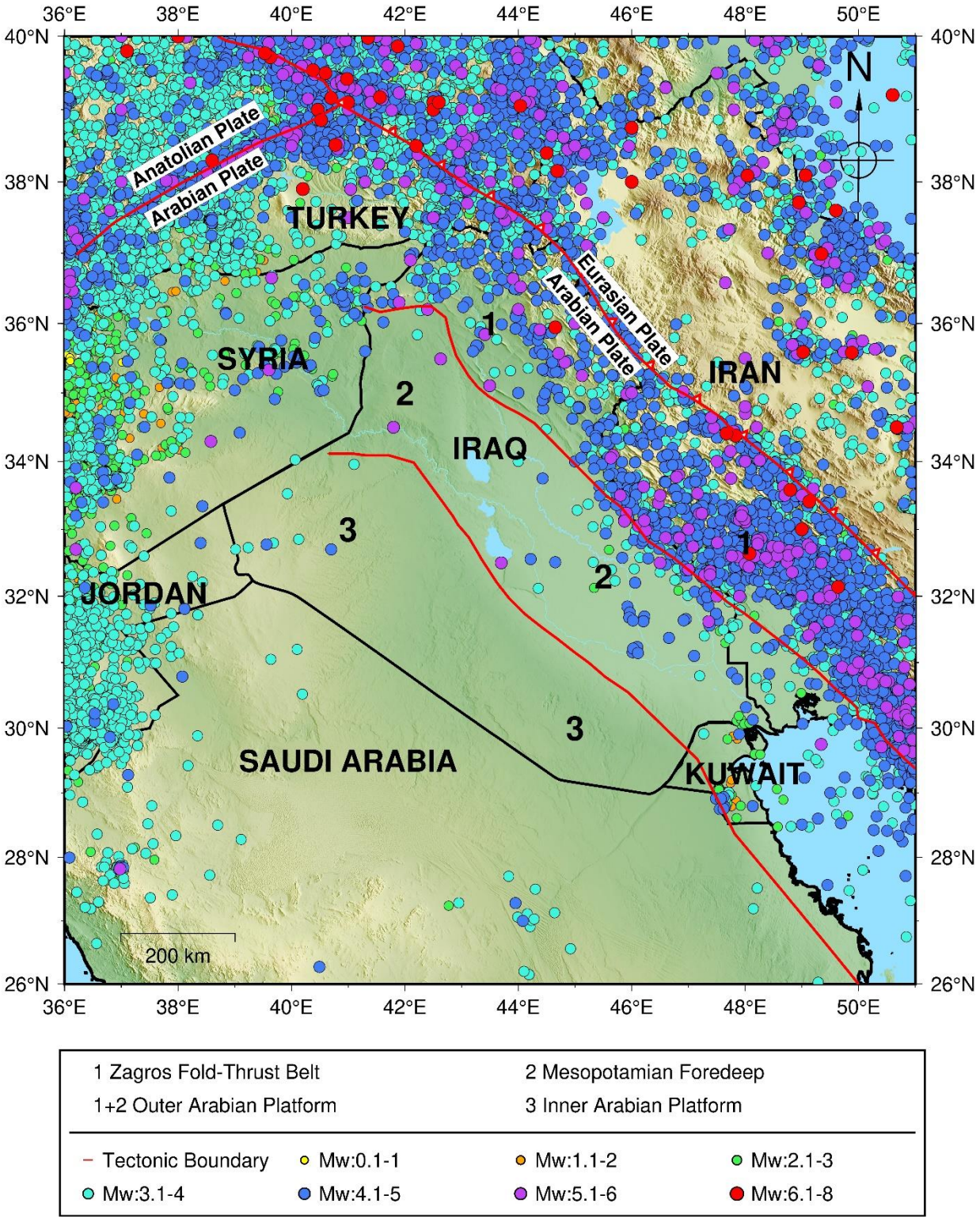

Figure 2: *The original earthquake catalog from 1900 to 2009 (Onur et al., 2017). The tectonic divisions are based on Fouad (2015).*

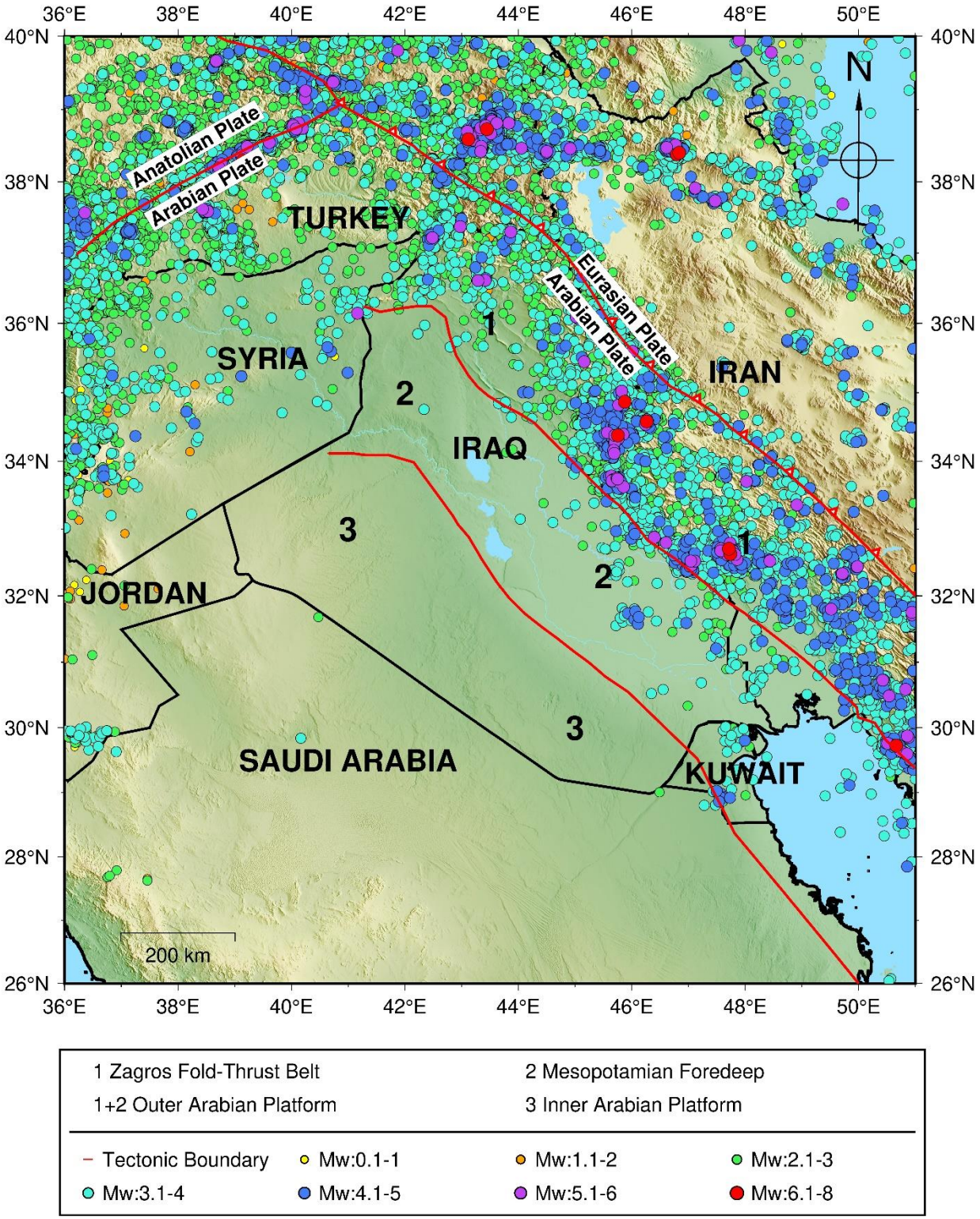

Figure 3: *Earthquake catalog from 2010 to 2021. The tectonic divisions are based on Fouad (2015).*

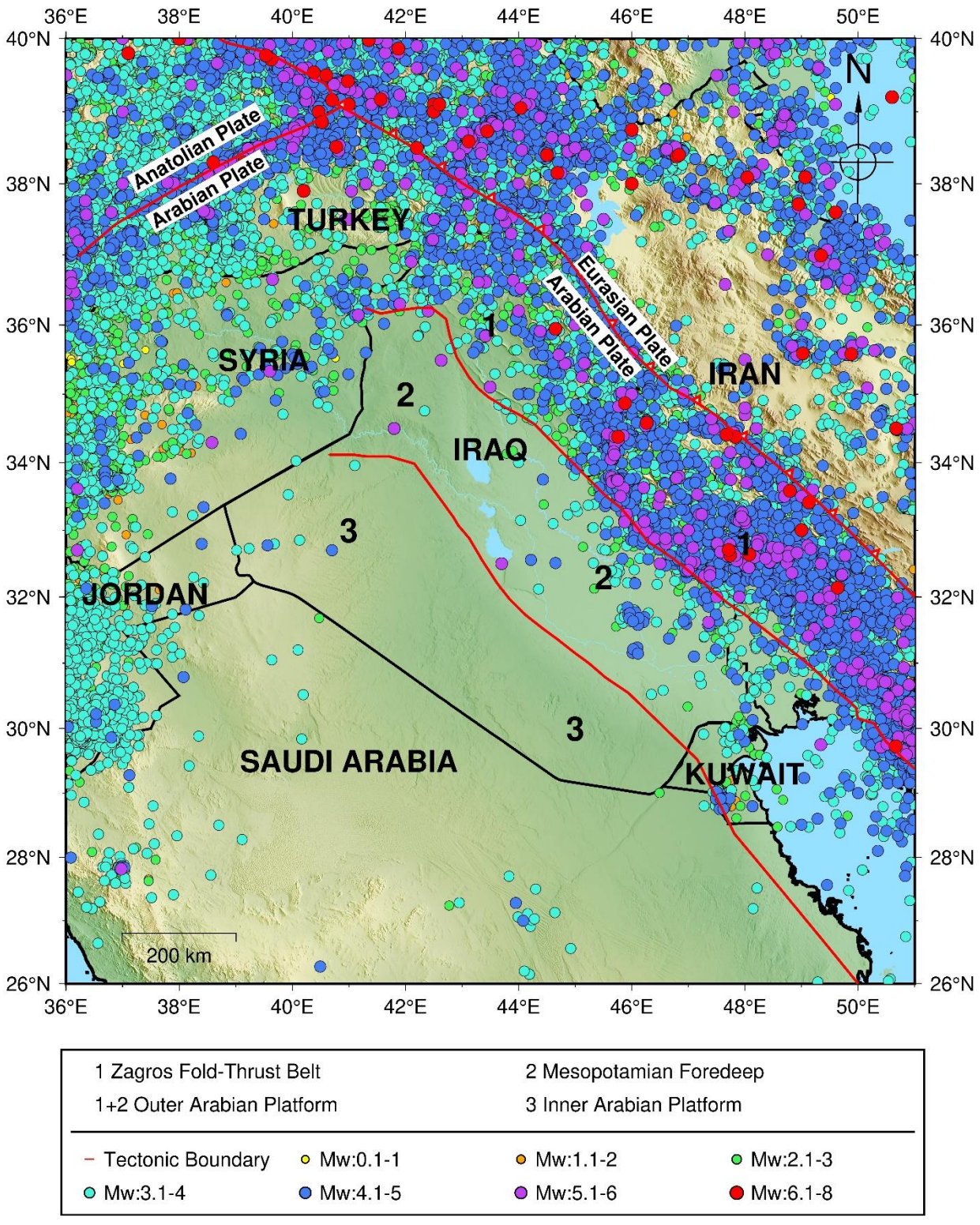

Figure 4: *Final updated earthquake catalog from 1900 to 2021. The tectonic divisions are based on Fouad (2015).*

2.2. Moment Magnitudes (Mw) Calculations

It is essential to include direct measurements of moment magnitude (Mw) whenever possible, particularly for large earthquakes. There are two main reasons for this: (1) directly calculated moment magnitudes provide a more reliable and robust estimate of the size of earthquakes, especially large ones, as other magnitude scales tend to saturate. (2) they also can be used to develop more accurate magnitude conversion relations for earthquakes where digital waveform data is unavailable (Onur *et al*., 2017).

For these reasons, the original catalog directly calculated moment magnitudes for about 1,000 Mw 2.5+ events between 1989 and 2009 (Onur *et al*., 2017). This updated catalog included more than 2,800 Mw 2.5+ events between 2010 and 2021 (Al-Kaabi *et al*., 2024). Both sets of calculations utilized the coda envelop model described in detail by Mayeda *et al*. (2003) and Gök *et al*. (2016). The coda envelope model is implemented in the Java-based Coda Calibration Tool (CCT; https://github.com/LLNL/coda-calibration-tool) developed by the Lawrence Livermore National Laboratory.

In Al-Kaabi *et al*. (2024) and Al-Kaabi (2025), data from the MPSN covering 2010 to 2021 were used to estimate Mw for over 2,800 earthquakes, ranging from M_W 2.5 to 7.35 (Figure 5). From 2010 to 2014, only one broadband station in northern Iraq was operational and was the sole station for calculating Mw. After 2014, nine stations were installed covering large territory of Iraq and employed for data processing. A simple 1D coda envelope model was used because coda waves have a low sensitivity to the source and path heterogeneity. Al-Kaabi *et al*. (2024) describes in detail the development of the 1D coda envelop model and the calculation of Mw used in this study.

Table 1 displays the distribution of direct Mw calculations from various sources, including AFAD, AMB, DDM, GCMT, GII, H, MED, ZUR, and others. Moment magnitudes from most of these sources were calculated by moment tensor solutions. Furthermore, direct Mw measurements proposed by Ambraseys (2001), Abdulnaby *et al*. (2014), and Onur *et al*. (2017) were taken into consideration. The total number of direct Mw measurements from all sources is 4,593.

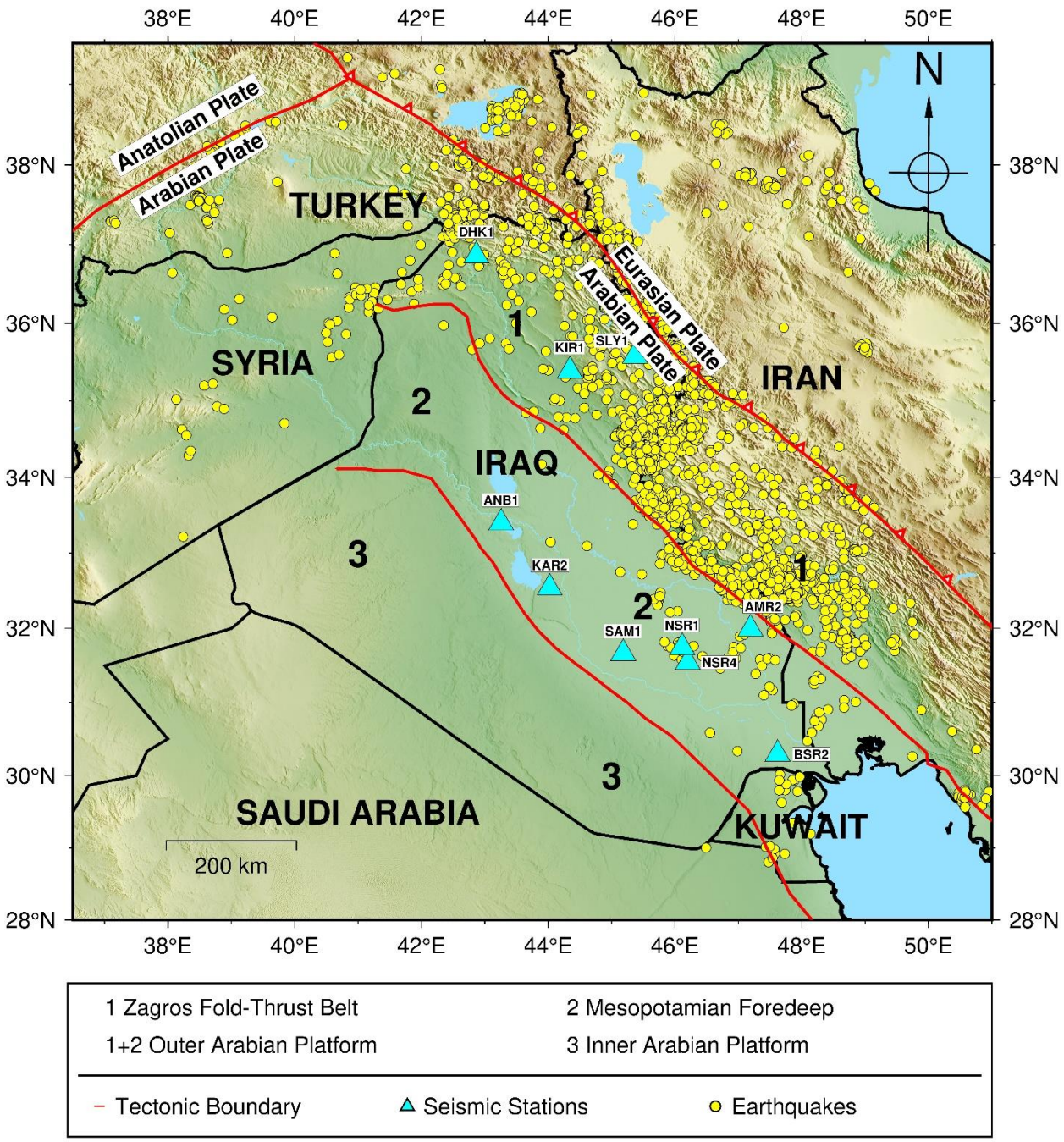

Figure 5: *Earthquakes with direct Mw measurements using CCT were done in this study. The tectonic divisions are based on Fouad (2015).*

Table 1. Distribution of direct Mw calculations by source.

Mw Source	Number of Earthquakes	Period	Magnitude Range
AFAD	246	2013-2021	2.5-6.8
AMB	24	1901-1975	5.6-7.4
DDA	21	2011	2.4-4.7
GCMT	159	1977-2021	4.7-7.4
GII	52	2001-2021	1.0-4.4
H	17	2004-2009	3.2-4.5
MED-RCMT	47	2010-2021	4.1-6.0
ZUR-RMT	114	2001-2005	4.2-5.2
AZER, CENT, CSEM, EMSC, GFZ, IPRG, NEIC, NIC, UPIES	26	1930-2021	2.2-7.7
Ambraseys (2001)	6	1965 - 1975	Mw > 5
Abdulnaby *et al*. (2014)	65	2004-2013	3.2-5.4
Onur et al. (2017)	988	1989-2009	2.3-6.0
Al-Kaabi *et al*. (2024)	2828	2010 - 2021	2.4-7.3
Total	4593	1901-2021	1.0-7.4

2.3. Magnitude Harmonization

Earthquake data, including date, time, location, depth, and magnitude from the various sources described above, were collected and merged to create a comprehensive instrumental catalog of earthquakes for Iraq and the surrounding regions (Table 2). During the process of merging catalogs, duplicate earthquakes were identified based on location and time, and lower-priority entries were eliminated from the catalog. Different prioritization schemes were used for location and magnitude. For instance, direct Mw values were prioritized for magnitudes, followed by ISC body-wave magnitude (mb) assignments. The magnitude of the majority (40.1%) of earthquakes in the resulting catalog are expressed as MD (40.1 %). The rest are expressed as ML (38.4%), Mw (13.2%), and mb (6%). Earthquakes measured using other magnitude scales (M, Mc, MG, Mn, Mpv, and Ms) account for 1%. Therefore, MD–Mw, ML–Mw, and mb–Mw relationships are

necessary to convert all magnitudes to Mw. The next section describes the development of the magnitude conversion relationships.

Table 2: A selection of earthquakes from the final harmonized catalog.

Event-ID	ISC Event-ID	Source	Year	Mo.	Da.	Ho.	Mi.	Sec.	Lat.	Lon.	Depth (km)	Source	M.T.	Mag.	Mw
35417	6.02E+08	TEH	2012	05	09	19	51	14.70	32.5640	46.7950	10	ISN	ML	3.0	3.1
35418	6.01E+08	ISC	2012	05	09	20	57	24.53	38.9310	43.6118	9.5	AFAD	ML	3.0	3.1
35419	6.02E+08	TEH	2012	05	09	21	12	21.70	32.5840	47.0640	3.6	ISN	ML	2.7	2.8
35420	6.01E+08	ISC	2012	05	10	00	35	30.64	32.7628	47.6178	15.3	Al-Kaabi *et al*	M_W	3.7	3.7
35421	6.02E+08	TEH	2012	05	10	02	22	21.80	32.9420	47.7660	10	ISN	ML	2.6	2.7
35422	6.01E+08	ISC	2012	05	10	02	40	28.94	38.6768	43.1684	10.2	AFAD	ML	2.8	2.9
35423	6.01E+08	ISC	2012	05	10	03	31	27.72	32.2941	50.0642	11	TEH	ML	3.5	3.6
35424	6.01E+08	ISC	2012	05	10	09	59	14.54	38.7654	43.1714	13.5	AFAD	ML	2.9	3.0
35425	6.01E+08	ISC	2012	05	10	10	57	15.60	39.0086	43.6431	1.3	AFAD	ML	3.6	3.7
35426	6.02E+08	ISC	2012	05	10	11	19	18.72	32.7860	47.5642	6.3	Al-Kaabi *et al*	M_W	3.6	3.6
35427	6.01E+08	ISC	2012	05	10	12	45	33.45	38.7172	43.1907	13.6	AFAD	ML	2.6	2.7
35428	6.02E+08	ISC	2012	05	10	23	15	02.00	29.7971	50.6792	22	TEH	ML	2.8	2.9
35429	6.01E+08	ISC	2012	05	11	11	01	55.81	37.3795	38.6003	6.1	AFAD	ML	2.7	2.8
35430	6.03E+08	ISC	2012	05	11	14	20	58.67	38.7682	41.6513	6	AFAD	ML	2.6	2.7
35431	6.01E+08	ISC	2012	05	11	15	32	17.63	39.3531	40.3671	8.2	AFAD	ML	2.3	2.4
35432	6.01E+08	ISC	2012	05	12	00	24	34.94	39.2117	42.3126	13.2	ISK	MD	2.6	2.5
35433	6.02E+08	TEH	2012	05	12	05	24	39.10	32.7440	46.9100	10	Al-Kaabi *et al*	M_W	3.5	3.5

2.4. Empirical Magnitude Conversion Relations

As we mentioned earlier, the resulting PSHA-ready catalog was supplemented by direct moment magnitude calculations for Iraq, using the coda calibration technique and moment tensor solutions. Where no directly calculated Mw was available, other magnitude scales were converted to Mw using relationships compatible with the local catalog. Therefore, regional magnitude conversion relations were developed to convert three dominant magnitude scales in the catalog (MD, ML, and mb) to Mw (Eqs. 1, 2, and 3). A general orthogonal regression was used to develop the relations (Figure 6) because it allows the uncertainty in the dependent and independent variables to be of a similar order of magnitude.

To develop these relationships, we use the entries in our catalog, which report multiple magnitudes of the same event. Instead of a least-squares fit to the data, which requires that the uncertainty on the independent variable (i.e., MD, ML, and mb) is at least one order of magnitude smaller than the one on the dependent variable (i.e., Mw), we utilize orthogonal regression, which allows both the dependent and independent variables to be affected by uncertainty (Castellaro *et al*., 2006). Consequently, instead of minimizing the sum of square differences between a dependent variable and its empirical estimation (ordinary least squares), we minimize the sum of square distances from each set of points to the regression line (orthogonal regression) to obtain regression coefficients for each magnitude conversion relation. Further discussion on the method, formulation, and examples for orthogonal regression can be found in Kendall and Stuart (1979), Castellaro *et al*. (2006), and Deniz and Yucemen (2010).

- $Mw = 1.142448\ MD - 0.496685$, $R^2 = 0.88$ …… (1)
- $Mw = 1.010884\ ML + 0.051675$, $R^2 = 0.89$ …… (2)

- Mw = 1.065713 mb - 0.28855, R^2 = 0.88 ……. (3)

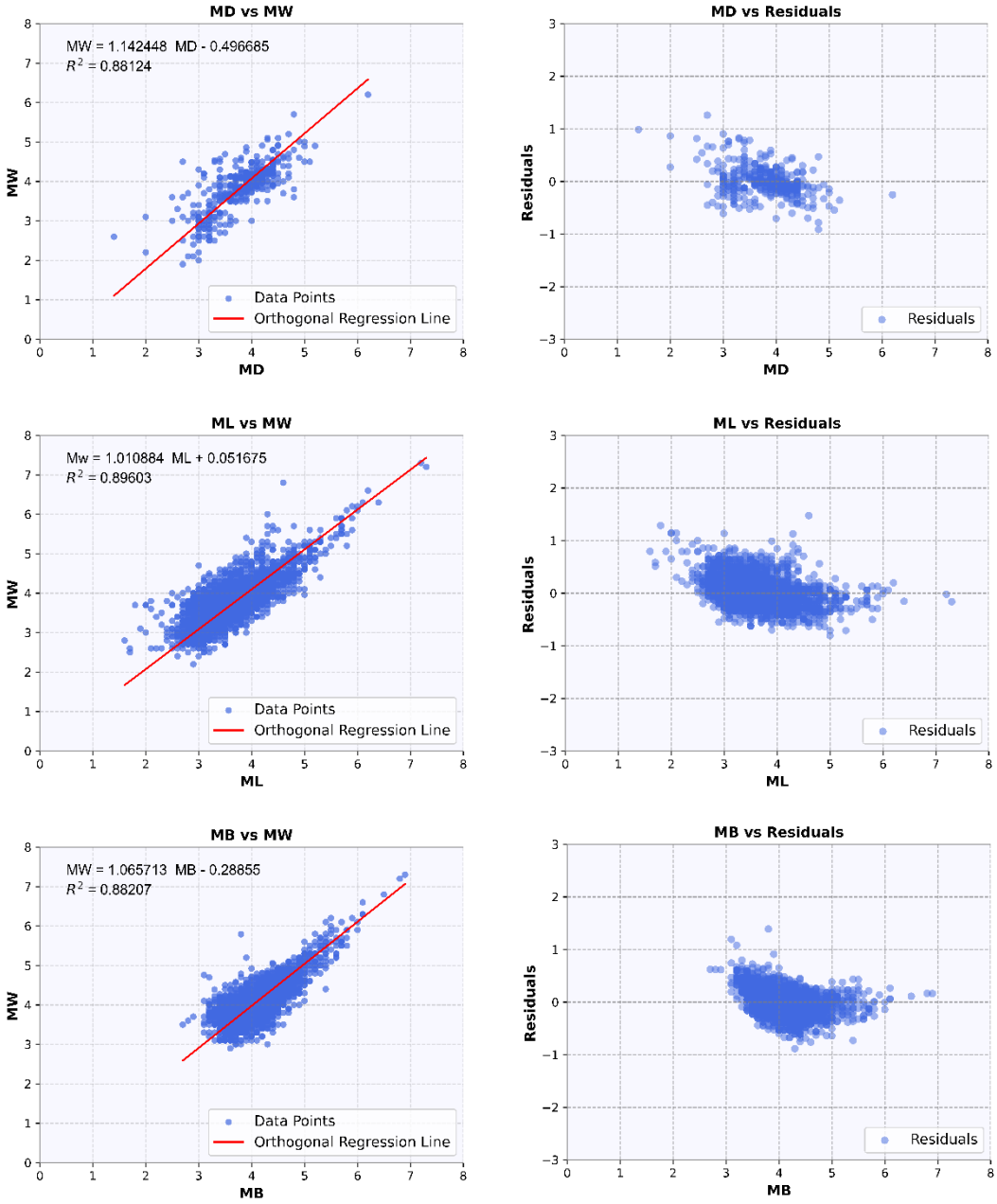

Figure 6: *Empirical magnitude conversion relations.*

2.5. Catalog Completeness

Completeness intervals depend on the sensitivity and density of seismic instrumentation over time and space. Catalog completeness is essential to estimate reliable seismic activity rates and recurrence parameters. Completeness intervals for the catalog developed for this study are derived from the logarithm of the cumulative rate of earthquakes against magnitude, prepared for various periods of time, and by noting at which magnitude the slope of the curve deviates from a straight line and the activity rates drop off. The resulting completeness intervals for the entire catalog are as follow: Mw 6.5 and above are complete since 1900, Mw 5.9 and above since 1924, Mw 5.0 and above since 1965, Mw 3.4 and above since 1995, Mw 3.3 and above since 2004, and Mw 3.2 and above since 2012 (Table 3, Figures 7 and 8). However, completeness intervals are also region-dependent in Iraq, due to the variable density and history of instrumentation. Broadly, the catalog is more complete in the Outer Platform region (more small earthquakes are recorded) and less complete in the Inner Platform region of Iraq (less small earthquakes are recorded). We take into account this regional variability in the calculation of recurrence parameters for the seismic source zones.

Table 3: Catalog completeness intervals.

Period	Completeness	Mw
1900-2021	1900-1923	6.5
1924-2021	1924-1964	5.9
1965-2021	1965-1994	5.0
1995-2021	1995-2003	3.4
2004-2021	2004-2012	3.3
2012-2021	2012-2021	3.2

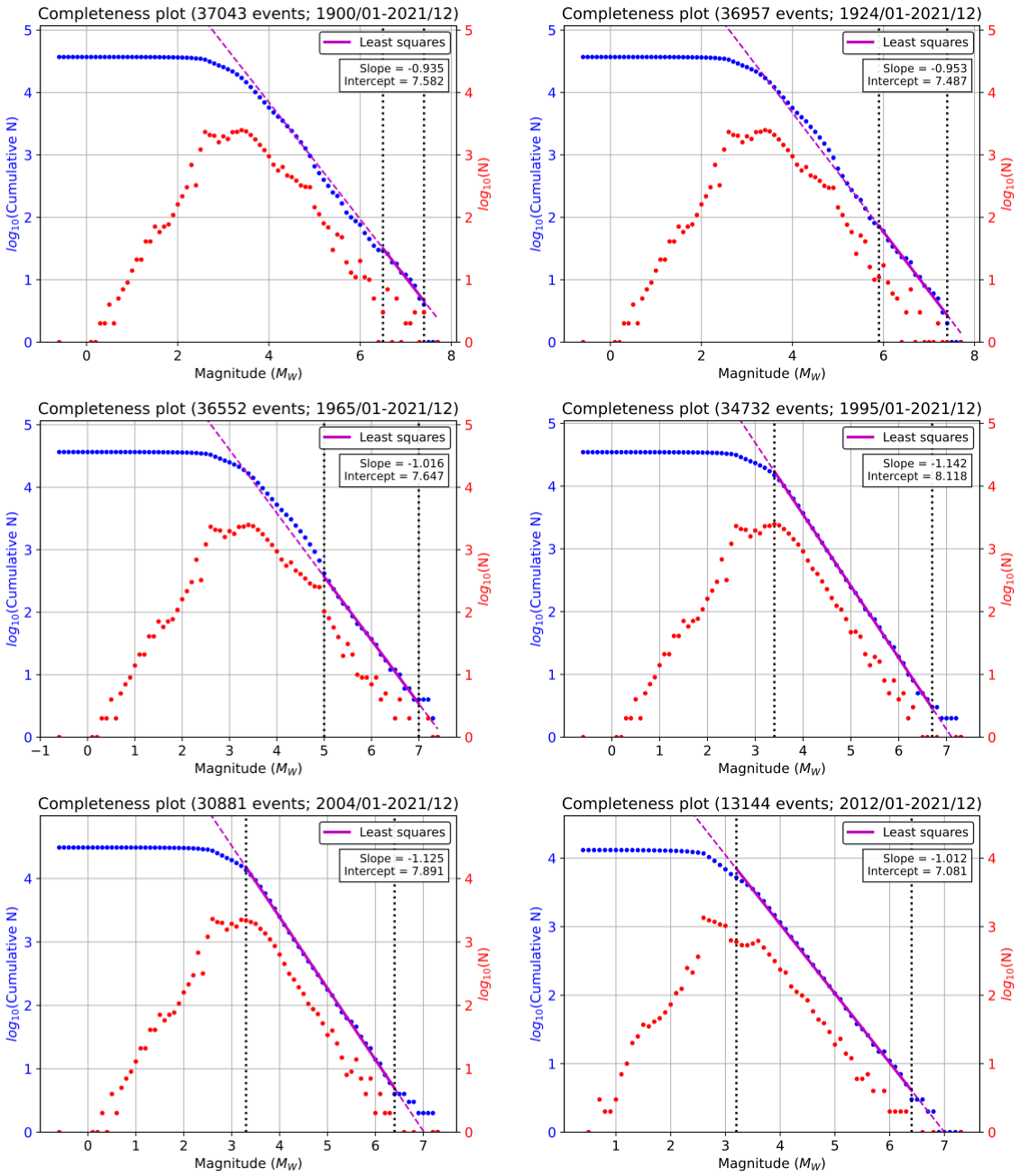

Figure 7: *Cumulative rate of earthquakes by magnitude for six selected time periods: 1900-2021, 1924-2021, 1965-2021, 1995–2021, 2004-2021, and 2012-2021.*

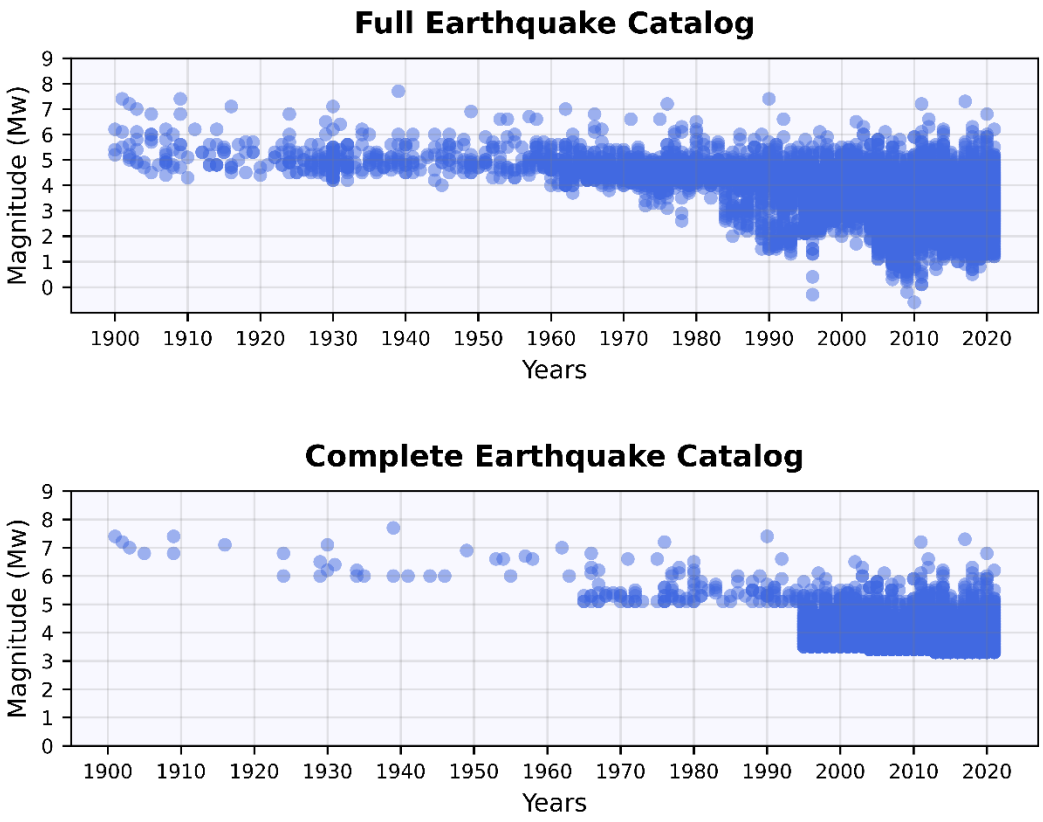

Figure 8: *Temporal distribution of earthquakes in the harmonized catalog. The upper panel is for the full earthquake catalog, and the lower panel is for the complete earthquake catalog.*

3. Updated PSHA

3.1. Stations and Data

The data from strong-motion seismic stations are crucial for understanding ground shaking characteristics during seismic events and their decay by distance. PSHA is highly sensitive to the Ground Motion Models (GMMs) that are used for ground motion characterization. The most commonly used ground motion parameters in PSHA are the Peak Ground Acceleration (PGA) values and response spectra. Strong-motion stations in Iraq and neighboring regions of Iran, as

well as the broadband seismic stations situated in Iraq were used to derive recorded PGA and the response spectra (Figure 9).

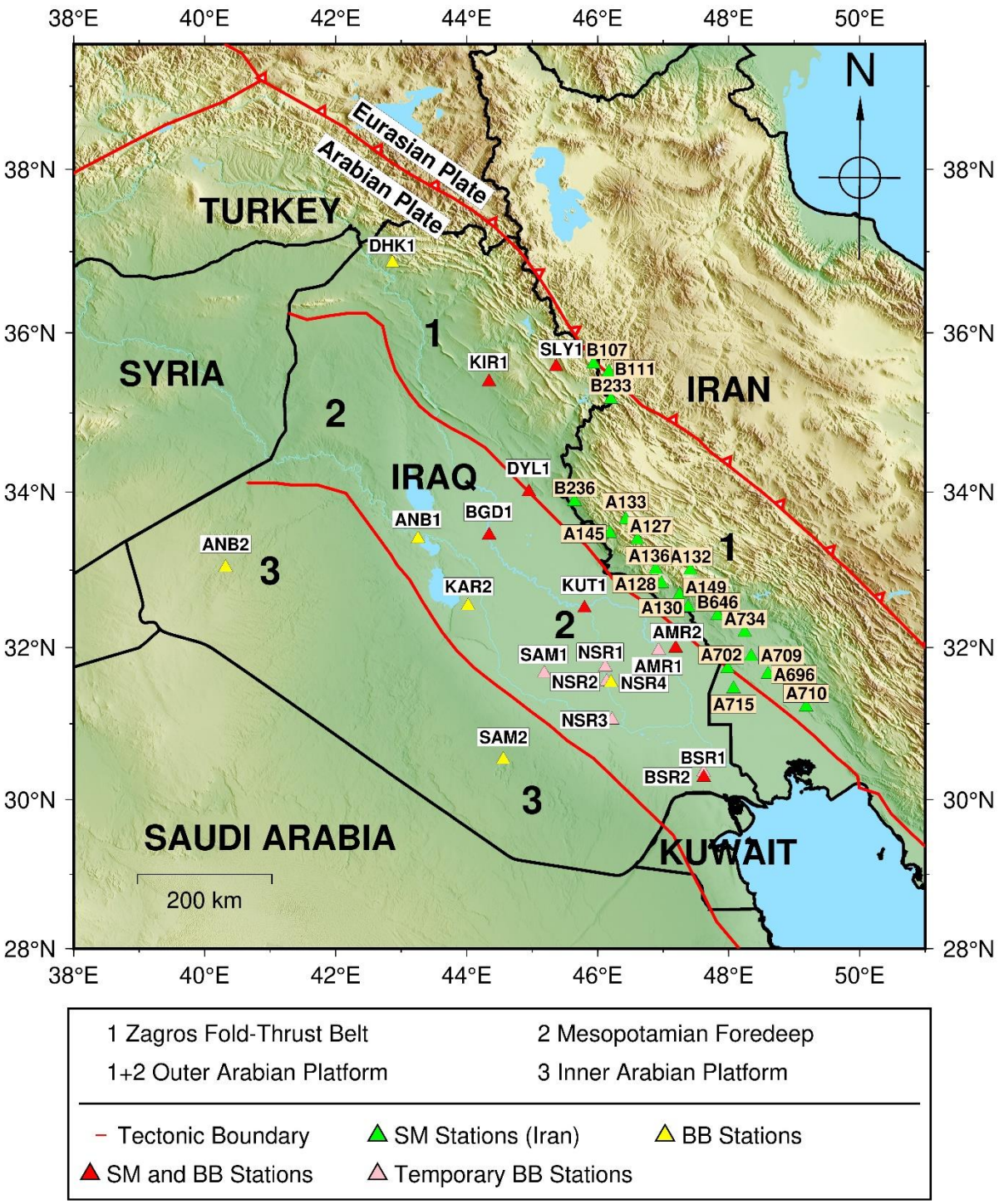

Figure 9: *Strong motion stations in Iraq and Iran and the broadband seismic stations in Iraq that were used in this study. The tectonic divisions are based on Fouad (2015).*

3.1.1. Strong Motion Stations in Iraq

Strong motion stations in Iraq, though limited, have seen significant progress. Two strong motion stations, one in Sulaymaniyah (SLY1) and the other in Basrah (BSR1), have operated from 2015 to 2017. Currently, we have seven strong motion stations in total in Iraq: Basrah (BSR1), Amarah (AMR), Kut (KUT1), Baghdad (BGD1), Diyala (DYL1), Kirkuk (KIR1), and Sulaymaniyah (SLY1). Table 4 lists the station names, codes, coordinates, and instrument types. In addition, the table shows the number of earthquakes that were analyzed and used in ground motion model validation (number of events with PGA ≥ 0.01g).

Table 4: *Strong motion stations in Iraq.*

No.	Station name	Station code	Lat.	Lon.	No. of analyzed events	No. of events with PGA ≥ 0.01g
01	Amarah, 2	AMR2	31.9899	47.1902	23	0
02	Baghdad, 1	BGD1	33.5092	44.3437	15	0
03	Basrah, 2	BSR2	30.2927	47.6191	3	0
04	Diyala, 1	DYL1	34.3745	45.3630	21	0
05	Kirkuk, 1	KIR1	35.3880	44.3419	11	0
06	Kut, 1	KUT1	32.5091	45.7974	7	0
07	Sulaymaniyah, 1	SLY1	35.5784	45.3667	4	0
Total records					**84**	**0**

3.1.2. Broadband Seismic Stations in Iraq

Currently, there are 13 operational broadband seismic stations in Iraq belonging to the Mesopotamian Seismological Network (MPSN). Table 5 shows the station names, codes, coordinates, instrument types, and number of analyzed and used earthquakes recorded by each station. We converted the velocity data obtained from the broadband seismic stations to acceleration data to compensate for the lack of acceleration data with adequately large amplitudes (PGA ≥ 0.01g) from the strong motion stations.

Table 5: *MP-network broadband seismic stations in Iraq.*

No.	Station name	Station code	Lat.	Lon.	No. of analyzed events	No. of events with PGA ≥ 0.01g
01	Amara, 1	AMR1	31.9590	46.9286	18	1
02	Amara, 2	AMR2	31.9899	47.1902	351	1
03	Anbar, 1	ANB1	33.4018	43.2576	94	0
04	Anbar, 2	ANB2	33.0375	40.3200	5	0
05	Baghdad, 1	BGD1	33.5092	44.3437	0	0
06	Basrah, 1	BSR1	30.3581	47.6153	194	0
07	Basrah, 2	BSR2	30.2927	47.6191	286	0
08	Duhok, 1	DHK1	36.8606	42.8665	686	4
09	Diyala, 1	DYL1	34.3745	45.3630	0	0
10	Karbala, 2	KAR2	32.5398	44.0224	293	0
11	Kirkuk, 1	KIR1	35.3880	44.3419	0	0
12	Kut, 1	KUT1	32.5091	45.7974	0	0
13	Nasiriya, 1	NSR1	31.7416	46.1151	171	2
14	Nasiriya, 2	NSR2	31.5550	46.1374	0	0
15	Nasiriya, 3	NSR3	31.0514	46.2199	0	0
16	Nasiriya, 4	NSR4	31.5399	46.2016	180	0
17	Samawa, 1	SAM1	31.6615	45.1834	0	0
18	Samawa, 2	SAM2	30.5295	44.5586	16	0
19	Sulaymaniyah, 1	SLY1	35.5784	45.3667	409	15
Total records					**2389**	**23**

3.1.3. Strong Motion Stations in Iran

The Building and Housing Research Center (BHRC) operates the Iranian Strong Motion Network (ISMN). This seismic network consists of over 1,260 active accelerometers and has collected over 14,129 earthquake recordings since 1973. The network plays a crucial role in monitoring seismic activity, providing data for earthquake research and engineering. It is distributed throughout Iran, focusing on major cities and earthquake-prone regions, ensuring comprehensive coverage.

Stations from this network that are near the Iraq-Iran border, to the west of the Zagros Thrust Belt were selected for our study. Table 6 lists the 18 strong motion stations selected from the ISMN. Data from 108 earthquakes recorded by these stations was collected and analyzed. Since most of

this data has relatively strong levels of shaking (PGA ≥ 0.01g), it supplements well the strong motion data available from Iraqi sources.

Table 6: *Strong motion stations in Iran that were used in this study.*

No.	Station code	Lat.	Lon.	No. of analyzed events	No. of events with PGA ≥ 0.01g
01	A127	33.388	46.606	3	3
02	A128	32.826	46.975	7	7
03	A130	32.518	47.379	27	26
04	A132	32.996	47.415	2	2
05	A133	33.646	46.428	1	1
06	A136	33.008	46.885	10	10
07	A145	33.470	46.186	10	10
08	A149	32.680	47.250	1	0
09	A696	31.648	48.599	4	4
10	A702	31.723	47.984	2	2
11	A709	31.879	48.344	5	5
12	A715	31.460	48.074	5	5
13	A734	32.193	48.245	10	10
14	B107	35.611	45.938	2	2
15	B111	35.510	46.170	1	0
16	B233	35.169	46.201	4	4
17	B236	33.875	45.644	12	10
18	B646	32.410	47.830	8	8
Total records				**108**	**103**

3.2. Data Preparation and Analyses

The data presented in Tables 4, 5, and 6 was collected and analyzed based on a list of earthquakes from the International Seismological Centre (ISC). We specifically focused on earthquakes within a 250 km radius of the seismic station with a Mw ≥ 4. The continuous waveforms were cut to include a 10-second window before the P-wave arrival time and a 10-second window after the coda wave. The header was prepared by adding the station coordinates, station code, station components (e.g. HNE, HNN, HNZ), and network name (e.g. MP). The earthquake source parameters, including earthquake date, time, coordinates, depth, and magnitude, were added to the header. All data are stored in SAC format.

The total number of analyzed earthquake records is 2,521, but we generally considered records with a Peak Ground Acceleration (PGA) of 0.01 g or higher, amounting to 126 records out of the full dataset of 2521. These data were processed and response spectra calculated using a Python script developed for this purpose, which is based on the method of Phillips et al. (2012). Figure 10 shows the moment magnitude versus distance for the data where PGA is 0.01 g or higher. The magnitudes range from 4 Mw to 7.3 Mw, while the distances range from 6 km to 295 km. Red triangles represent accelerations obtained by differentiating velocity data from Broadband stations, and blue circles are acceleration data directly from accelerometers.

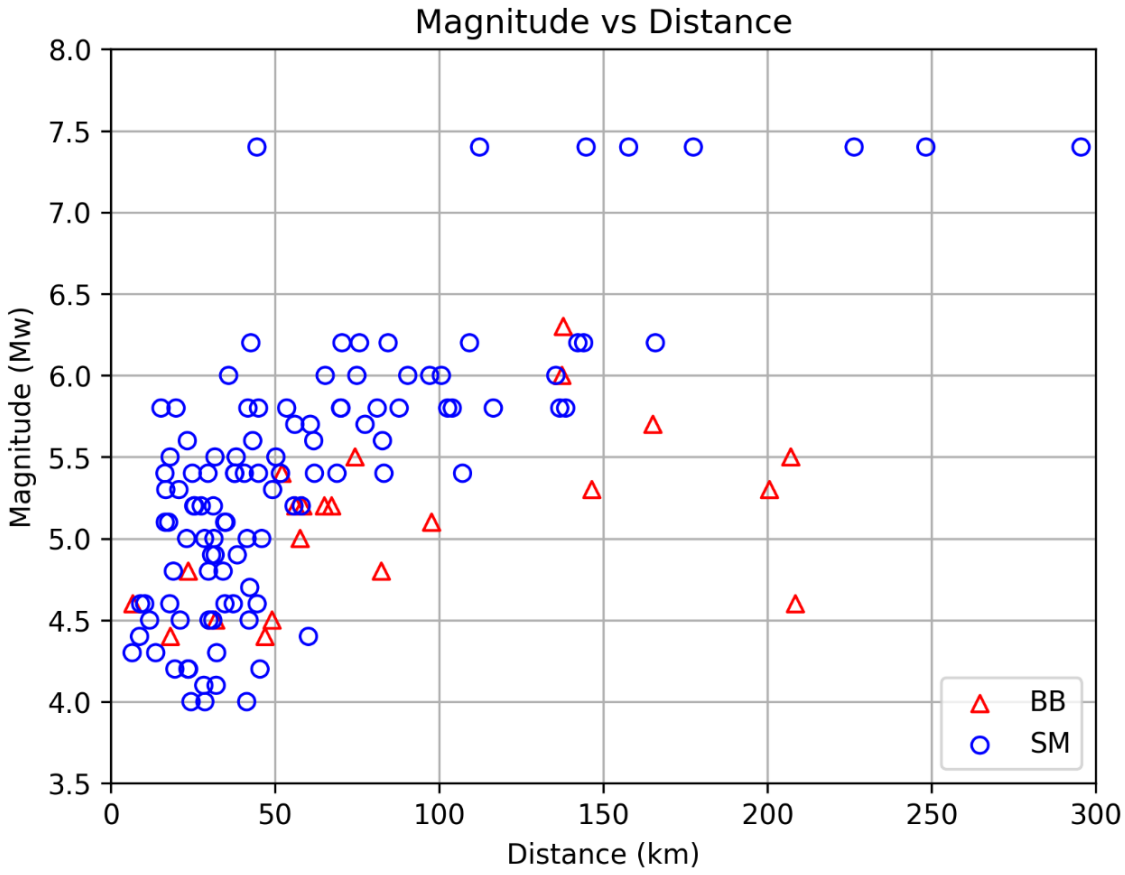

Figure 10: *Plot of magnitude versus distance for records from 126 earthquakes with PGA ≥ 0.01g (based on Tables 4 and 5). BB refers to broadband seismometer and SM strong motion accelerometer.*

3.2.1. Ground Motion Characteristics from Strong Motion Stations in Iraq

Data for 24 earthquakes were collected from the strong motion stations in Iraq, as shown in Table 4. The PGA from these recordings are all below 0.01 g.

3.2.2. Ground Motion Characteristics from Broadband Seismic Stations in Iraq

Data for 2,389 earthquakes were collected from the broadband seismic stations in Iraq, but only 23 records had PGA ≥ 0.01 g (Table 5). These are from earthquakes recorded by AMR1, AMR2, DHK1, NSR1, and SLY1. Table 6 lists the earthquakes recorded by these stations and the PGA values for each of the three components. Note that some of these components are clipped. Figure 11 represents an example of the PGA and response spectra results derived from the SLY1 broadband seismic station.

Table 6: *PGA values from broadband seismic stations in Iraq. The cross (×) refers to clipped components, and the asterisk (*) refers to the PGA value < 0.01g.*

Station	Date	Time (UTC)	Lat.	Lon.	Depth (km)	Mw	Dist. (km)	PGA (g)		
								HNE	HNN	HNZ
AMR1	20150925	061024	32.7964	46.6067	13.0	5.1	97.68	0.013	0.011	0.003*
AMR2	20180115	142745	31.5925	46.925	10.0	4.2	49.09	0.042	0.038	0.014
DHK1	20120614	055253	37.2159	42.4833	11.3	5.4	52.12	0.044×	0.043×	0.025
	20120805	203723	37.3725	42.9766	15.2	5.0	57.64	0.010	0.010	0.004*
	20130311	145708	36.6124	43.4167	12.9	5.2	56.33	0.047×	0.047×	0.018
	20130313	062302	36.6100	43.2901	13.9	5.4	46.95	0.025×	0.029	0.009*
NSR1	20170602	160952	31.5783	46.1086	0.7	4.4	18.12	0.146×	0.131×	0.101×
	20170818	101843	31.6820	46.1253	12.6	4.4	06.68	0.163×	0.149×	0.109×
SLY1	20170823	134254	36.0921	45.0199	14.7	5.2	65.04	0.025	0.019	0.012
	20171211	140957	35.0219	45.8227	19.3	5.5	74.37	0.039×	0.045×	0.020×
	20171211	144241	34.9393	45.8276	19.4	4.8	82.38	0.024	0.028	0.012
	20180111	065931	33.7388	45.7501	19.4	5.5	207.1	0.020	0.014	0.008*
	20180111	072135	33.7135	45.6516	16.1	5.2	208.5	0.021	0.013	0.006*
	20180111	072150	33.7844	45.6413	13.3	5.3	200.6	0.021	0.013	0.006*
	20180825	221325	34.5828	46.2641	11.1	6.0	137.4	0.012	0.014	0.010
	20180916	150342	35.2910	45.3516	10.0	3.6	31.91	0.025	0.023	0.012
	20181125	163732	34.3783	45.7559	17.3	6.3	137.8	0.023×	0.019×	0.013×
	20181125	170937	34.2875	45.7050	19.8	5.3	146.5	0.012	0.016	0.005*
	20190106	134159	34.1146	45.6928	18.3	5.7	165.1	0.020×	0.020×	0.010
	20201109	231824	35.4481	45.1614	7.4	4.8	23.57	0.016	0.023	0.007*
	20210406	151225	35.5959	46.0114	15.2	5.2	58.46	0.009*	0.012	0.007*
	20230316	183251	35.3022	46.0259	10.0	5.2	67.24	0.036	0.030	0.016

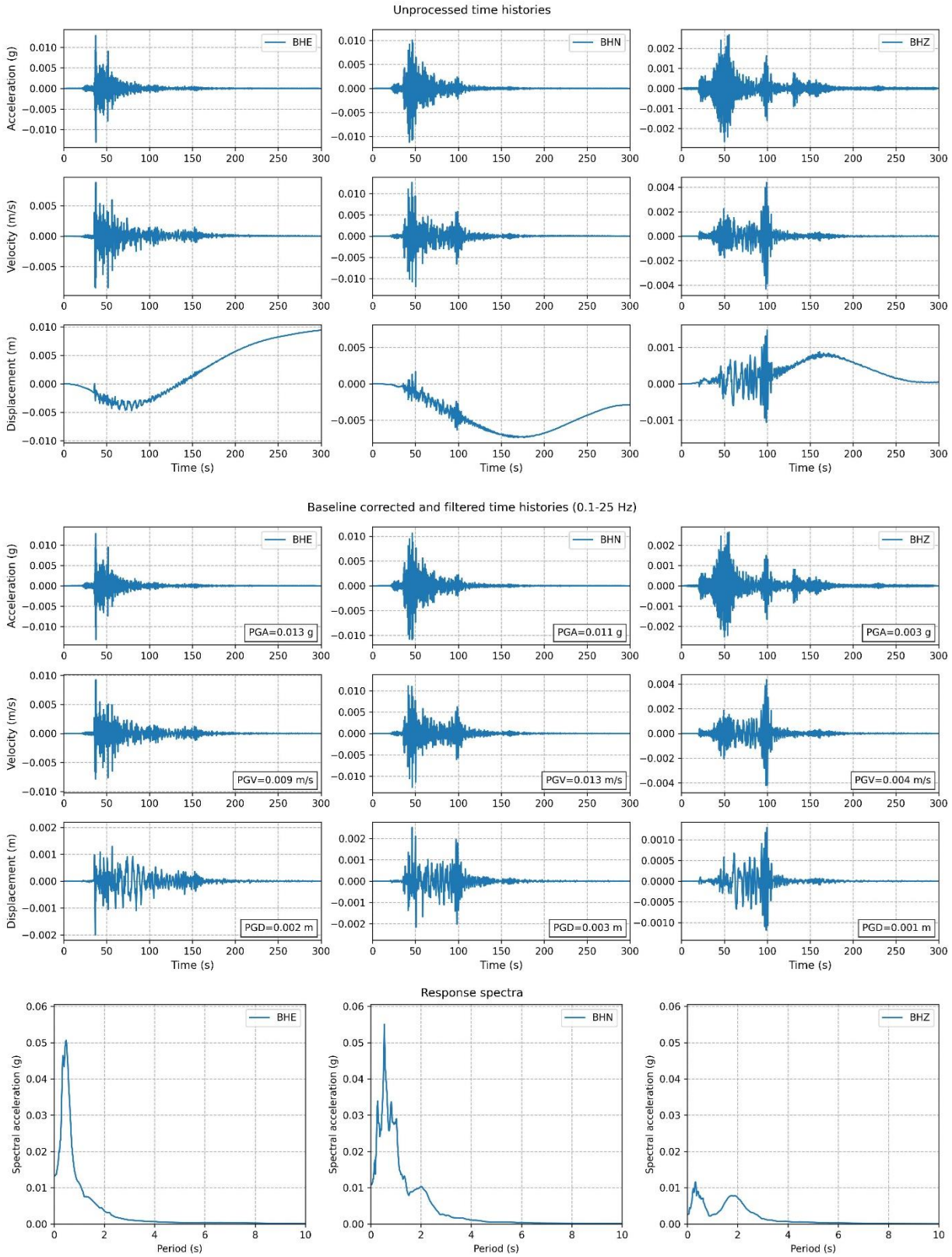

Figure 11: *An example of the PGA and response spectra from analyzing earthquake (20150925-061024-5.2Mw) recorded by AMR1 broadband seismic station.*

3.2.3. Ground Motion Characteristics from Strong Motion Stations in Iran

Data for 108 earthquakes were collected, and 103 had a PGA of 0.01 g or higher (Table 5). Table 7 lists the earthquakes recorded by these stations and the PGA values in the three components. Figure 12 represents an example of the PGA and response spectra results derived from the A130 strong motion station.

Table 7: *PGA values from selected strong motion stations in Iran. The asterisk (*) refers to PGA < 0.01g.*

Station	Date	Time (UTC)	Lat.	Lon.	Depth (km)	Mw	Dist. (km)	PGA (g)		
								HNE	HNN	HNZ
A127	20010323	052412	32.8317	46.5409	29.6	5.4	61.99	0.048	0.061	0.019
	20010329	063250	33.1588	46.7748	13.0	4.0	29.89	0.018	0.017	0.008*
	20171112	181817	34.8685	45.8783	20.1	7.4	177.41	0.096	0.089	0.058
A128	20010323	052412	32.8317	46.5409	29.6	5.4	40.65	0.040	0.039	0.030
	20020715	085458	32.8162	46.6730	22.0	4.2	28.30	0.021	0.019	0.015
	20140818	023205	32.7052	47.7125	12.9	6.2	70.39	0.021	0.020	0.016
	20140818	180824	32.6268	47.7386	14.4	6.0	74.91	0.029	0.022	0.020
	20140820	101416	32.6198	47.8230	15.4	5.6	82.71	0.011	0.012	0.006*
	20150925	061024	32.7964	46.6067	13.0	5.1	34.64	0.052	0.029	0.030
	20171112	181817	34.8685	45.8783	20.1	7.4	248.24	0.013	0.015	0.010
A130	20080827	215239	32.3402	47.4018	19.3	5.8	19.83	0.563	0.469	0.132
	20080903	224315	32.3692	47.3650	30.6	5.1	16.55	0.213	0.133	0.124
	20080903	231440	32.3209	47.2637	4.7	3.7	24.40	0.025	0.007	0.010
	20080906	235334	32.3420	47.2940	44.5	4.1	21.09	0.036	0.036	0.049
	20081026	052027	32.3431	47.3595	32.6	4.1	19.48	0.019	0.017	0.006*
	20120324	052538	32.5584	46.9720	35.0	4.9	38.49	0.013	0.013	0.005*
	20120418	184301	32.6406	47.1117	31.6	5.0	28.54	0.020	0.019	0.009*
	20120418	200408	32.4632	47.0440	20.0	4.7	32.06	0.016	0.016	0.008*
	20120420	012108	32.5209	47.1102	19.2	5.2	25.25	0.021	0.024	0.009*
	20120420	033141	32.4559	46.9015	16.3	4.3	45.40	0.011	0.010	0.004*
	20120420	035203	32.3733	46.9737	20.0	4.8	41.35	0.012	0.008*	0.004*
	20120420	153706	32.3997	47.0434	39.6	4.8	34.17	0.013	0.011	0.007*
	20120420	161752	32.4903	47.0466	32.0	5.0	31.38	0.027	0.021	0.008*
	20120421	023916	32.4415	47.0207	30.2	4.8	34.73	0.023	0.025	0.012
	20120421	052512	32.4603	47.0540	37.6	5.2	31.20	0.011	0.011	0.005*
	20120422	081355	32.3911	47.0849	20.0	3.4	31.02	0.008*	0.006*	0.006*
	20120503	100935	32.7890	47.7351	14.2	5.4	44.93	0.020	0.014	0.007*
	20140818	052551	32.6839	47.7780	12.6	5.8	41.72	0.016	0.013	0.010
	20140818	080528	32.6517	47.5059	27.6	4.8	19.02	0.018	0.009*	0.008*
	20140818	112303	32.6553	47.5973	12.8	5.2	25.53	0.025	0.018	0.011
	20140818	115134	32.6736	47.5690	15.7	5.4	24.81	0.021	0.023	0.010
	20140818	180824	32.6268	47.7386	14.4	6.0	35.85	0.028	?	?
	20140819	213217	32.7058	47.5706	13.3	5.2	27.51	0.018	0.017	0.014
	20140820	101416	32.6198	47.8230	15.4	5.6	43.19	0.026	0.032	0.015
	20140822	104000	32.6975	47.6424	13.3	4.9	31.74	0.011	0.007*	0.005*

	20141015	133554	32.5458	47.8565	8.1	5.8	44.96	0.016	0.020	0.010
	20171112	181817	34.8685	45.8783	20.1	7.4	295.50	0.027	0.023	0.012
A132	20120503	100935	32.7890	47.7351	14.2	5.4	37.73	0.066	0.082	0.051
	20140818	023205	32.7052	47.7125	12.9	6.2	42.61	0.200	0.224	0.100
A133	20171112	181817	34.8685	45.8783	20.1	7.4	144.75	0.075	0.061	0.032
A136	20010323	052412	32.8317	46.5409	29.6	5.4	37.65	0.053	0.052	0.023
	20120308	182140	32.8121	46.9680	27.1	5.0	23.07	0.087	0.107	0.040
	20120418	184301	32.6406	47.1117	31.6	5.0	45.94	0.014	0.018	0.010
	20120420	012108	32.5209	47.1102	19.2	5.2	57.99	0.014	0.014	0.007*
	20120420	030542	32.5230	47.0428	17.2	5.2	55.78	0.013	0.010	0.008*
	20120503	100935	32.7890	47.7351	14.2	5.4	83.16	0.013	0.011	0.004*
	20140818	023205	32.7052	47.7125	12.9	6.2	84.42	0.015	0.020	0.010
	20140818	180824	32.6268	47.7386	14.4	6.0	90.42	0.012	0.015	0.005*
	20150925	061024	32.7964	46.6067	13.0	5.1	35.05	0.027	0.020	0.010
	20171112	181817	34.8685	45.8783	20.1	7.4	226.38	0.029	0.028	0.016
A145	19980805	142704	33.1070	46.2933	50.6	5.6	41.48	0.023	0.030	0.011
	20041016	100436	33.5029	45.8687	32.3	4.8	29.71	0.029	0.022	0.008*
	20050125	113920	33.4496	45.8570	41.1	4.9	30.66	0.029	0.044	0.020
	20060405	173344	33.4463	46.0965	11.0	4.0	8.72	0.028	0.012	0.008*
	20090830	140438	33.1799	46.3882	31.7	4.6	37.27	0.018	0.012	0.005*
	20140818	023205	32.7052	47.7125	12.9	6.2	165.84	0.011	0.011	0.006*
	20171112	181817	34.8685	45.8783	20.1	7.4	157.70	0.016	0.016	0.014
	20180111	065931	33.7388	45.7501	19.4	5.5	50.25	0.011	0.013	0.009*
	20180111	071415	33.7517	45.7428	16.3	5.4	51.65	0.013	0.015	0.008*
	20180111	080040	33.7047	45.7355	19.5	5.3	49.25	0.011	0.011	0.004*
A696	20080827	215239	32.3402	47.4018	19.3	5.8	136.71	0.011	0.009	0.004*
	20140818	023205	32.7052	47.7125	12.9	6.2	143.99	0.012	0.012	0.004*
	20140818	052551	32.6839	47.7780	12.6	5.8	138.53	0.012	0.019	0.004*
	20140818	180824	32.6268	47.7386	14.4	6.0	135.53	0.009*	0.019	0.003*
A702	20080827	215239	32.3402	47.4018	19.3	5.8	87.79	0.015	0.016	0.008*
	20140823	200518	32.6733	47.7810	16.5	5.4	107.10	0.011	0.011	0.003*
A709	19990710	050542	32.1448	48.2063	10.0	4.4	32.21	0.031	0.023	0.011
	20080827	215239	32.3402	47.4018	19.3	5.8	102.58	0.011	0.013	0.005*
	20140818	023205	32.7052	47.7125	12.9	6.2	109.23	0.011	0.013	0.005*
	20140818	052551	32.6839	47.7780	12.6	5.8	103.96	0.014	0.015	0.004*
	20140818	180824	32.6268	47.7386	14.4	6.0	100.65	0.014	0.012	0.003*
A715	20080827	215239	32.3402	47.4018	19.3	5.8	116.48	0.011	0.010	0.004*
	20140818	023205	32.7052	47.7125	12.9	6.2	142.23	0.011	0.020	0.003*
A734	19990710	050542	32.1448	48.2063	10.0	4.4	6.47	0.040	0.042	0.027
	20080827	215239	32.3402	47.4018	19.3	5.8	81.10	0.017	0.013	0.005*
	20140818	023205	32.7052	47.7125	12.9	6.2	75.71	0.020	0.020	0.008*
	20140818	052551	32.3402	47.4018	19.3	5.8	69.94	0.048	0.031	0.016
	20140820	101416	32.6198	47.8230	15.4	5.6	61.77	0.014	0.015	0.005*
	20140823	200518	32.6733	47.7810	16.5	5.4	68.85	0.012	0.012	0.004*
	20141015	133554	32.5458	47.8565	8.1	5.8	53.54	0.040	0.064	0.017
	20141015	134523	32.4750	47.9081	16.4	4.3	44.54	0.009*	0.013	0.004*
	20141015	223142	32.4670	47.9358	14.4	4.5	42.08	0.030	0.022	0.007*
	20171112	181817	34.8685	45.8783	20.1	7.4	369.28	0.017	0.018	0.012
B107	20001222	090413	35.8212	45.8938	35.0	4.2	23.66	0.066	0.059	0.032
	20010528	085701	35.8590	46.0253	35.0	3.7	28.62	0.022	0.035	0.036
B233	20171112	181817	34.8685	45.8783	20.1	7.4	44.48	0.047	0.050	0.044
	20171211	140957	35.0219	45.8227	19.3	5.5	38.15	0.040	0.062	0.026
	20180722	100726	34.5381	46.2426	10.8	5.8	70.09	0.041	0.038	0.018

	20180825	221325	34.5828	46.2641	11.1	6.0	65.28	0.044	0.027	0.023
B236	20030105	094848	33.9396	35.5842	35.0	4.6	9.05	0.012	0.013	0.004*
	20131122	065127	34.4192	45.5706	21.7	5.7	60.74	0.047	0.037	0.012
	20131122	183059	34.3777	45.7022	18.9	5.7	56.01	0.049	0.051	0.018
	20131124	180541	34.1591	45.6801	12.1	5.5	31.68	0.018	0.012	0.006*
	20171112	181817	34.8685	45.8783	20.1	7.4	112.29	0.056	0.061	0.027
	20180111	065931	33.7388	45.7501	19.4	5.5	18.02	0.164	0.252	0.086
	20180111	070053	33.7258	45.6703	17.6	5.2	16.72	0.081	0.106	0.031
	20180111	071415	33.7517	45.7428	16.3	5.4	16.45	0.049	0.069	0.033
	20180111	072135	33.7135	45.6516	16.1	5.2	17.92	0.432	0.273	0.281
	20180111	080040	33.7047	45.7355	19.5	5.3	20.70	0.122	0.105	0.036
	20180825	221325	34.5828	46.2641	11.1	6.0	97.10	0.008*	0.009*	0.003*
	20181017	031655	34.4087	45.5274	18.0	4.4	60.16	0.006*	0.005*	0.002*
B646	20140820	101416	32.6198	47.8230	15.4	5.6	23.27	0.271	0.137	0.080
	20140820	102837	32.6105	47.7507	12.3	3.7	23.45	0.011	0.015	0.007*
	20140823	200518	32.6733	47.7810	16.5	5.4	29.55	0.110	0.091	0.035
	20140824	024452	32.5630	47.7812	19.5	5.1	17.57	0.020	0.018	0.013
	20141015	133554	32.5458	47.8565	8.1	5.8	15.26	0.201	0.138	0.093
	20141015	134523	32.4750	47.9081	16.4	4.3	10.29	0.035	0.043	0.025
	20141015	223142	32.4670	47.9358	14.4	4.5	11.78	0.015	0.032	0.013
	20141015	235043	32.4783	47.9506	17.4	4.0	13.637	0.018	0.040	0.015

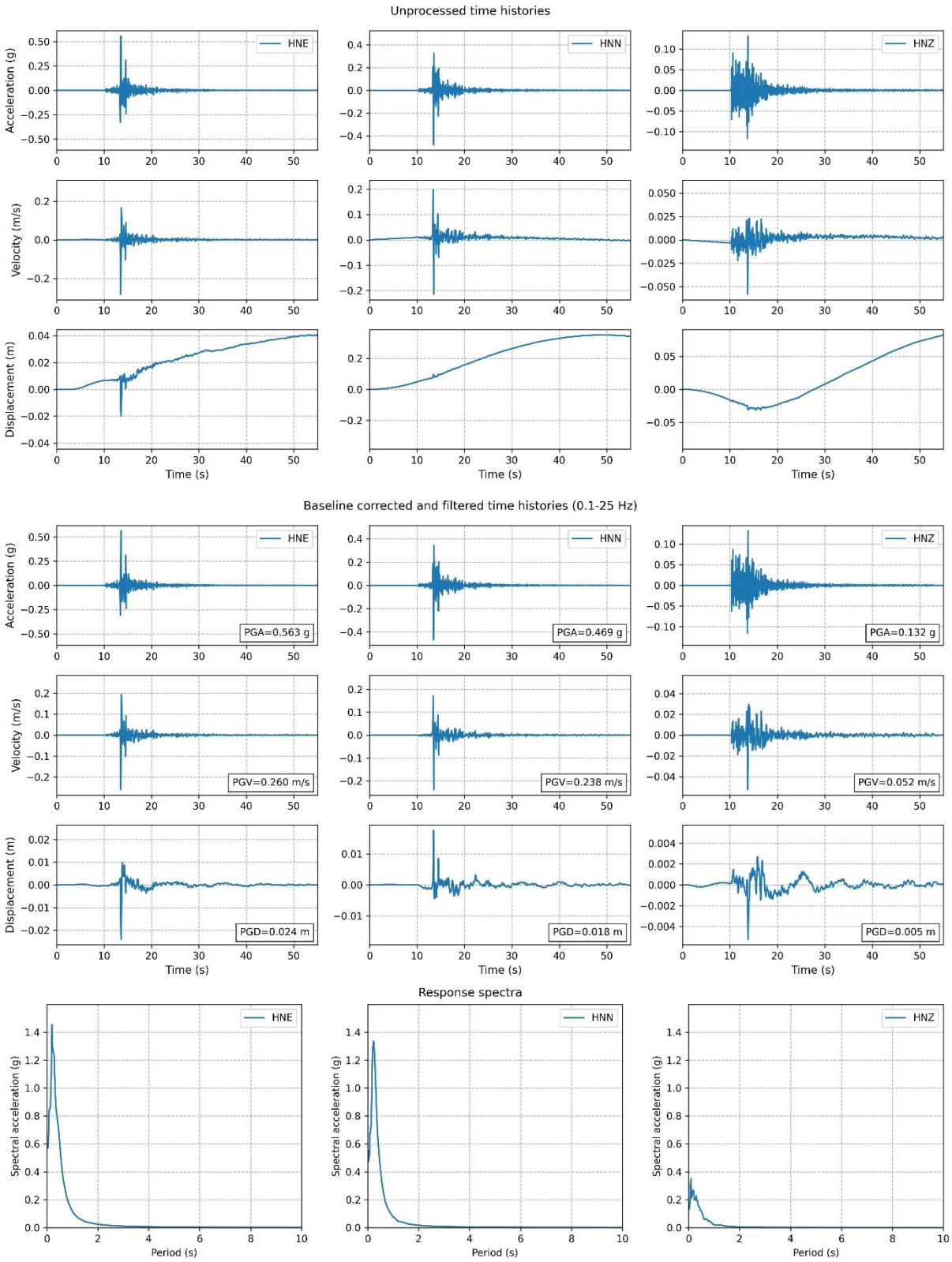

Figure 12: *An example of the PGA and response spectra resulting from analyzing earthquake (20080827-215239-5.3Mw) recorded by A130 strong motion station.*

3.3. Ground Motion Models (GMMs)

The choice of GMMs used in PSHA to characterize strong ground motion is dependent on the tectonic setting of the study area and availability of strong-motion data. In order of the decreasing amount of data, the options are to (1) empirically derive region-specific GMMs, (2) choose regionally or globally derived GMMs based on comparisons and/or validations against locally recorded strong-motion data, and (3) choose regionally or globally derived GMMs based on the local attenuation characteristics (Abdulnaby *et al*., 2020). This study utilizes the second option, because while strong motion data availability is increasing in the region, the amount of data is still not enough to empirically derive region-specific GMMs for Iraq.

Global GMMs generally fall into one of the following tectonic groupings: (a) active tectonic regions with shallow crustal seismicity, (b) stable continental regions, and (c) subduction zones. Iraq is primarily situated in a region characterized by active tectonic regions with shallow crustal seismicity, with most of its earthquake activity occurring in active tectonic areas that border Turkey and Iran. This active tectonic region is represented by the Outer Arabian Platform that consists of the Zagros Fold-Thrust Belt and the Mesopotamian Foredeep (Figure 1). The relatively quiet tectonic region is represented by the Inner Arabian Platform, which is occupied by the Western and Southern Deserts of Iraq. However, it should be noted that past attenuation tomography studies indicated that the attenuation in Iraq is in between what is typical of active tectonic regions and stable continental regions (Onur *et al*., 2017).

Consequently, two GMMs from Next Generation Attenuation (NGA) West-2 project (active tectonic regions) and one GMM from NGA East project (stable continental regions) with four variations, were used in this project through a logic tree approach. NGA West-2 GMMs that were considered are Boore *et al*. (2014), referred to as BSSA14 in the rest of the study; and Campbell

and Bozorgnia (2014), CB14. The NGA East GMM that was considered is Darragh *et al*. (2015)–DASG15, with the following variations: single-corner variable stress parameter (1CVSP), single-corner constant stress parameter (1CCSP). These GMMs were selected based on their fit to the available strong motion data.

For this project, we use a logic tree approach to weigh attenuation relations from active tectonic regions against stable continental regions based on the comparison between the observed strong motion data and the GMMs (Figures 13, 14, and 15). Our weighting scheme is period-dependent as suggested by the data, weights on the two variations of DASG15 increasing by increasing vibration period.

Ground motions from all GMMs were computed for three site classes. Site classification is based on the National Earthquake Hazard Reduction Program (NEHRP) site classes (BSSC 2001), which uses the average shear-wave velocity of the top 30 m of the site to characterize ground conditions.

As more strong-motion data from recently installed instruments becomes available, the ground-motion characterization can be updated and further refined in a more informed manner. Recorded strong-motion data may also reveal the need for new GMMs for regions like Iraq, where the attenuation appears to be not as fast as California or Turkey, and not as slow as stable craton regions. A region-specific ground-motion modeling study, also accounting for the thick sedimentary deposits in the Mesopotamian Foredeep, would be invaluable for future PSHA studies in Iraq.

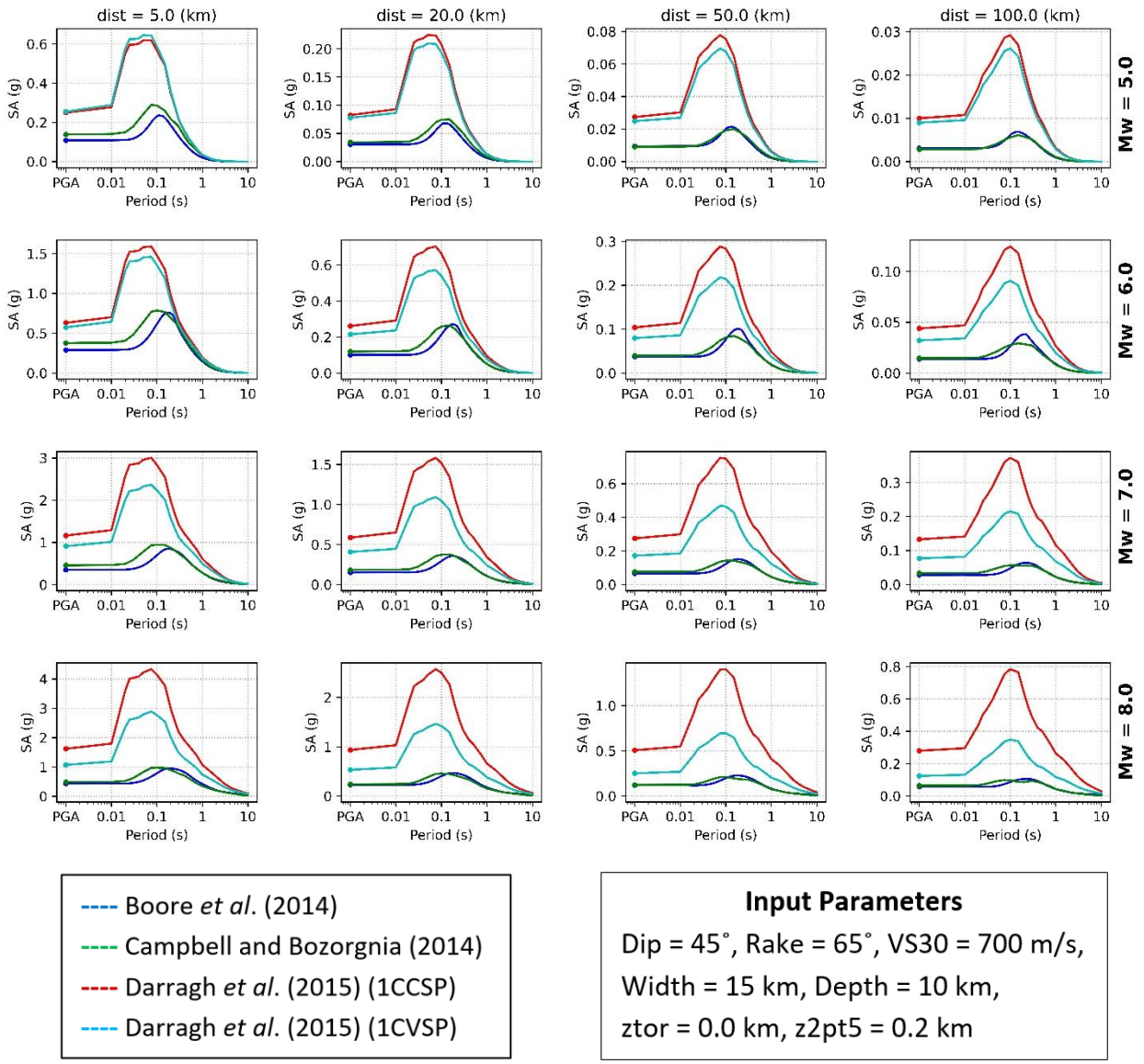

Figure 13: *Trellis plot comparing the GMMs used in the hazard assessment. Dip is the dip angle of the fault, Rake is the slip direction of the fault, VS30 is the estimated average shear-wave velocity in the upper30 m, Depth is the hypocentral depth, ztor is the depth-to-top of rupture, and z2pt5 is the vertical distance from earth surface to the layer where seismic waves start to propagate with a speed above 2.5 km/s.*

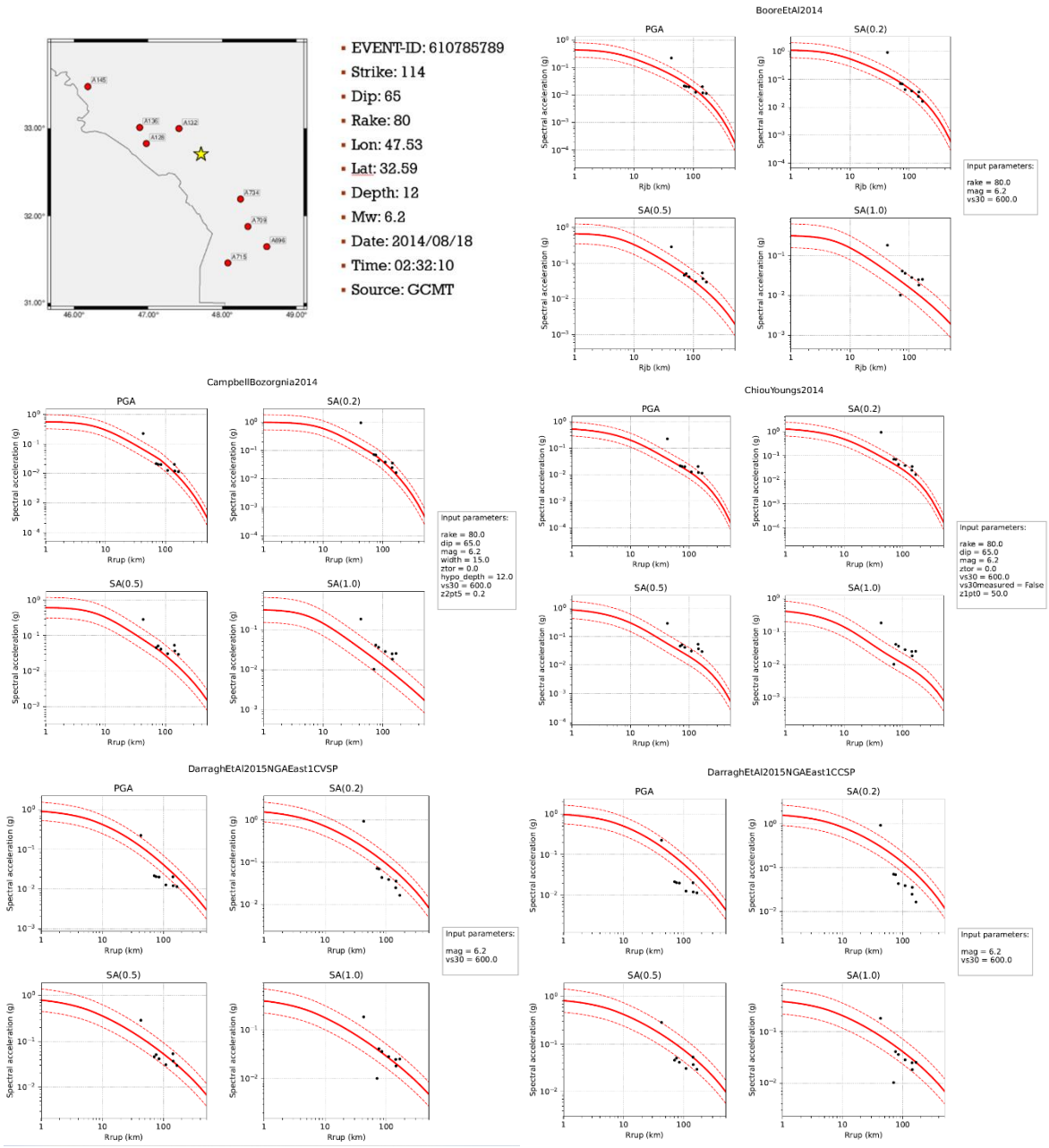

Figure 14: *Trellis plot comparing the GMMs used in the hazard assessment with the strong-motion measured values.*

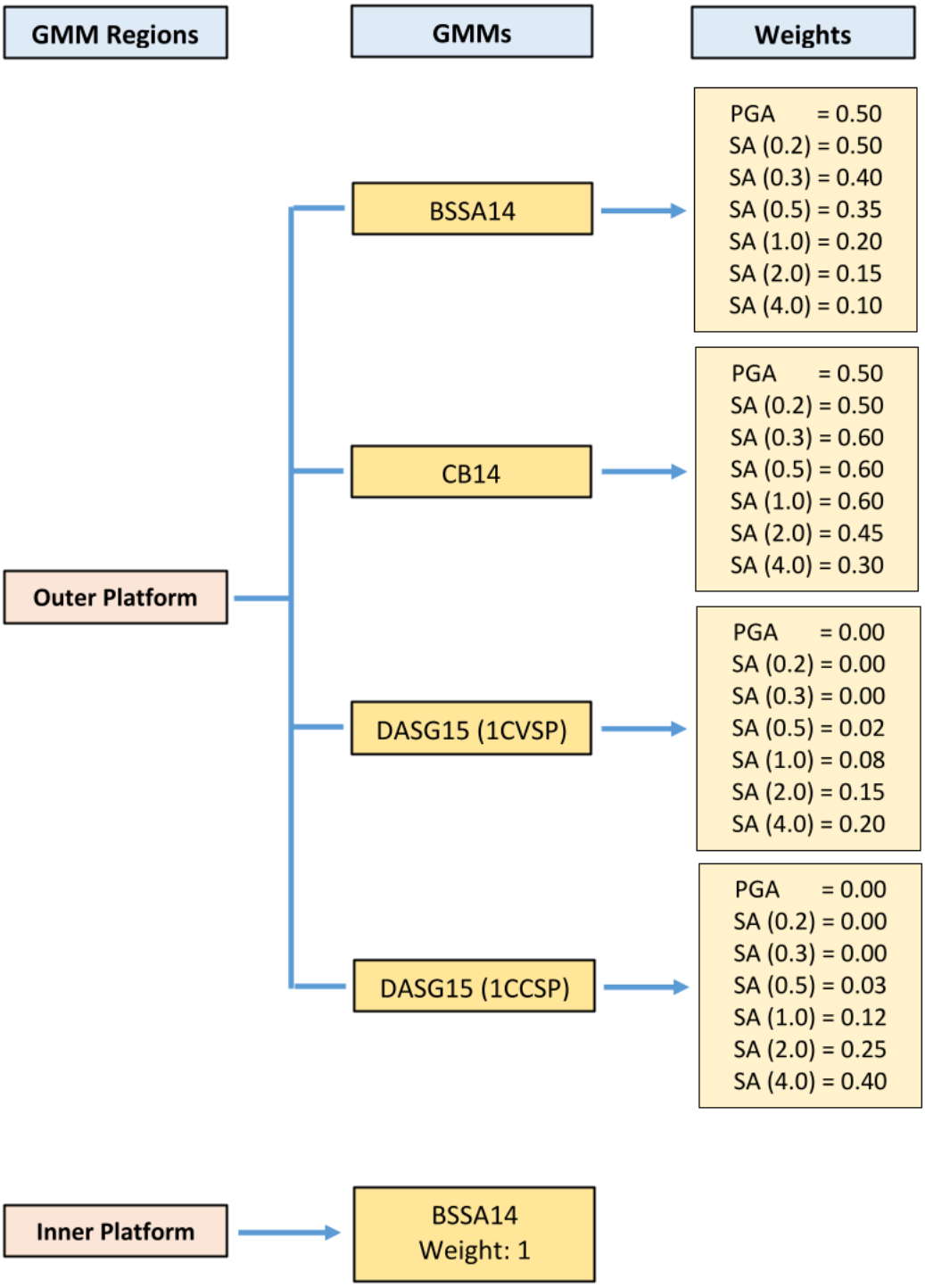

Figure 15: *The logic tree used for ground-motion characterization.*

3.4. Seismic Source Characterization

Since good quality fault-specific information (particularly geologic slip rates) are generally unavailable in Iraq, area sources were used in PSHA to characterize seismic activity in the region. When delineating the source zones, the tectonics of the region, geometry of known faults, and the seismicity patterns were considered (Figure 16). The area sources broadly follow the main tectonic features in the region, as described below.

Zones 3, 4, 5, 6, 7, 8, 9, 11, 12, and 16 characterize, in ten different segments, the main axis of the Bitlis–Zagros Fold and Thrust Belt. Although they have similar tectonic origins, zone 4 to the northwest has less present-day activity than other zones. Zones 1 and 7 roughly coincide with the Mesopotamian Foredeep. Zone 1 represents the Inner Platform. Zone 9 characterizes the seismicity in and around Sinjar Uplift and zone 19 along the Palmyrides and the northernmost section of the Euphrates fault system. Zones 17 and 18 capture the intense seismic activity in Eastern Turkey. Zones 13 and 14 represent the relatively low seismic activity northeast of the Zagros Fold and Thrust Belt. Zone 20 represents the seismic activities near the eastern region of the Dead Sea Fault. The detail level for the geographic characterization of the source zones is generally lower for zones that are relatively distant from Iraq (e.g., zones 17, 18, 19, and 20).

Maximum magnitudes were assigned to each source zone based on various considerations such as the maximum historical earthquake inside the zone (maximum magnitude cannot be lower than the magnitude of the largest observed earthquake), length of known faults within each zone, potential for segmentation and possibility of multiple-segment ruptures, and other relevant tectonic information (faulting mechanism, kinematics of the fault, etc.). For the sources characterizing the multiple segments of the Bitlis–Zagros Fold and Thrust Belt, the lengths of the segments were used as a guiding consideration as well. The geometry and length of the faults were taken into

account using Wells and Coppersmith (1994) magnitude scaling relations between rupture length/area and magnitude.

The choice of maximum magnitude often depends on whether an active fault is characterized as a linear source. If yes, the maximum magnitude assigned to the surrounding area source can be lowered, if no other major fault features are available inside the source zone. In our case, while some known active faults exist in the region, the information necessary to characterize them as linear sources is largely unavailable. Therefore, we assign relatively large maximum magnitudes to the area sources that are accommodating for known active fault features.

For each source, Gutenberg–Richter recurrence parameters (a- and b-values) were calculated using maximum likelihood estimation and least squares regression based on the earthquake catalog developed for this project (Figure 17 and Table 8). Maximum likelihood was generally preferred, however in some cases where earthquake activity is low, least squares regression or an average of maximum likelihood and least squares provided better fit parameters. Truncated Gutenberg–Richter relations were used for the hazard analyses, with a minimum magnitude of 4.5 for all sources and maximum magnitudes varying by source (Table 8).

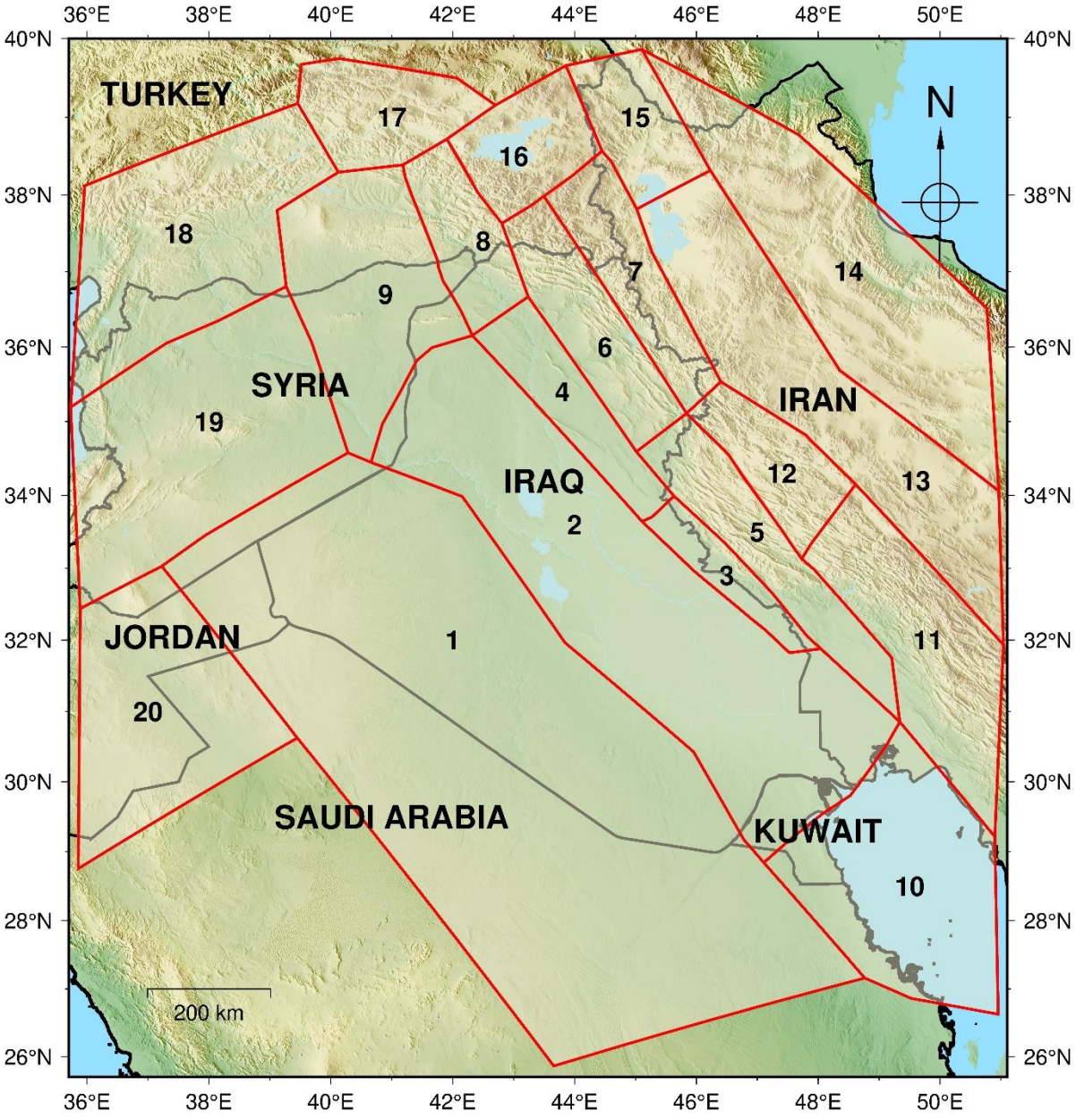

Figure 16: *Delineation of seismic source zones in Iraq and adjacent areas.*

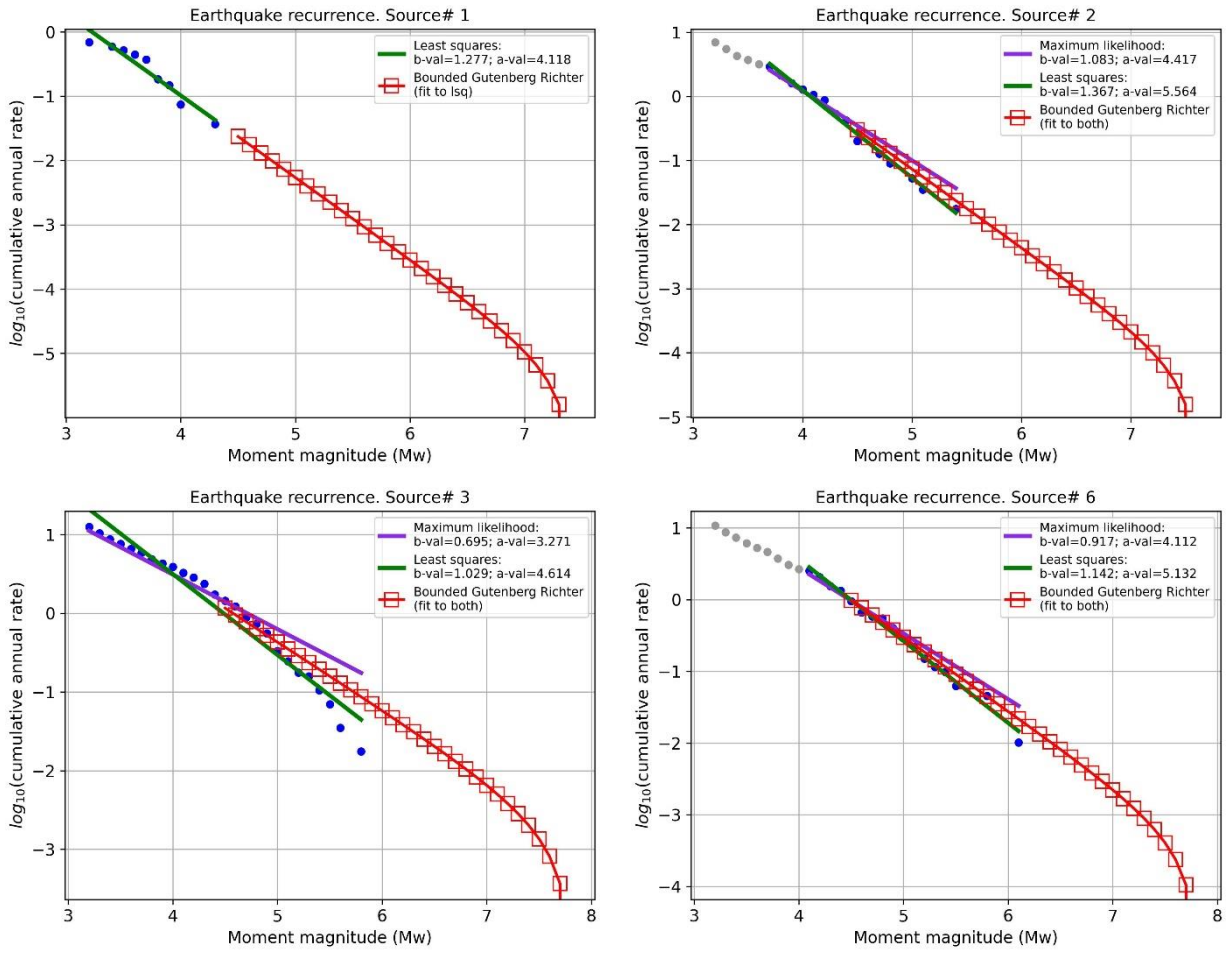

Figure 17: *Examples of cumulative number of earthquakes per annum plotted against magnitude for four different source zones. Blue circles indicate observed seismicity, and red squares indicate modeled seismicity (bounded Gutenberg-Richter model). Source number 1 is for the Iraqi desert, source number 2 is for the Mesopotamian Foredeep, source number 3 is for the Mandili-Badra-Teeb fault, and source number 6 is for the High-Folded zone. The gray data points indicate adjustments, where necessary, to the completeness magnitude for each individual source zone.*

Table 8: *Recurrence parameters for source zones.*

Source zone no.	Source zone name	Observed Mmax	Theoretical Mmax	G-R b-value	G-R a-value
01	Iraqi Desert	4.3	7.4	1.277	4.118
02	Mesopotamia	5.4	7.6	1.225	4.990
03	Mandili-Badra-Teeb	5.8	7.8	0.862	3.942
04	Low Folded	5.1	7.6	0.936	3.554
05	Ilam-Dezful	7.3	7.8	1.080	5.351
06	High Folded	6.1	7.8	1.029	4.622
07	Thrust	7.1	7.8	0.918	4.168
08	Duhok-Sirnak	6.0	7.8	1.134	4.573
09	Sinjar	6.2	7.6	0.858	3.460
10	Arabian Gulf	5.0	7.6	1.390	5.564
11	Kazerun	7.4	8.0	1.102	5.678
12	Sarpol	6.7	8.0	0.896	3.900
13	Central Iran	4.8	7.6	1.305	5.000
14	Caspian Sea	7.4	7.8	0.918	4.433
15	Caucas	5.6	7.9	1.100	5.463
16	Iran-Turkey	7.2	7.9	1.142	5.761
17	Eastern Turkey	6.9	7.9	0.988	4.797
18	Syria-Turkey	6.8	7.9	1.101	5.345
19	Western Syria	5.5	7.8	1.119	4.467
20	Jordan	5.0	7.9	1.577	5.855

4. Results

This study uses the open-source PSHA software OpenQuake (Pagani *et al*., 2014) to calculate the seismic hazard. The ground motions are presented for a probability of exceedance of 2% in 50 years (corresponding to a return period of 2,475 years). The ground motions were computed for Vs30 (the average shear-wave velocity in the upper 30 m) values of 760 m/s, 500 m/s, and 180 m/s. The PSHA results can be divided into four categories: seismic hazard maps, uniform hazard spectra, hazard curves, and hazard deaggregations. Each of these categories is further discussed below.

4.1. Seismic Hazard Maps

The ground motions were calculated for a 2% chance of being exceeded in 50 years, or a return period of 2,475 years, as required by the building code of Iraq. Results are presented in hazard maps of PGA and spectral accelerations at periods of 0.2 s, 0.3 s, 0.5 s, 1.0 s, 2.0 s, and 4.0 s (Figures 18 through 24). The maps presented herein are for a reference site with a Vs30 of 760 m/s. Please note that the color scale is shown separately for each map and varies from map to map.

Hazard maps were calculated for the three Vs30 site conditions mentioned above: 180 m/s, 500 m/s, and 760 m/s. Figures 18 through 24 depict the hazard maps for the 760 m/s site condition. The results for the other Vs30 values are provided in Appendix A.

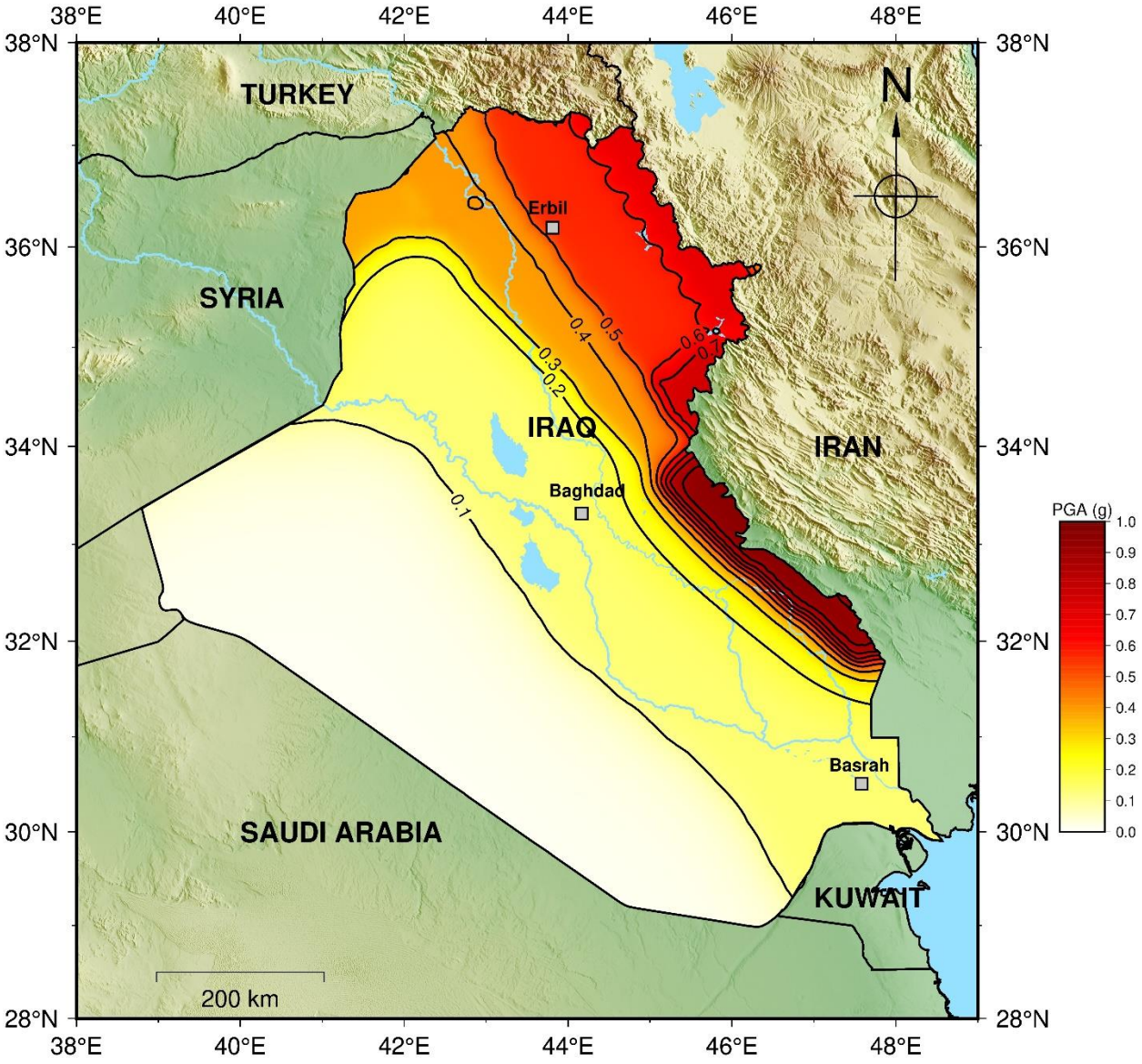

Figure 18: *Probabilistic seismic hazard in Iraq with a 2% chance of exceedance in 50 years on site with a Vs30 of 760 m/s in terms of PGA.*

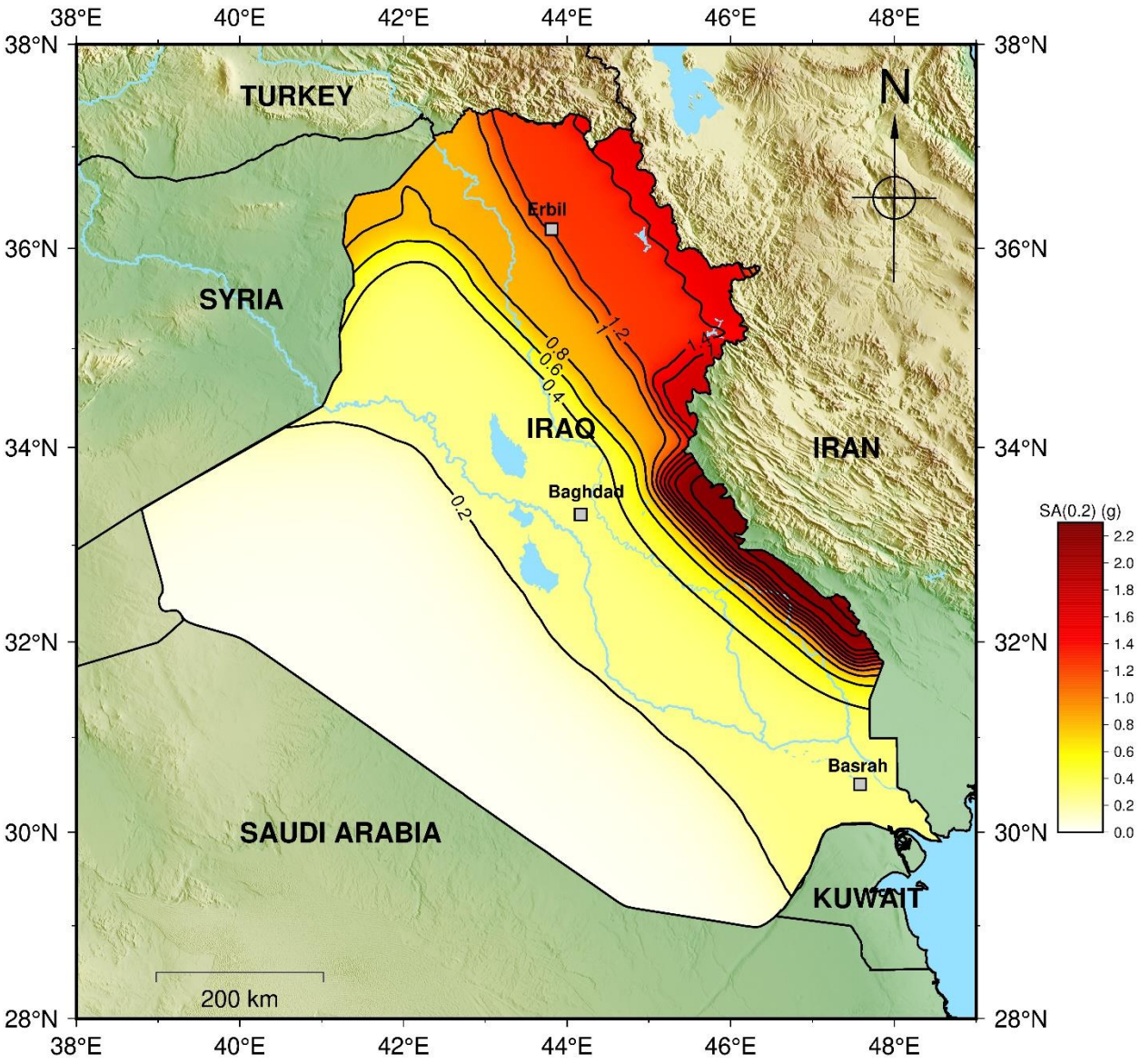

Figure 19: *Probabilistic seismic hazard in Iraq with a 2% chance of exceedance in 50 years on site with a Vs30 of 760 m/s in terms of spectral acceleration (SA) at 0.2 s.*

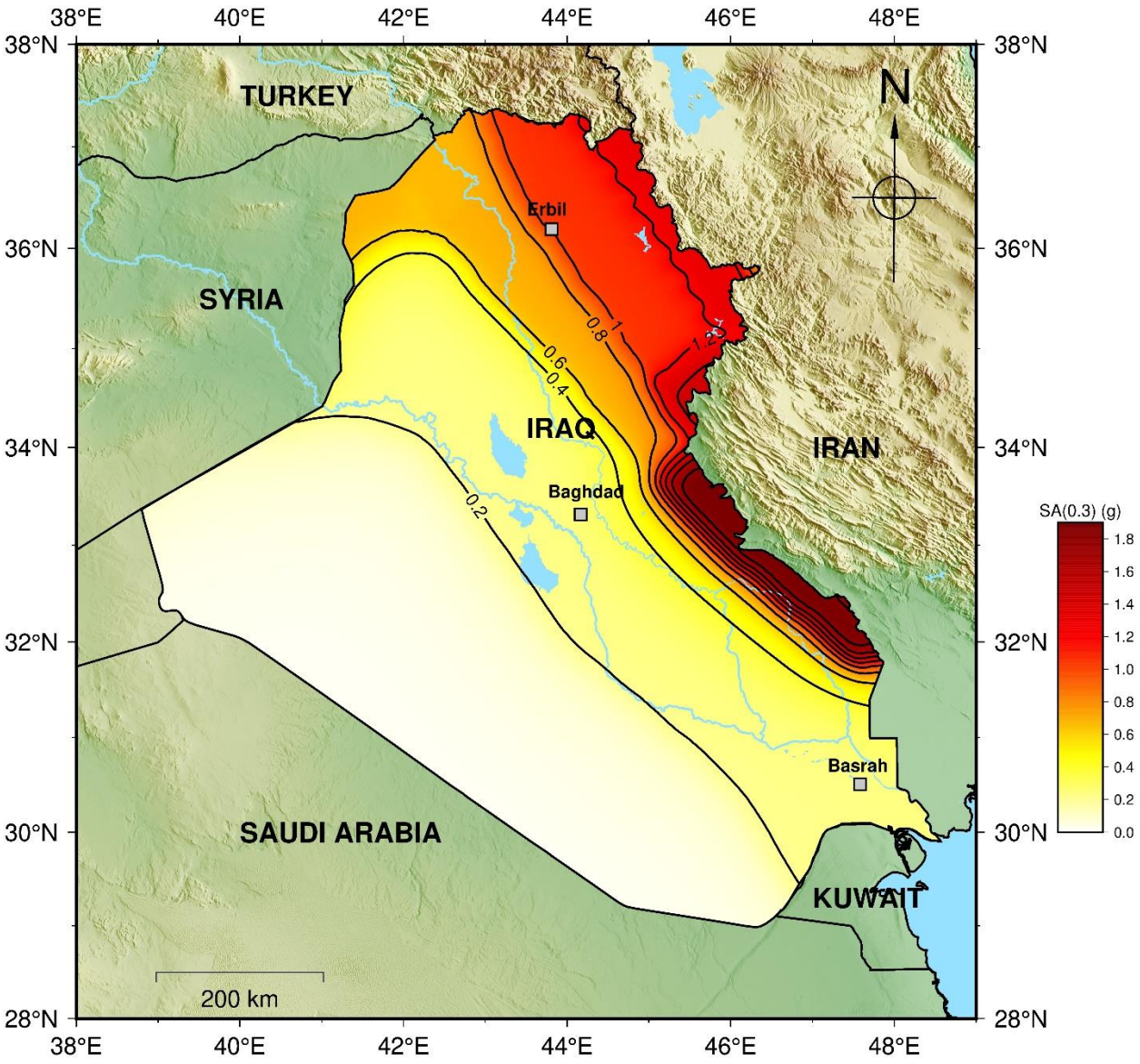

Figure 20: *Probabilistic seismic hazard in Iraq with a 2% chance of exceedance in 50 years on site with a Vs30 of 760 m/s in terms of spectral acceleration (SA) at 0.3 s.*

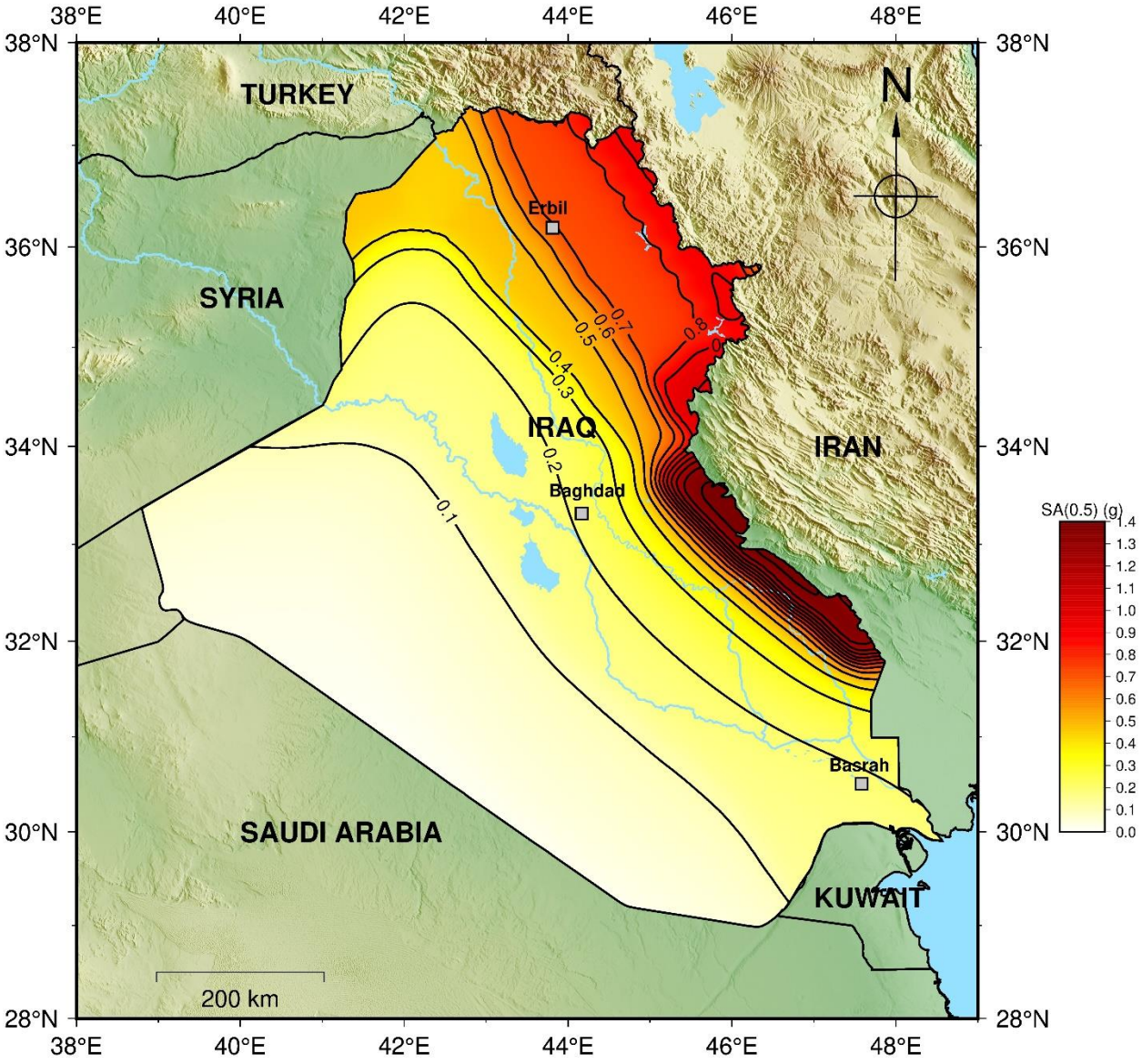

Figure 21: *Probabilistic seismic hazard in Iraq with a 2% chance of exceedance in 50 years on site with a Vs30 of 760 m/s in terms of spectral acceleration (SA) at 0.5 s.*

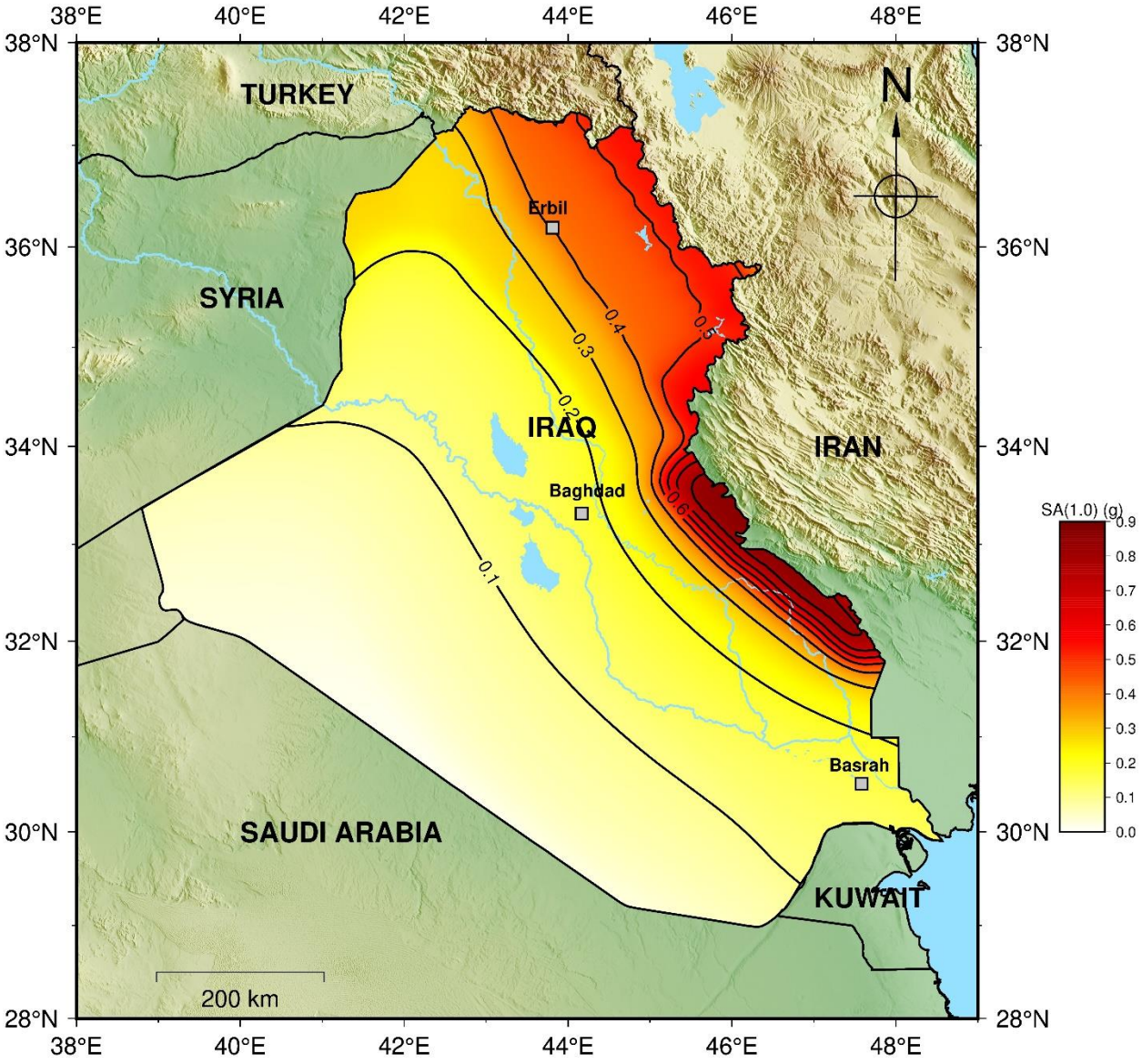

Figure 22: *Probabilistic seismic hazard in Iraq with a 2% chance of exceedance in 50 years on site with a Vs30 of 760 m/s in terms of spectral acceleration at 1.0 s*

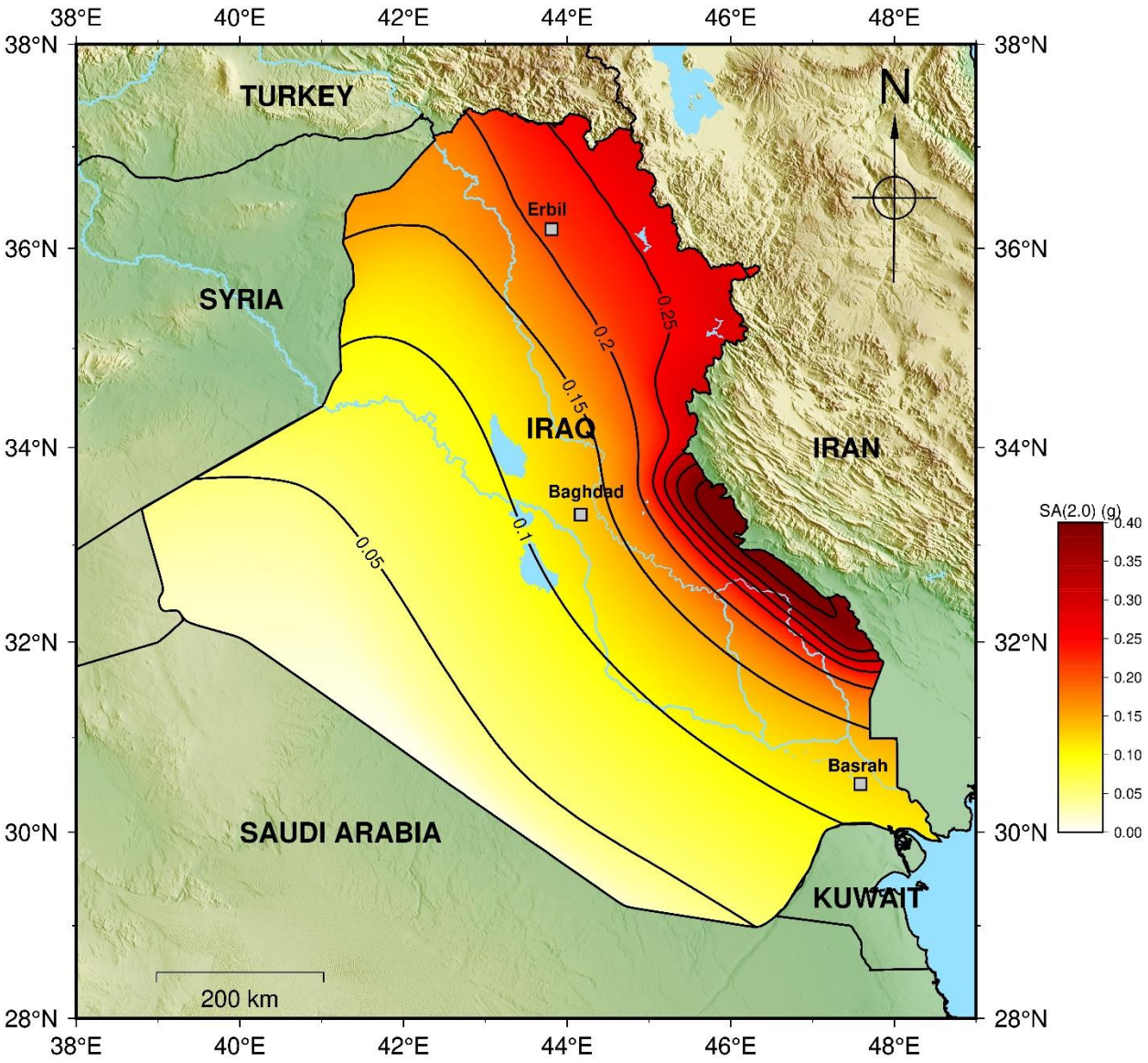

Figure 23: *Probabilistic seismic hazard in Iraq with a 2% chance of exceedance in 50 years on site with a Vs30 of 760 m/s in terms of spectral acceleration (SA) at 2.0 s.*

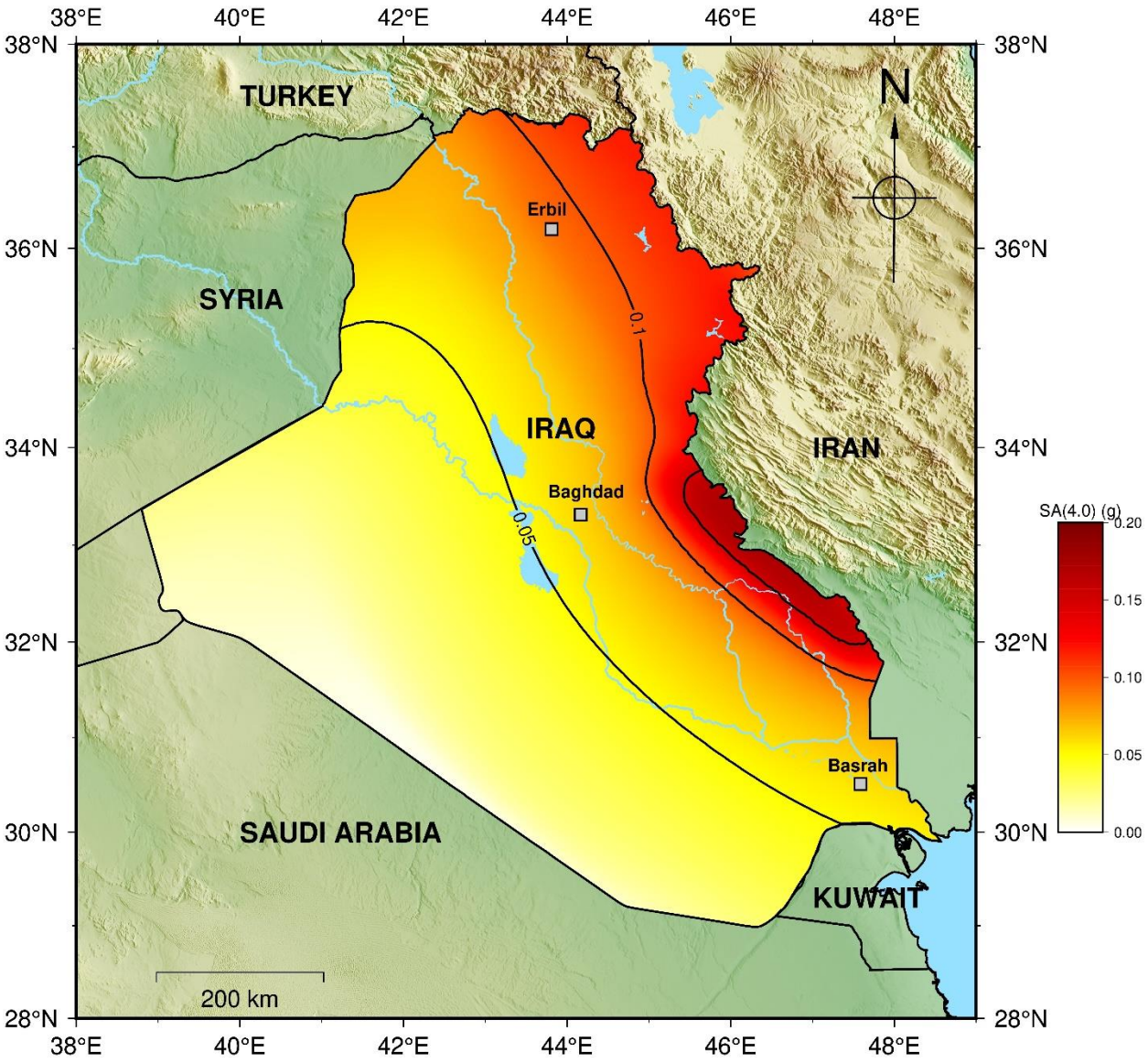

Figure 24: *Probabilistic seismic hazard in Iraq with a 2% chance of exceedance in 50 years on site with a Vs30 of 760 m/s in terms of spectral acceleration (SA) at 4.0 s.*

4.2. Uniform Hazard Spectra (UHS)

The results are presented in terms of uniform hazard spectra (UHS) at a 2% probability of exceedance for selected cities (Anbar, Baghdad, Basrah, Duhok, Erbil, Maysan, Kut, and Sulaymaniyah) in Figures 25, 26, and 27. All UHS were calculated for the three Vs30 site conditions mentioned above, which are 180 m/s, 500 m/s, and 760 m/s.

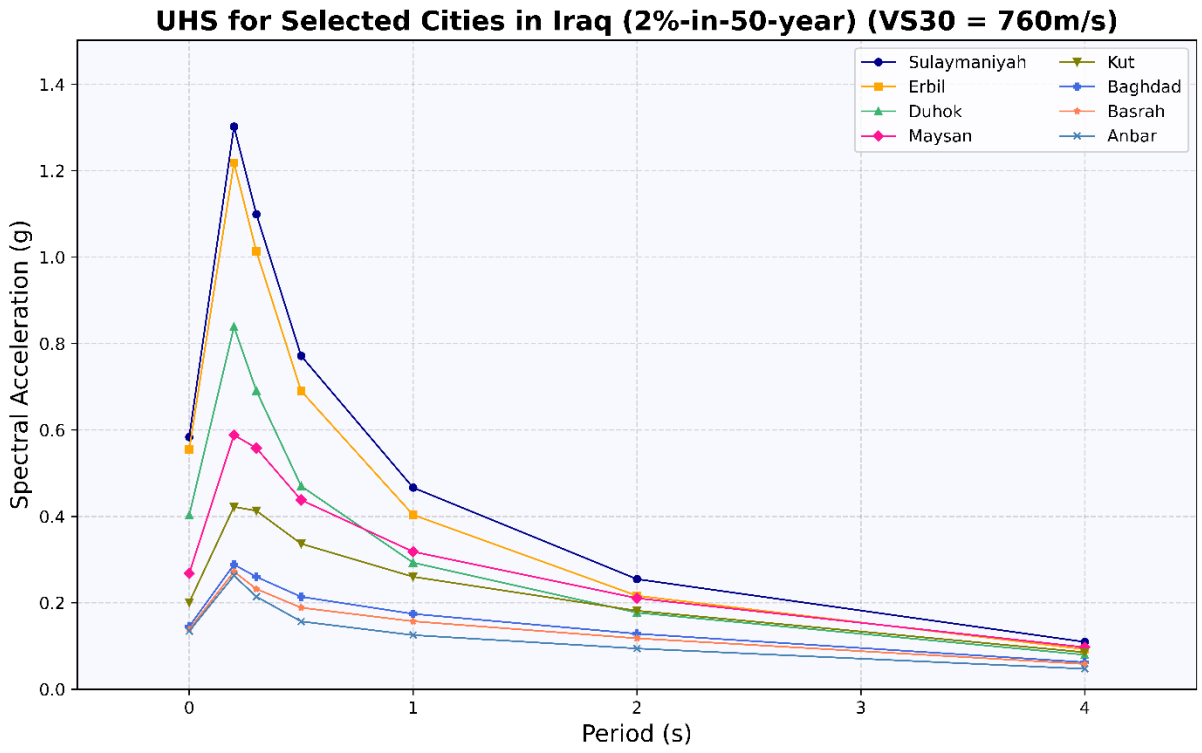

Figure 25: *Uniform hazard spectra for selected cities in Iraq with a probability of exceedance of 2% in 50 years in terms of site conditions of Vs30 of 760 m/s.*

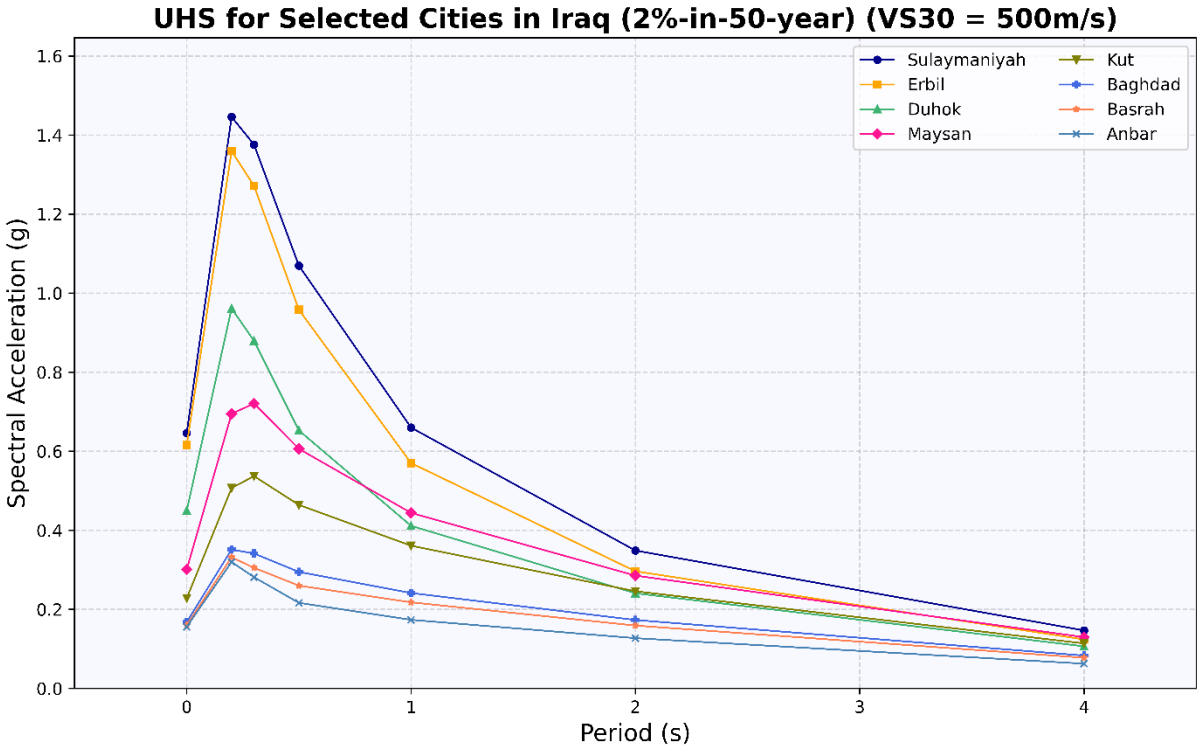

Figure 26: *Uniform hazard spectra for selected cities in Iraq with a probability of exceedance of 2% in 50 years in terms of site conditions of Vs30 of 500 m/s.*

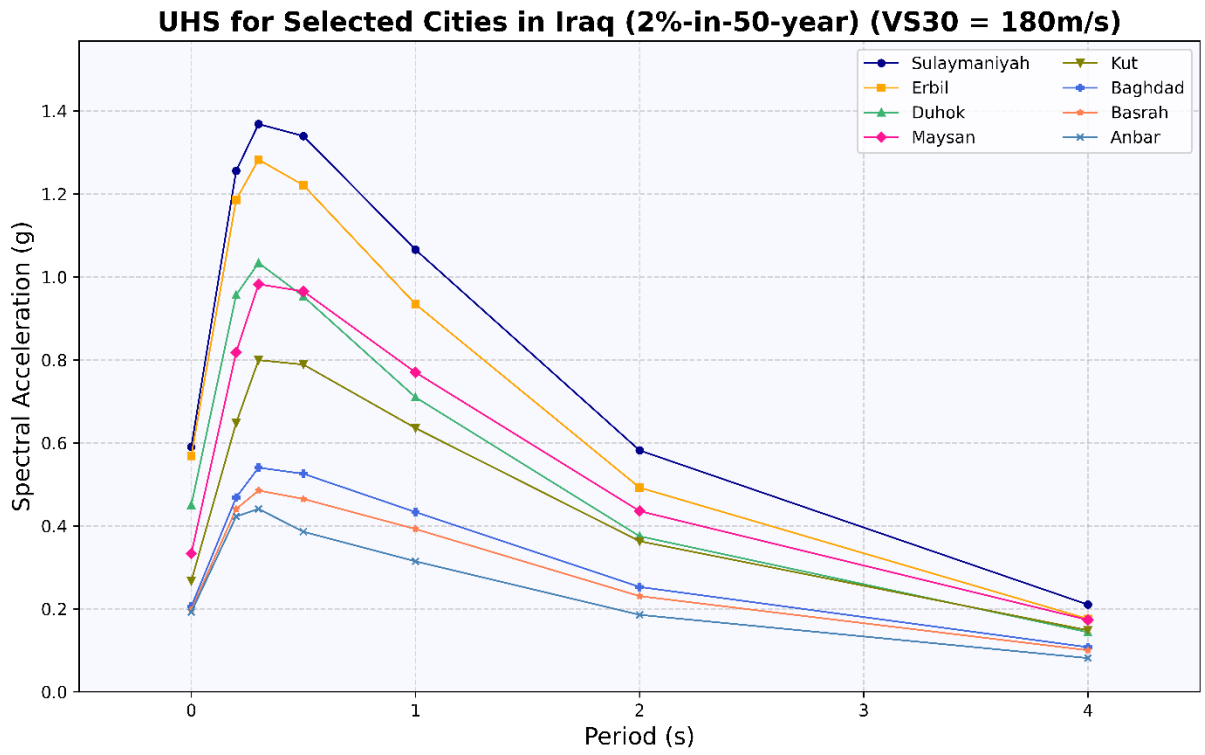

Figure 27: *Uniform hazard spectra for selected cities in Iraq with a probability of exceedance of 2% in 50 years in terms of site condition of Vs30 of 180 m/s.*

4.3. Hazard Curves

Figures 28, 29, and 30 present the hazard curves in terms of PGA, spectral acceleration at 0.2 s, and spectral acceleration at 1.0 s, respectively, for selected cities (Anbar, Baghdad, Basrah, Duhok, Erbil, Maysan, Kut, and Sulaymaniyah). All hazard curves were calculated for the three Vs30 site conditions mentioned above, which are 180 m/s, 500 m/s, and 760 m/s, along with mean, median, and 84th percentile. Figures 28, 29, and 30 depict the hazard curves for the site condition of 760 m/s. The hazard curves for the other two Vs30 values are provided in Appendix B.

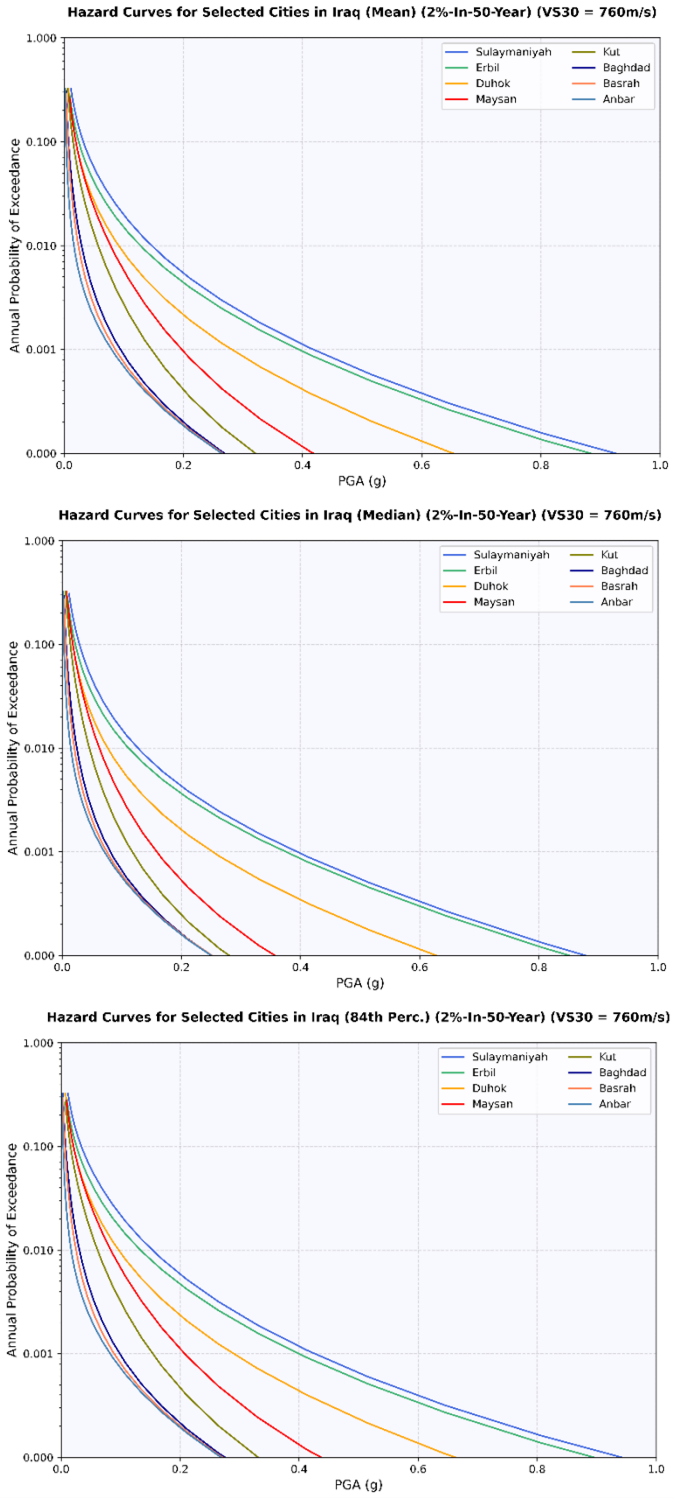

Figure 28: *Mean hazard curves for selected cities in terms of PGA represented by mean, median, and 84th percentile, with reference site of Vs30 of 760 m/s.*

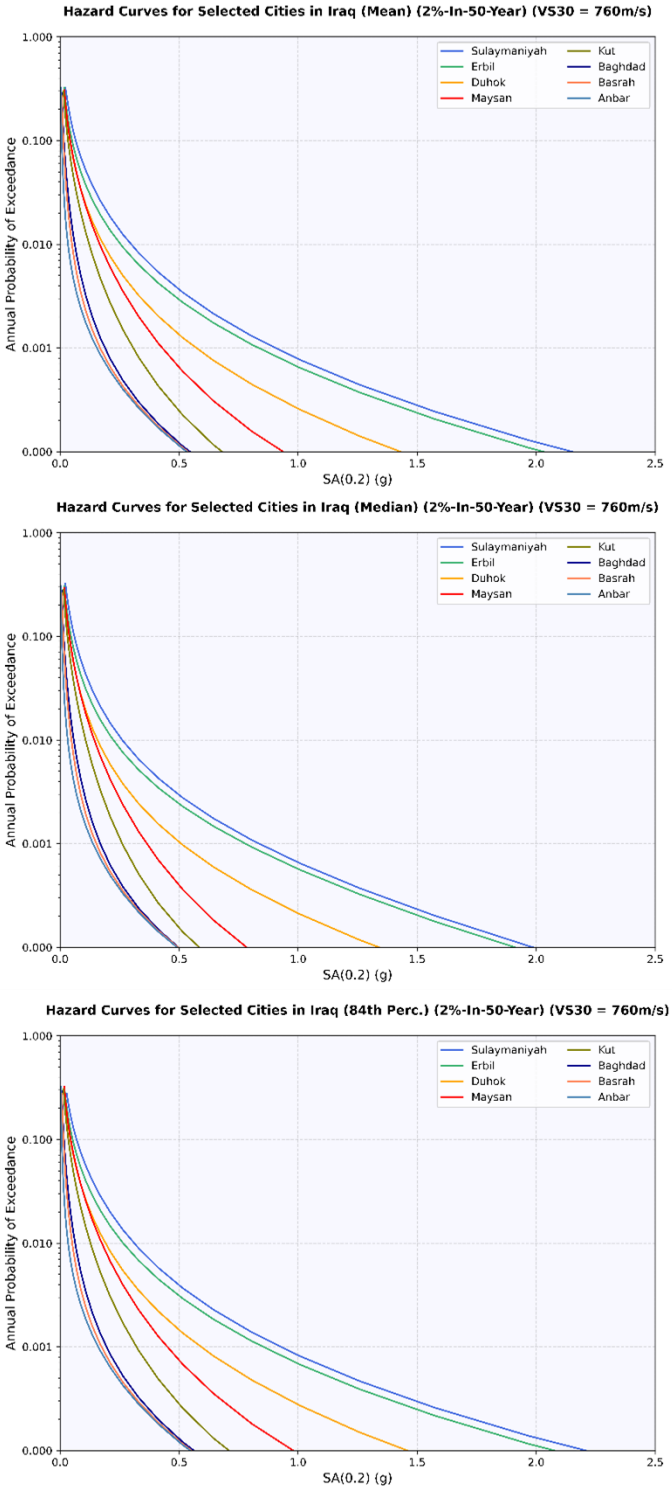

Figure 29: *Hazard curves for selected cities in terms of spectral acceleration (SA) at 0.2s represented by mean, median, and 84th percentile, with reference site of Vs30 of 760 m/s.*

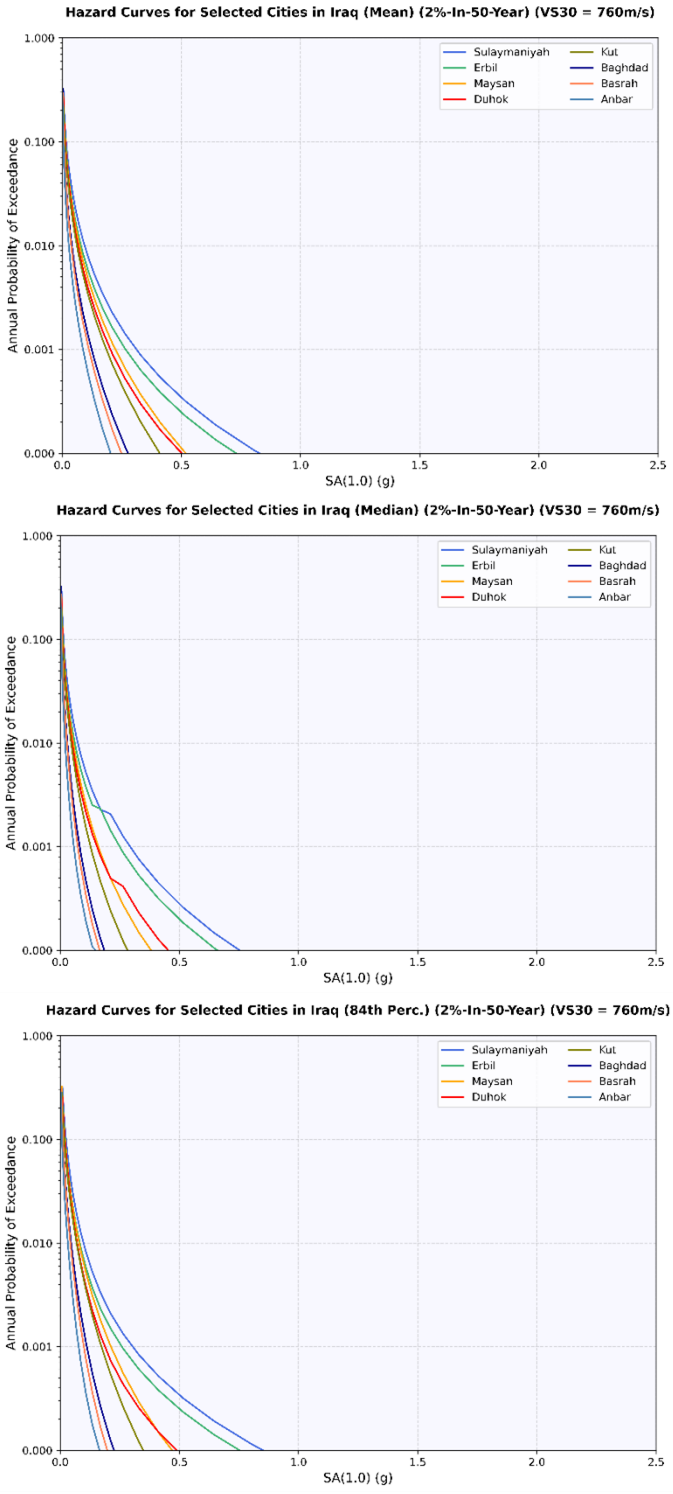

Figure 30: *Hazard curves for selected cities in terms of spectral acceleration (SA) at 1.0s represented by mean, median, and 84th percentile, with reference site of Vs30 of 760 m/s.*

4.4. Hazard Deaggregations

Figures 31, 32, and 33 represent hazard deaggregations for Erbil, Baghdad, and Basrah for PGA and spectral accelerations at periods of 0.2 sec and 1.0 sec, with a 2% probability of exceedance in 50 years. These hazard deaggregations were calculated for a reference site with Vs30 = 760 m/s. Hazard deaggregations calculated for the other two Vs30 site conditions mentioned above, which are 180 m/s and 500 m/s are provided in Appendix C.

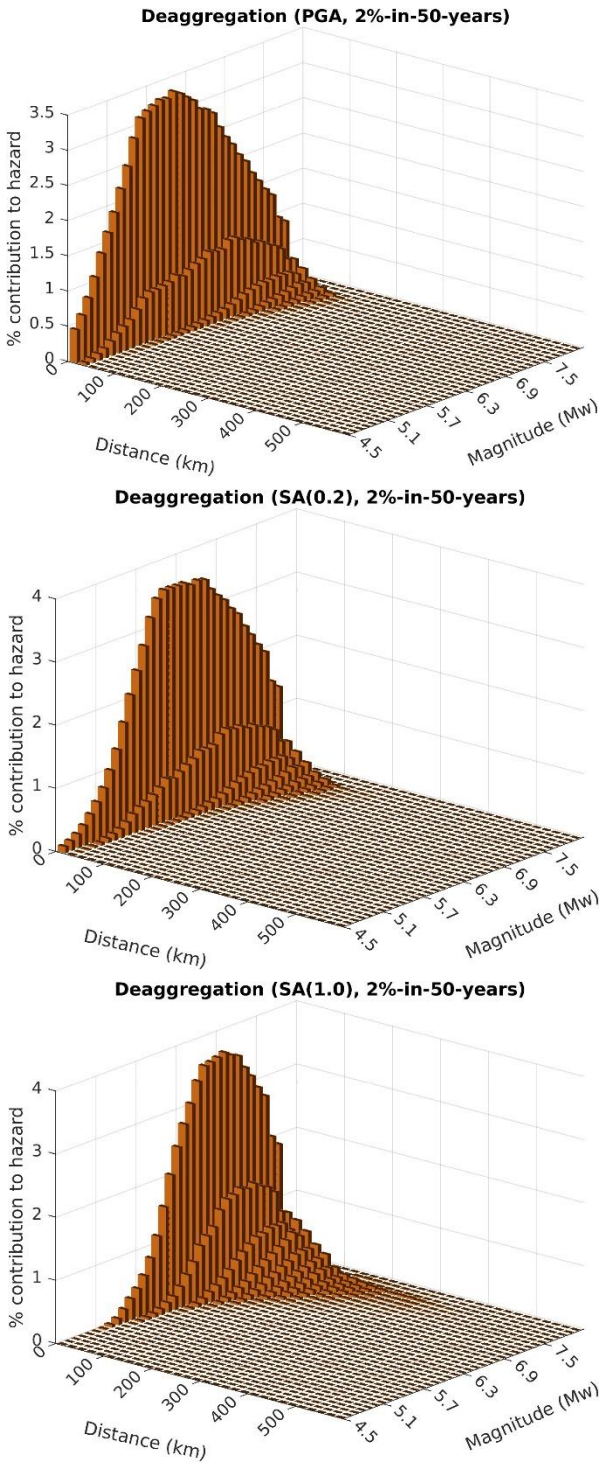

Figure 31: *Hazard deaggregations for Erbil in terms of PGA and spectral accelerations at periods of 0.2 sec and 1.0 sec, with 2% probability of exceedance in 50 years and reference site of Vs30 of 760 m/s.*

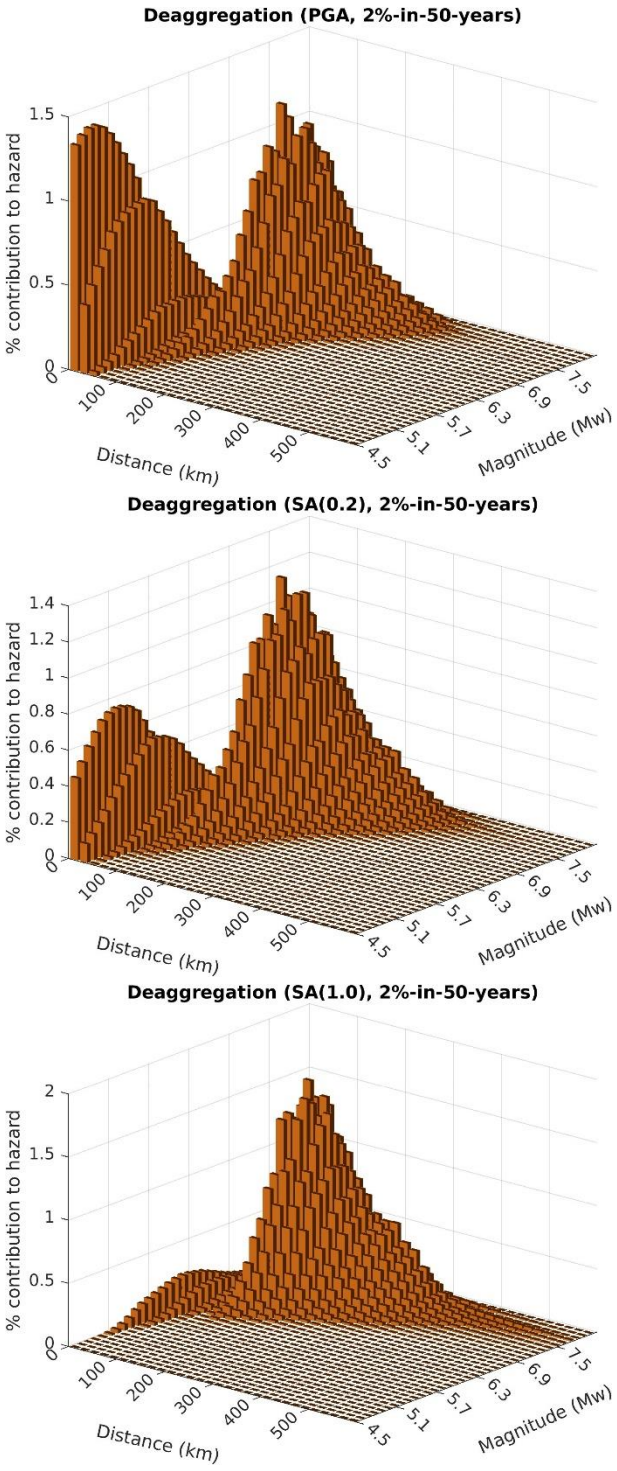

Figure 32: *Hazard deaggregations for Baghdad in terms of PGA and spectral accelerations at periods of 0.2 sec and 1.0 sec, with 2% probability of exceedance in 50 years and reference site of Vs30 of 760 m/s.*

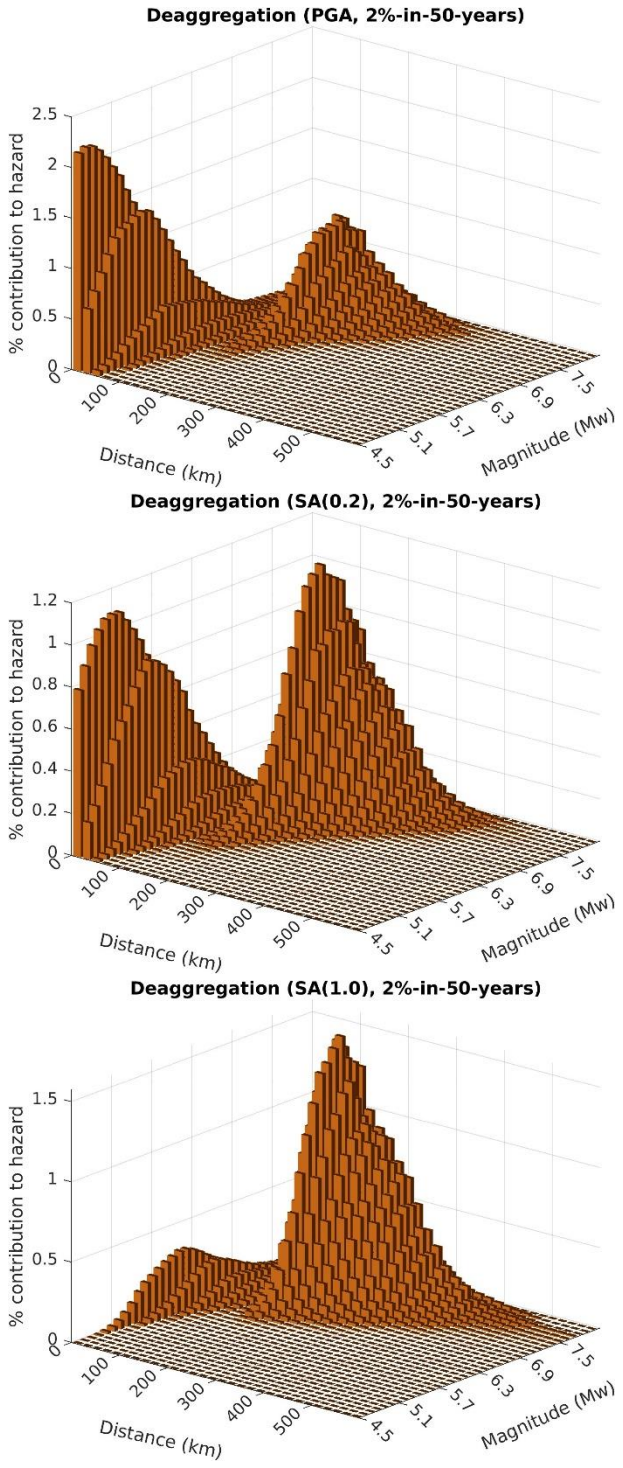

Figure 33: *Hazard deaggregations for Basrah in terms of PGA and spectral accelerations at periods of 0.2 sec and 1.0 sec, with 2% probability of exceedance in 50 years and reference site of Vs30 of 760 m/s.*

5. Discussion and Conclusions

This study represents the latest effort to understand seismic hazard in a region with considerable gaps in seismic data and knowledge. The resulting maps aim to benefit not only the updated building code but also enhance the understanding and reduction of seismic risk in the region.

A PSHA study for Iraq was conducted to support the update of the seismic provisions in Iraq's building code. As required by the new building code, the PSHA results are presented for a 2% chance of being exceeded in 50 years and for three ground conditions characterized by Vs30 of 180 m/s, 500 m/s, and 760 m/s. Data from strong motion stations located within the Outer Arabian Platform were used to identify the most suitable GMMs, significantly aiding in further understanding the ground motion attenuation characteristics in Iraq, which does not conform to the typical categories of "active tectonic" or "stable continental" GMMs.

The highest seismic hazard is estimated in areas near the Mandili-Badra-Teeb fault in eastern Iraq, which has ruptured many times in history, causing major damage to nearby communities. While this fault was not modeled as a "fault source" due to lack of detailed information needed, it may be a candidate to be considered for a deterministic cap for ground motions used in the building code of Iraq.

Significant seismic hazard is also estimated of northern Iraq, where the fold and thrust belt experiences frequent major earthquakes (such as the Mw7.3 earthquake on 12 November 2017). Seismic activity is relatively rare in central and western Iraq and these regions have a lower seismic hazard compared to the rest of the country; however, a major earthquake cannot be ruled out anywhere in Iraq.

Since the Mandili-Badra-Teeb fault is such a significant contributor to seismic hazard in the country, detailed tectonic studies of this fault are recommended to allow for a better characterization of it in future PSHA studies.

Acknowledgments

The authors would like to thank all participants in the PSHA training sessions for their valuable comments and suggestions, which significantly contributed to the improvement of this manuscript. We are also grateful to the Iraqi Universities and Research Farms for hosting the MPSN seismic stations. Our thanks extend to the regional agencies for providing seismic data utilized in this research. We thank Martitia Tuttle for her helpful and constructive reviews of this report. We acknowledge the support of Lawrence Livermore National Laboratory and the U.S. Department of Energy for providing the necessary resources to carry out this work. Chiang's work was performed under the auspices of the U.S. Department of Energy by Lawrence Livermore National Laboratory (LLNL) under Contract Number DE-AC52-07NA27344. This is document LLNL-TR-2006187.

Disclaimer

This is a project report and the application of the results is the responsibility of the reader. All information and data provided as part of this report (presented in any form, including any attachments to this report or other email communications) are the authors' best estimates on a subject that is susceptible to large uncertainties and varying interpretations. In no event shall the authors of this report be liable to any party for direct, indirect, special, incidental, or consequential damages, including injuries, loss of life, loss of property or any form of financial loss, arising out of the use of the information and data described herein.

References

Abdulnaby W. (2019). Chapter 4 - Structural Geology and Neotectonics of Iraq, Northwest Zagros. Editor: Ali Farzipour Saein, Developments in Structural Geology and Tectonics, Elsevier, 3, 53-73, https://doi.org/10.1016/B978-0-12-815048-1.00004-4.

Abdulnaby W., Mahdi H., Al-Shukri H., Numan N.M.S. (2014). Stress patterns in northern Iraq and surrounding regions from formal stress inversion of earthquake focal mechanism solutions. Pure Appl Geophys. 171:2137–2153. https://doi.org/10.1007/s00024-014-0823-x

Abdulnaby W., Mahdi M., Al-Mohmed R. (2016b). Seismicity and recent stress regime of Diyala City, Iraq–Iran border. Model Earth System Environ 2. https://doi.org/10.1007/s40808-016-0201-z

Abdulnaby W., Mahdi M., Al-Mohmed R., Mahdi H. (2016a). Seismotectonics of Badra-Amarah fault, Iran-Iraq border. IOSR J Appl Geol Geophys (IOSR-JAGG) 4(3):27–33

Abdulnaby W., Onur T., Gök R., Shakir A.M., Mahdi H., Al-Shukri H., Numan N.M.S., Abd N.A., Chlaib H.K., Taher H. Ameen T.H., Ramthan A. (2020). Probabilistic Seismic Hazard Assessment for Iraq. Journal of Seismology, 24:595–611. https://doi.org/10.1007/s10950-020-09919-2

Al-Kaabi M., Mayeda K., Roman-Nieves J., Chiang A., Mahdi H., Al-Shukri H. (2024). Using a 1D Radially Symmetric Coda Envelope Model for Robust Moment Magnitude (Mw) Estimation in Iraq's Tectonically Diverse Zones. Bulletin of the Seismological Society of America 2024. Doi: https://doi.org/10.1785/0120240113

Al-Kaabi (2025). Calculating Moment Magnitude Using the Coda Calibration Technique to Update the Earthquake Catalog of Iraq (1900-2021). University of Arkansas at Little Rock, Master thesis, P57.

Al-Qayim B., Omer A., and Koyi H., 2012. Tectonostratigraphic overview of the Zagros Suture Zone, Kurdistan Region, Northeast Iraq. GeoArabia, 17(4), 109-156.

Ambraseys N.N. (2001). Reassessment of earthquakes, 1900–1999, in the eastern Mediterranean and the Middle East. Geophysical Journal International, 145:471-485.

Berberian M. (1995). Master "blind" thrust faults hidden under the Zagros folds: active basement tectonics and surface morphotectonics. Tectonophysics, 241, 193-224.

Boore D.M., Stewart J.P., Seyhan E., Atkinson G.A. (2014). NGAWest2 equations for predicting PGA, PGV, and 5% damped PSA for shallow crustal earthquakes. Earthquake Spectra 30:1057–1085

Building Seismic Safety Council (BSSC) (2001). NEHRP recommended provisions for seismic regulations for new buildings and other structures, 2000 edition, part 1: provisions, prepared by the Building Seismic Safety Council for the Federal Emergency Management Agency (Report FEMA 368), Washington, D.C.

Campbell K.W., Bozorgnia Y. (2014). NGA-WEST2 ground motion model for the average horizontal components of PGA, PGV, and 5% damped linear acceleration response spectra. Earthquake Spectra, 30:1087–1115

Castellaro S., Mulargia F., and Kagan Y.Y., (2006). Regression problems for magnitudes. Geophys. J. Int., 165:913–930.

Darragh R.B., Abrahamson N.A., Silva W.J., Gregor N (2015). Development of hard rock ground-motion models for region 2 of Central and Eastern North America, In NGA-East: median ground-motion models for the Central and Eastern North America region, PEER Report no. 2015/04, PP. 51–84

Deniz A., and M.S. Yucemen (2010). Magnitude conversion problem for the Turkish earthquake data, Nat. Hazards 55, 333–352.

Fouad, S.F. (2015). Geological Map of Iraq, scale 1:1000000, 3rd edition. Iraqi Bulletin of Geology and Mining, 11, 1-7.

Gök R., Kaviani A., Matzel E.M., Pasayanos M.E., Mayeda K., Yetirmishli G., El-Hussain I., Al-Amri A., Al-Jeri F., and Godoladze T. (2016). Moment magnitude of local/regional events from 1D coda calibrations in the broader Middle East region, Bull. Seismol. Soc. Am. 106(5), 1926–1938.

Kendall M.G. and Stuart A. (1979). The Advanced Theory of Statistics, Fourth Ed., Vol. 2, Charles Griffin & Co. Ltd., London, United Kingdom, 758 pp.

Mayeda K., Hofstetter A., O'Boyle J.L., and Walter W.R. (2003). Stable and transportable regional magnitudes based on coda-derived moment rate spectra. Bull. Seism. Soc. Am., 93, 224–239.

Numan N.M.S. (1997). A plate tectonic scenario for the Phanerozoic succession in Iraq. Iraqi Geological Journal, 30(2):85–119

Onur T., Gök R., Abdulnaby W., Mahdi H., Numan N., Al-Shukri H, Shakir A.M., Chlaib H.K., Ameen T.H., Abd N.A. (2017). A comprehensive earthquake catalog for Iraq in terms of moment magnitude. Seismological Research Letters, 88(3):798–811

Pagani M., Monelli D., Weatherill G., Danciu L., Crowley H., Silva V., Henshaw P., Butler L., Nastasi M., Panzeri L., Simionato M., Vigano D. (2014). OpenQuake Engine: An open hazard (and risk) software for the Global Earthquake Model. Seismological Research Letters, 85(3):692–702.

Phillips C., Kottke A.R., Hashash Y.M., and Rathje E.M. (2012). Significance of ground motion time step in one dimensional site response analysis. Soil Dynamics and Earthquake Engineering, 43, 202-217.

Wells D.L., Coppersmith K.J. (1994). New empirical relationships among magnitude, rupture length, rupture width, rupture area, and surface displacement. Bull Seismol Soc Am, 84:974–1002.

Appendix A

The hazard maps for the 500 m/s and 180 m/s site conditions in terms of PGA and spectral accelerations at periods of 0.2 s, 0.3 s, 0.5 s, 1.0 s, 2.0 s, and 4.0 s (Figures A1 through A14).

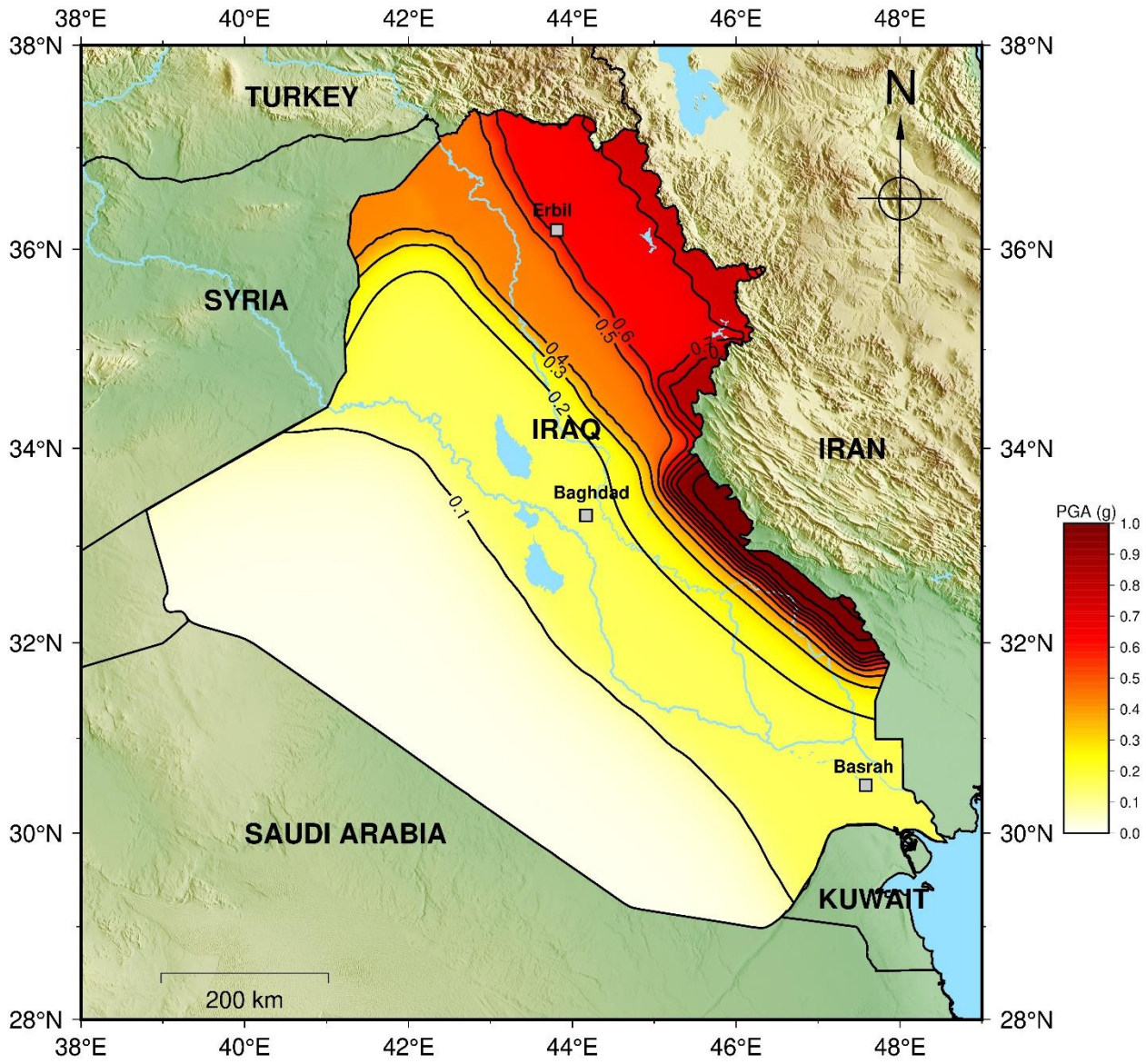

Figure A1: *Probabilistic seismic hazard in Iraq with a 2% chance of exceedance in 50 years on site with a Vs30 of 500 m/s in terms of PGA.*

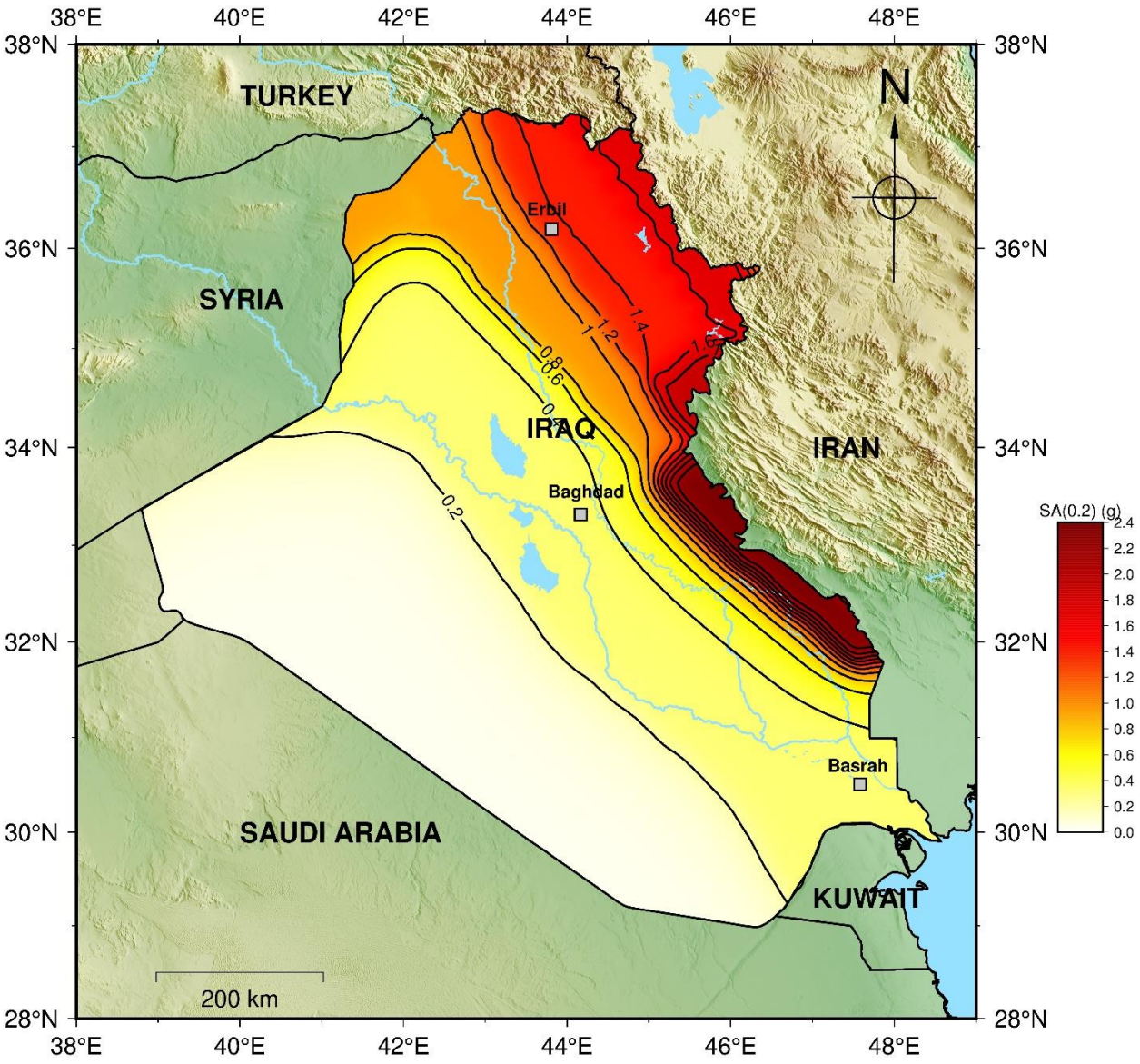

Figure A2: *Probabilistic seismic hazard in Iraq with a 2% chance of exceedance in 50 years on site with a Vs30 of 500 m/s in terms of spectral acceleration (SA) at 0.2 s.*

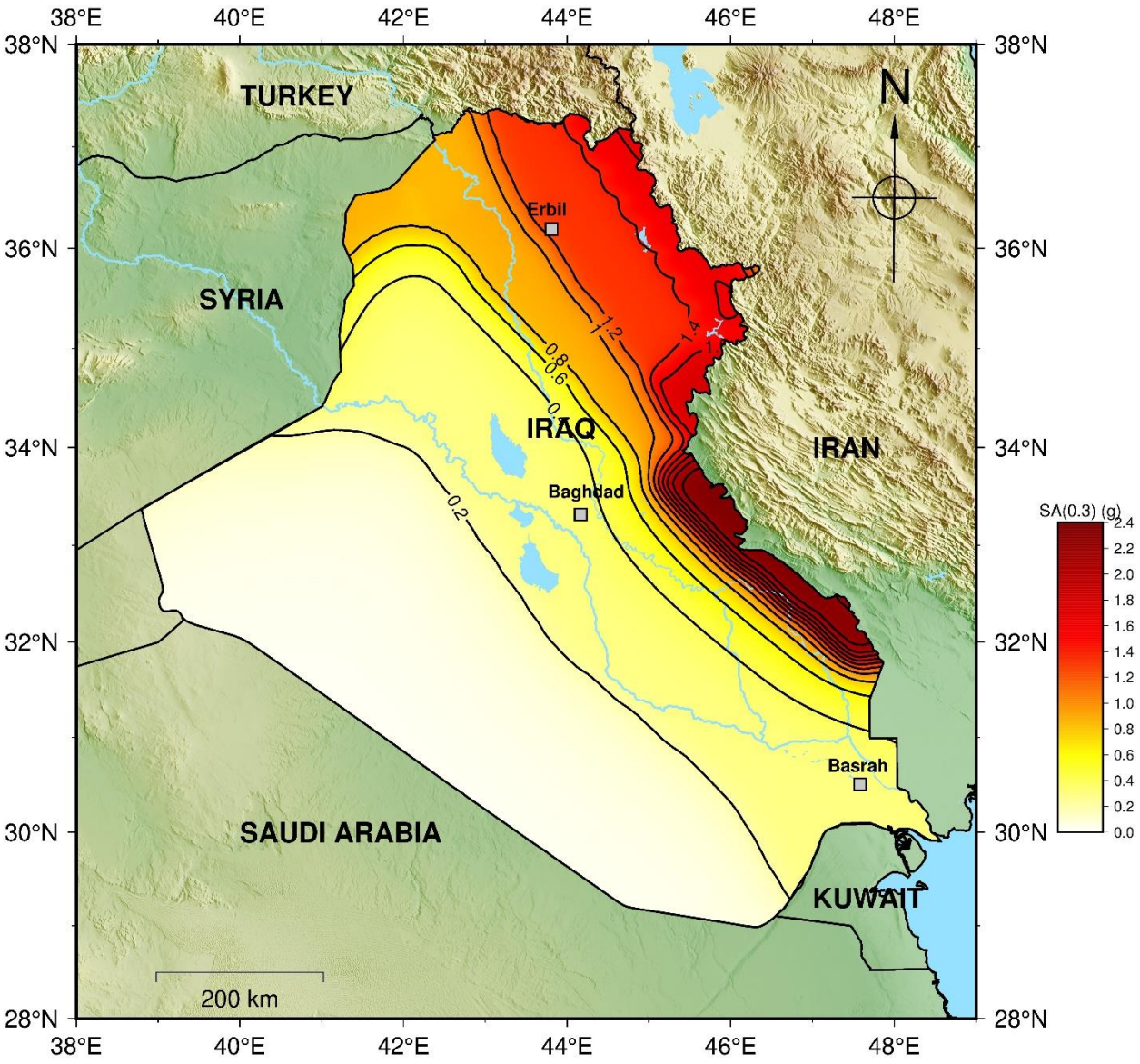

Figure A3: *Probabilistic seismic hazard in Iraq with a 2% chance of exceedance in 50 years on site with a Vs30 of 500 m/s in terms of spectral acceleration (SA) at 0.3 s.*

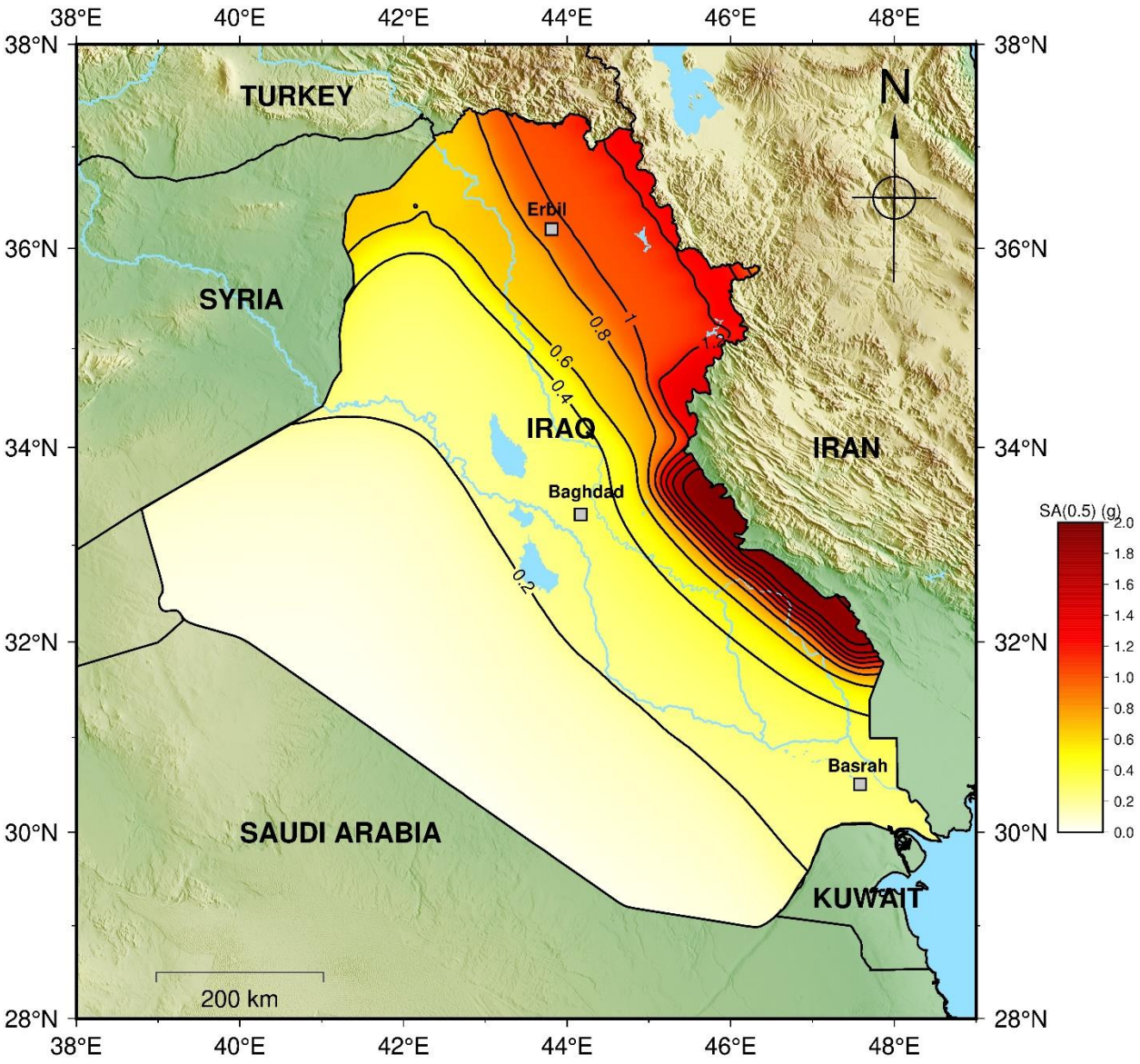

Figure A4: *Probabilistic seismic hazard in Iraq with a 2% chance of exceedance in 50 years on site with a Vs30 of 500 m/s in terms of spectral acceleration (SA) at 0.5 s.*

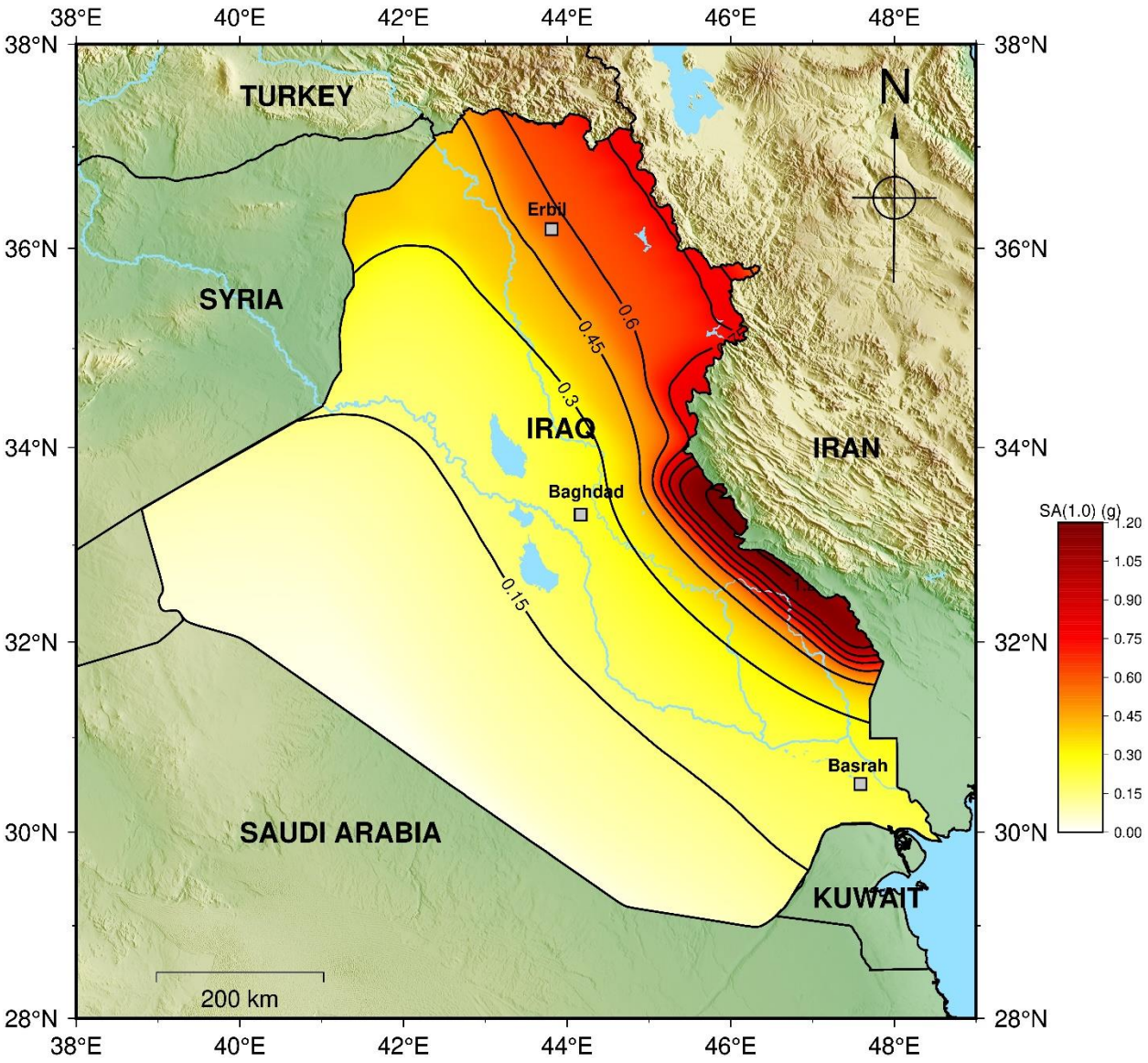

Figure A5: *Probabilistic seismic hazard in Iraq with a 2% chance of exceedance in 50 years on site with a Vs30 of 500 m/s in terms of spectral acceleration (SA) at 1.0 s.*

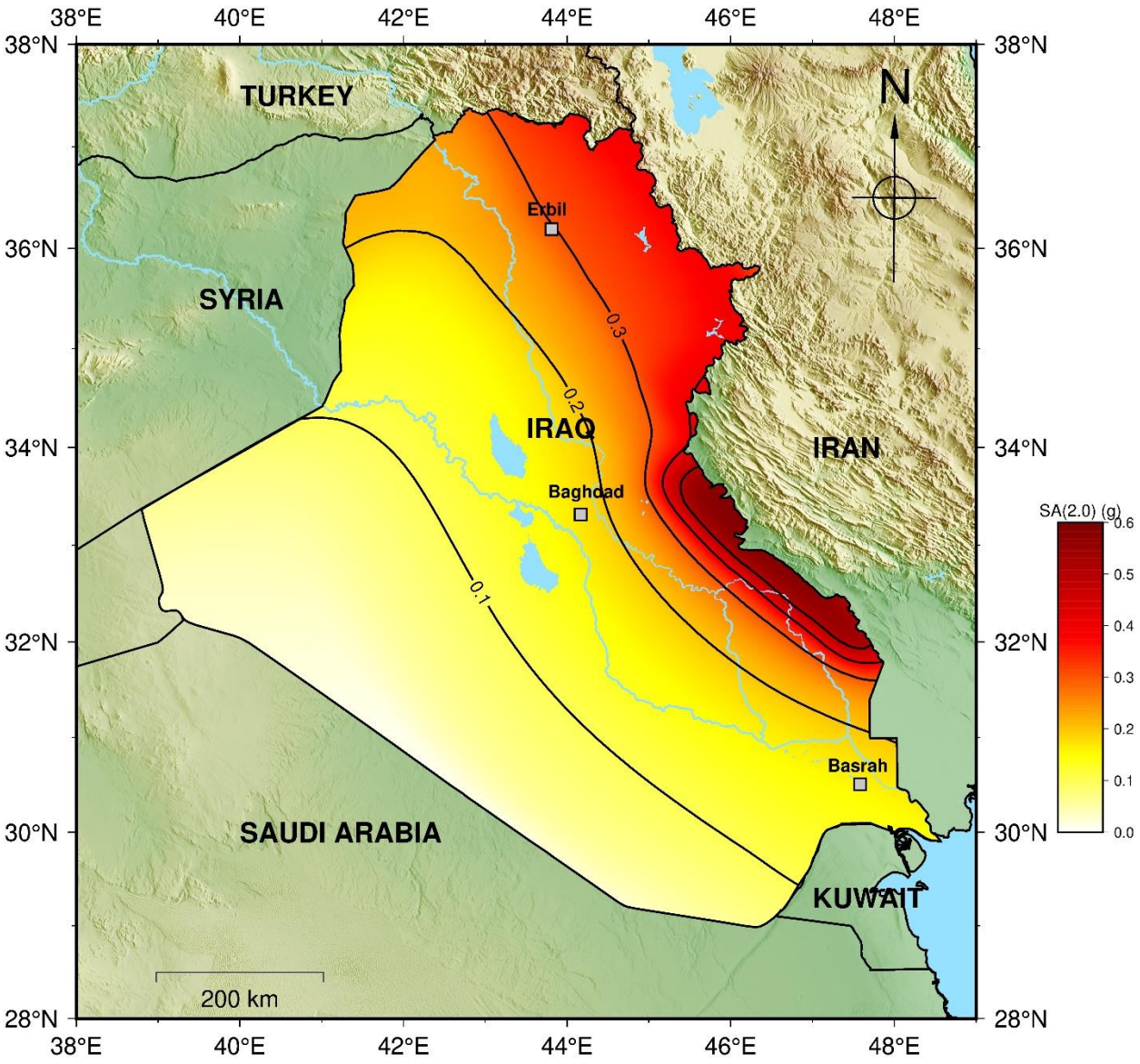

Figure A6: *Probabilistic seismic hazard in Iraq with a 2% chance of exceedance in 50 years on site with a Vs30 of 500 m/s in terms of spectral acceleration (SA) at 2.0 s.*

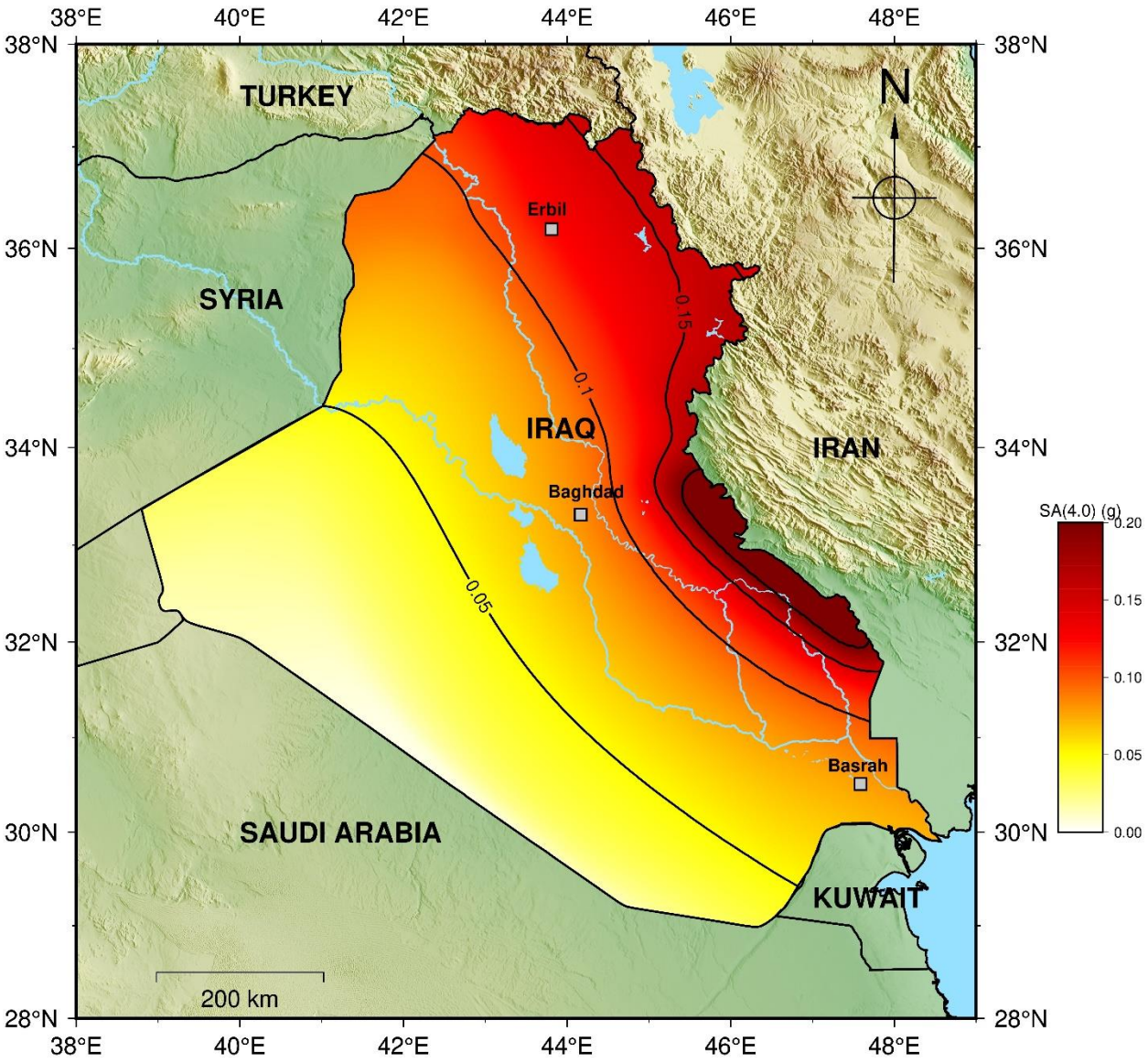

Figure A7: *Probabilistic seismic hazard in Iraq with a 2% chance of exceedance in 50 years on site with a Vs30 of 500 m/s in terms of spectral acceleration (SA) at 4.0 s.*

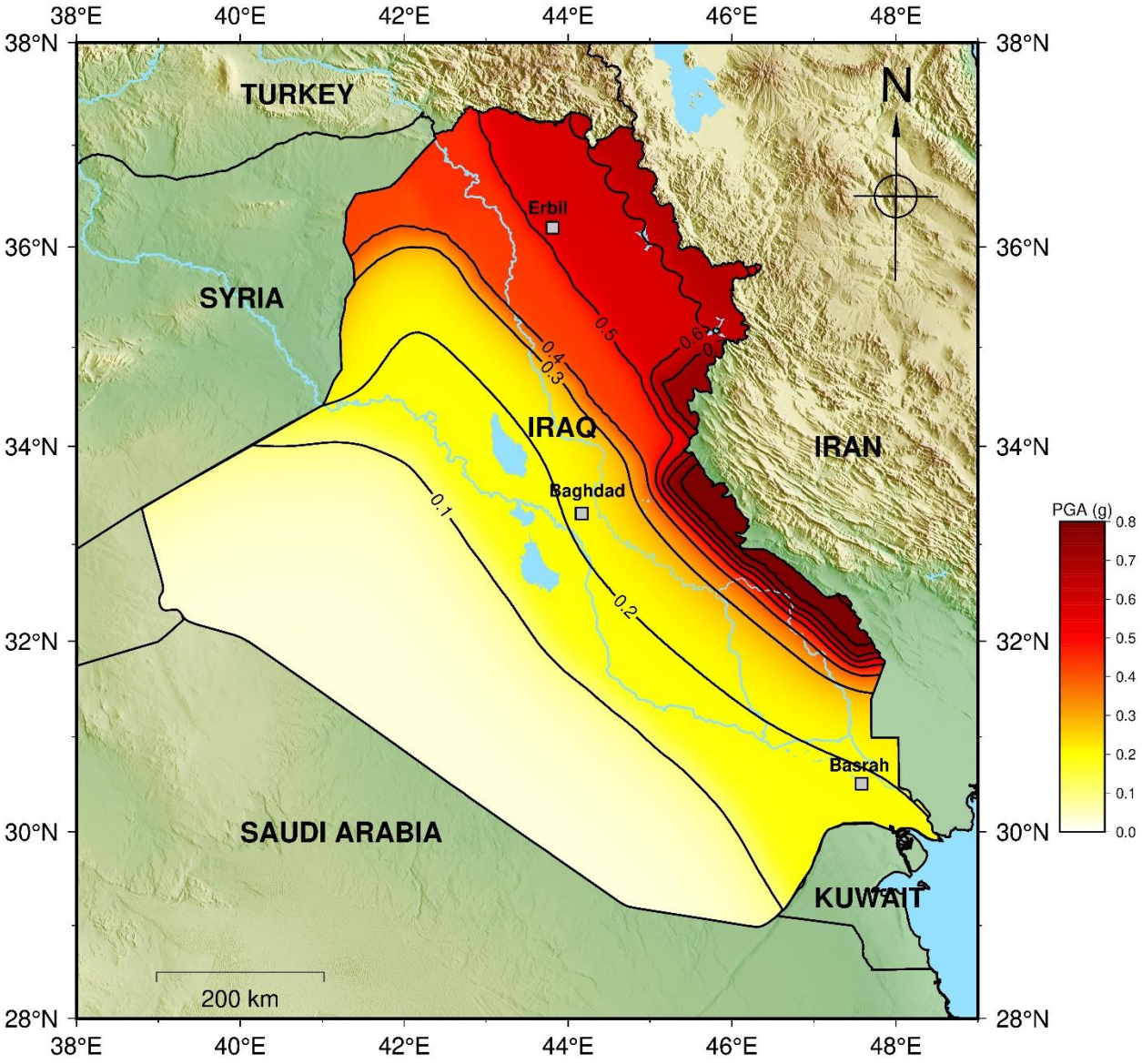

Figure A8: *Probabilistic seismic hazard in Iraq with a 2% chance of exceedance in 50 years on site with a Vs30 of 180 m/s in terms of PGA.*

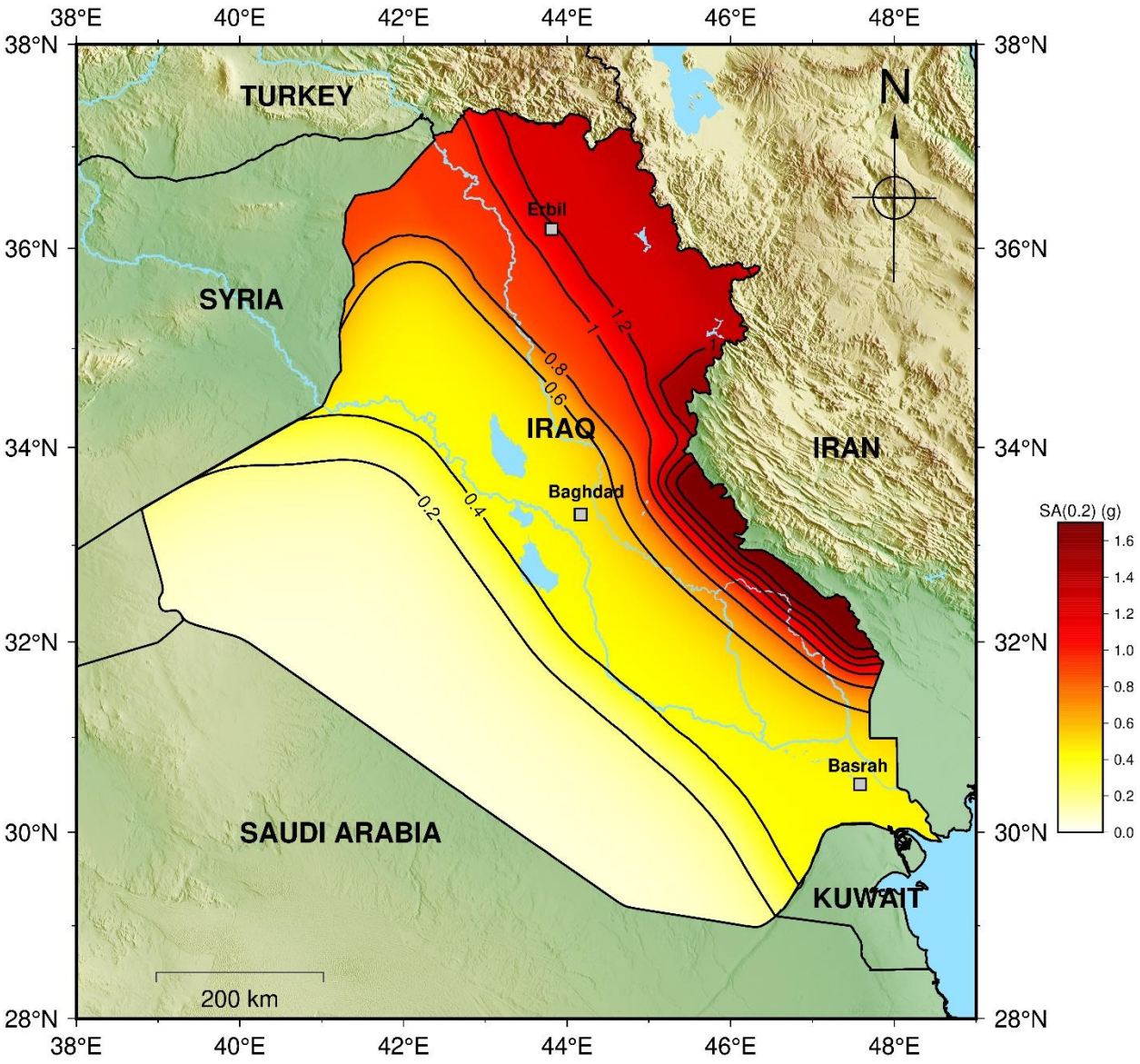

Figure A9: *Probabilistic seismic hazard in Iraq with a 2% chance of exceedance in 50 years on site with a Vs30 of 180 m/s in terms of spectral acceleration (SA) at 0.2 s.*

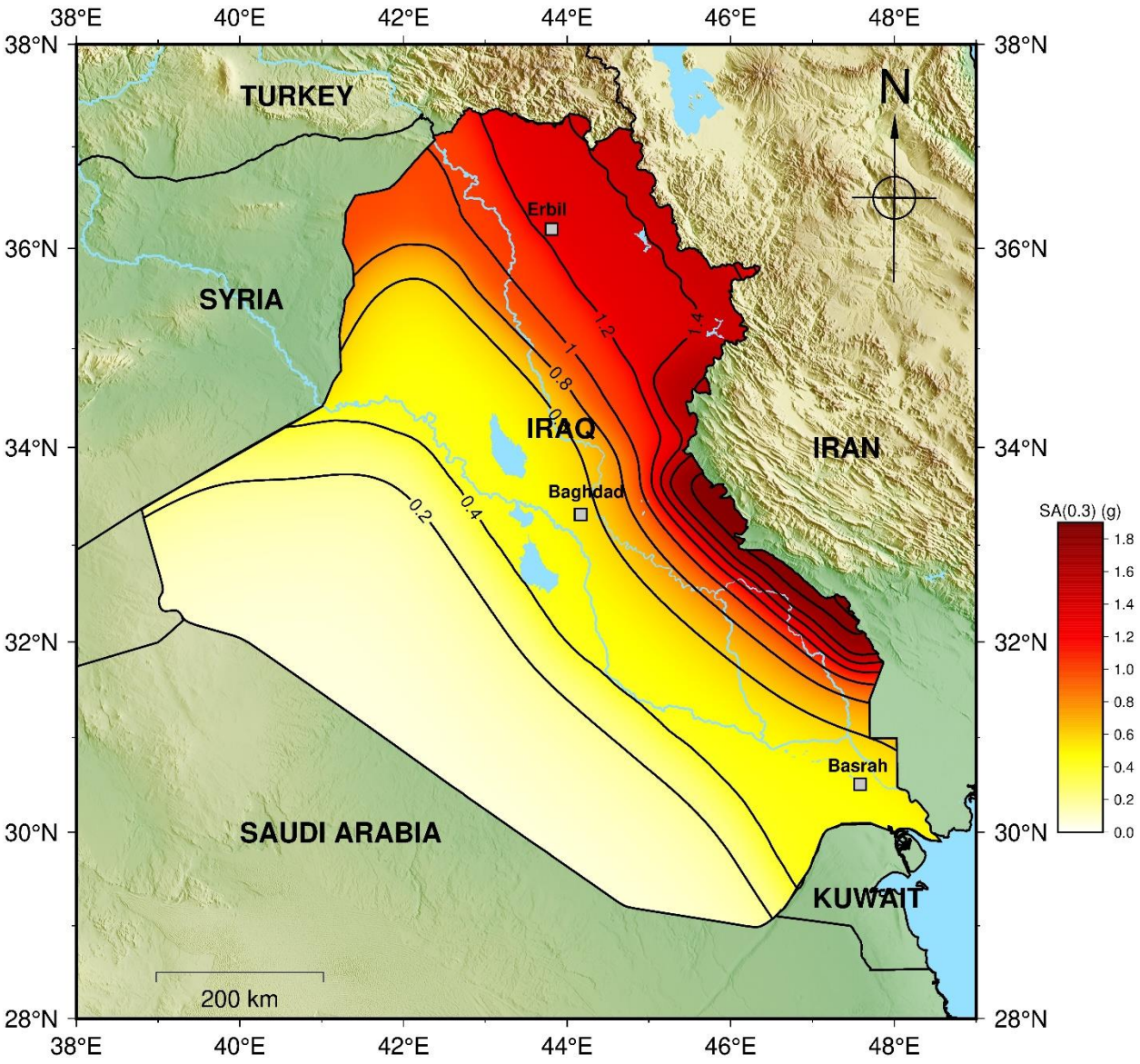

Figure A10: *Probabilistic seismic hazard in Iraq with a 2% chance of exceedance in 50 years on site with a Vs30 of 180 m/s in terms of spectral acceleration (SA) at 0.3 s.*

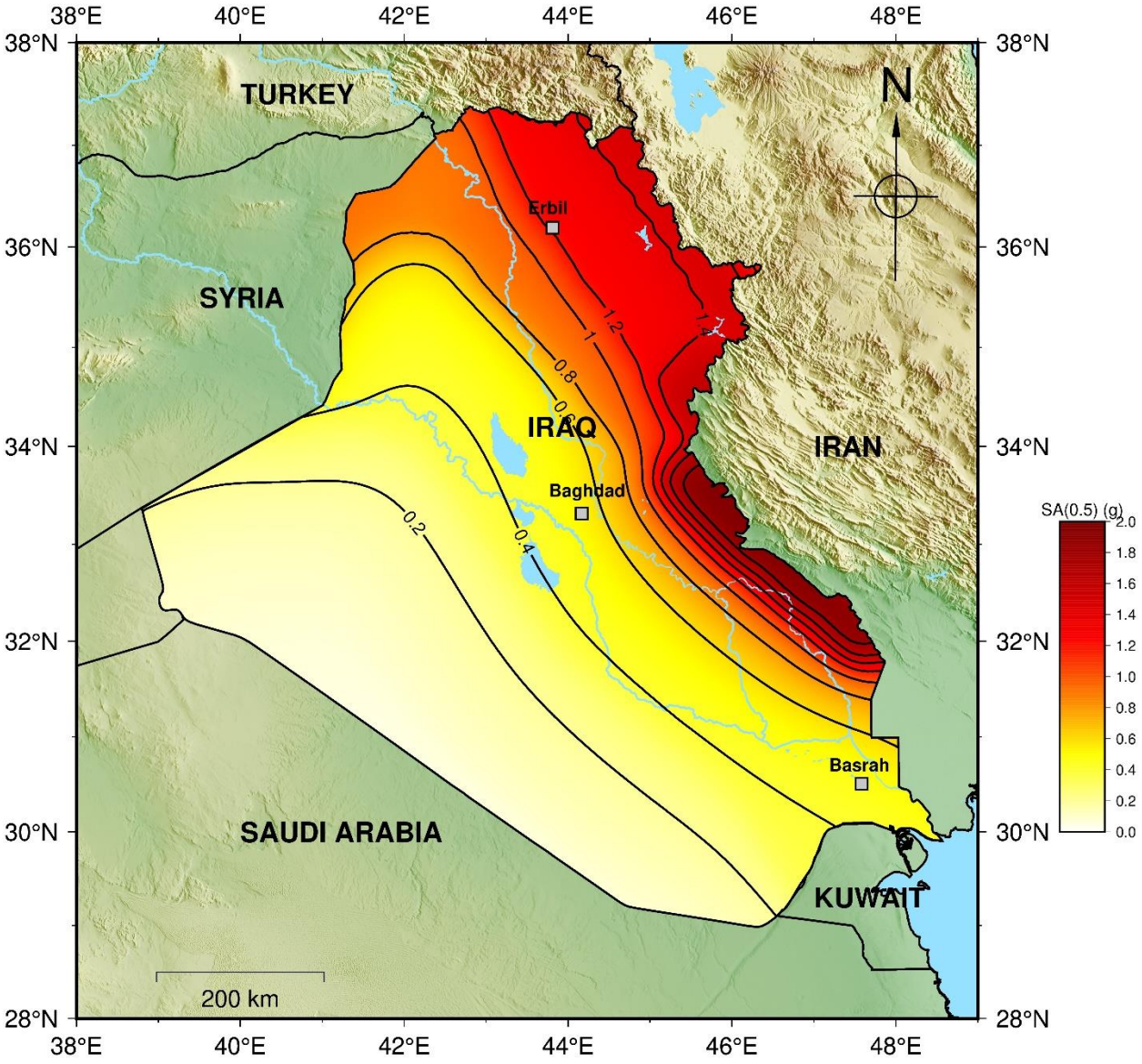

Figure A11: *Probabilistic seismic hazard in Iraq with a 2% chance of exceedance in 50 years on site with a Vs30 of 180 m/s in terms of spectral acceleration (SA) at 0.5 s.*

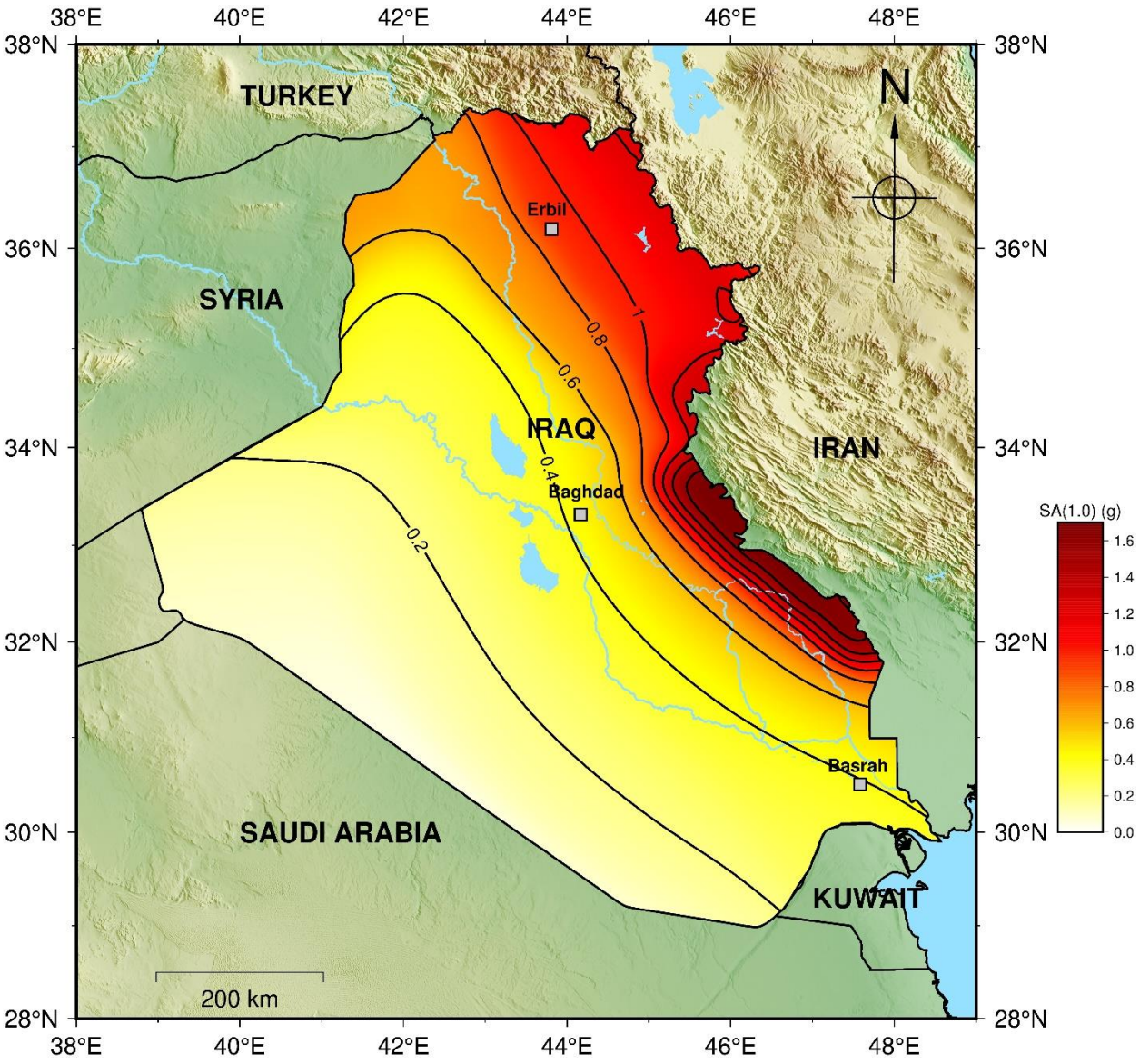

Figure 12: *Probabilistic seismic hazard in Iraq with a 2% chance of exceedance in 50 years on site with a Vs30 of 180 m/s in terms of spectral acceleration (SA) at 1.0 s.*

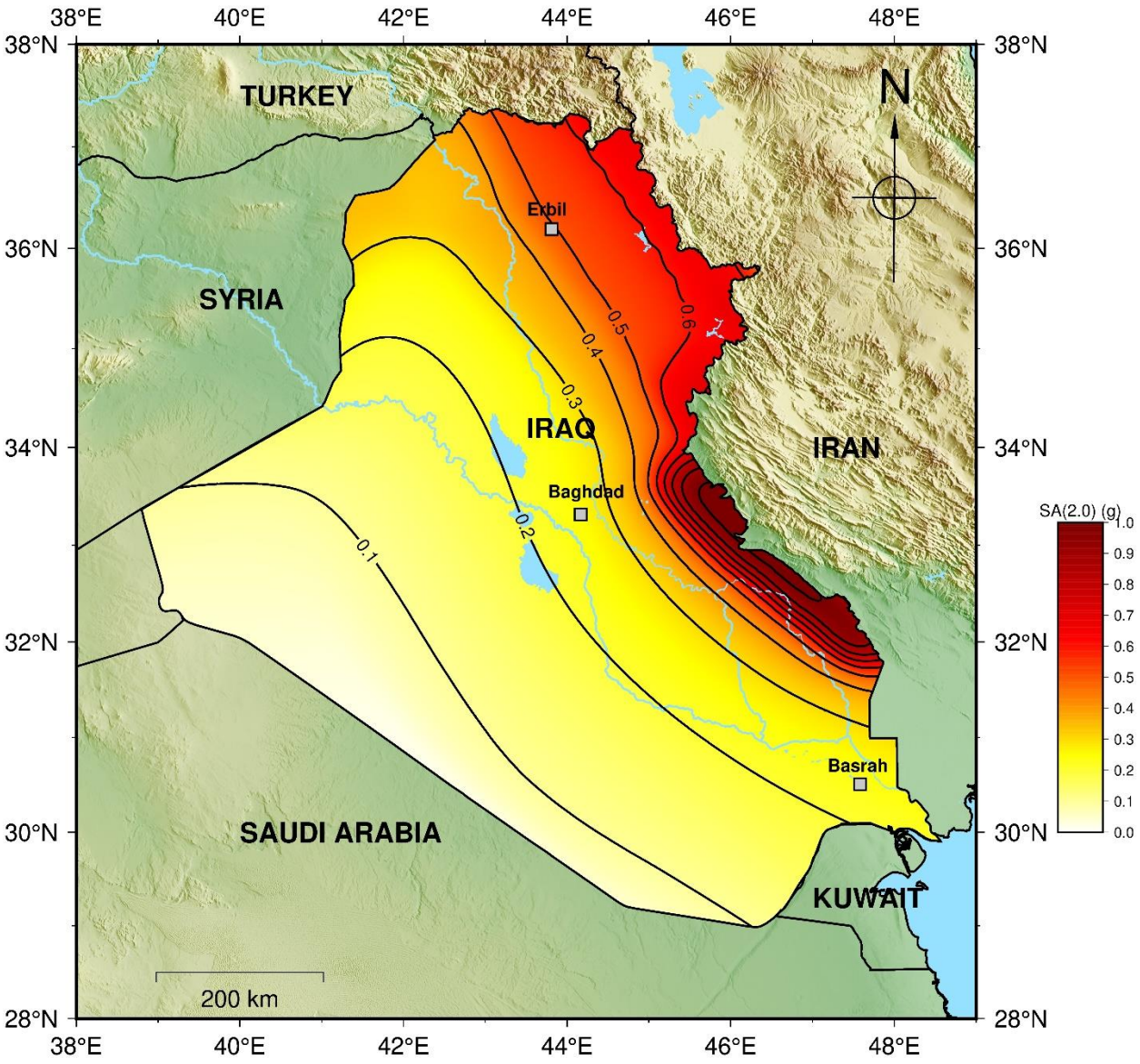

Figure A13: *Probabilistic seismic hazard in Iraq with a 2% chance of exceedance in 50 years on site with a Vs30 of 180 m/s in terms of spectral acceleration (SA) at 2.0 s.*

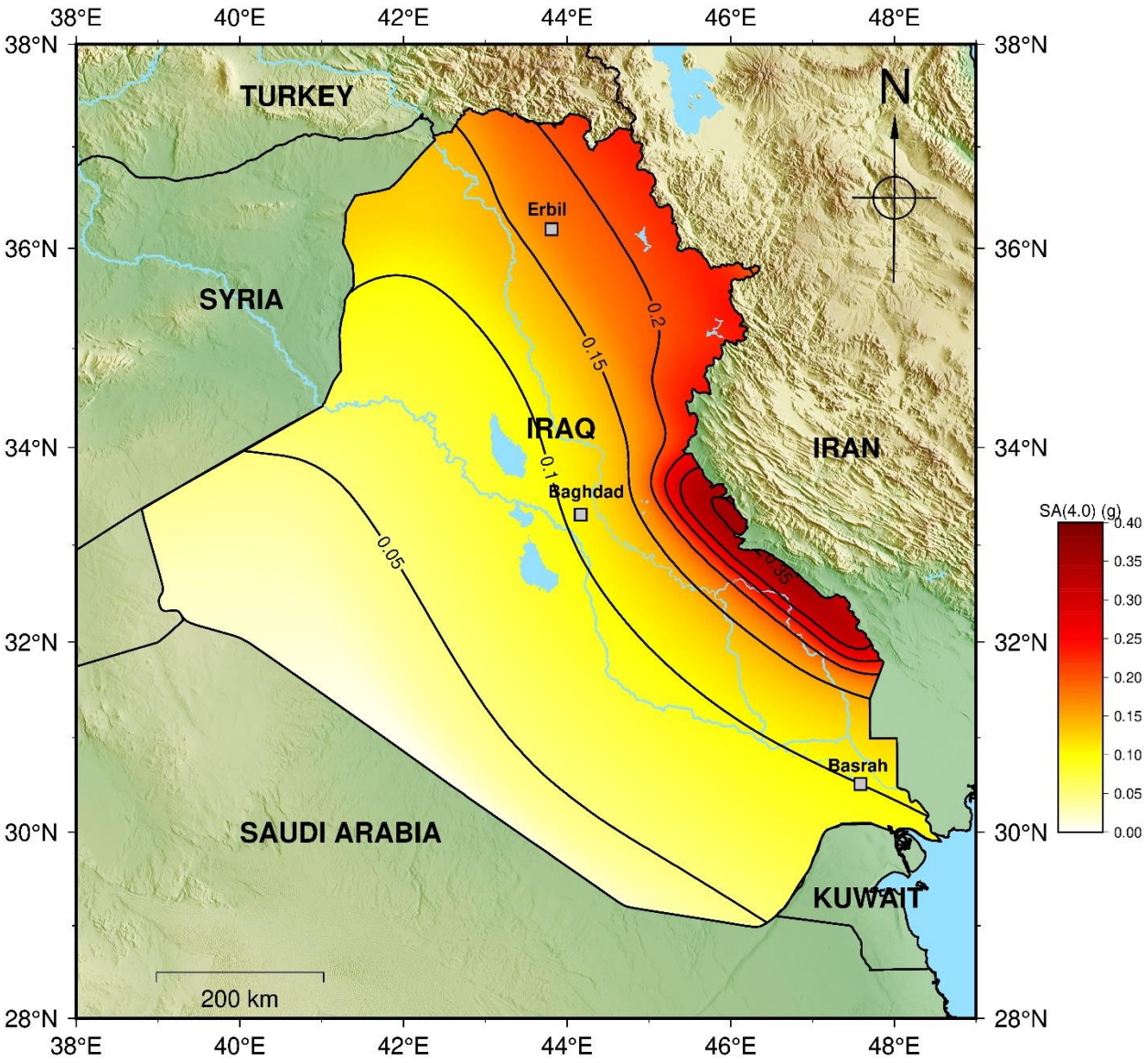

Figure A14: *Probabilistic seismic hazard in Iraq with a 2% chance of exceedance in 50 years on site with a Vs30 of 180 m/s in terms of spectral acceleration (SA) at 4.0 s.*

Appendix B

Figures B1 through B6 show the hazard curves in terms of PGA, spectral acceleration at 0.2 s, and spectral acceleration at 1.0 s, for selected cities (Anbar, Baghdad, Basrah, Duhok, Erbil, Maysan, Kut, and Sulaymaniyah). These hazard curves were calculated for the Vs30 site conditions of 180 m/s and 500 m/s, along with mean, median, and 84th percentile

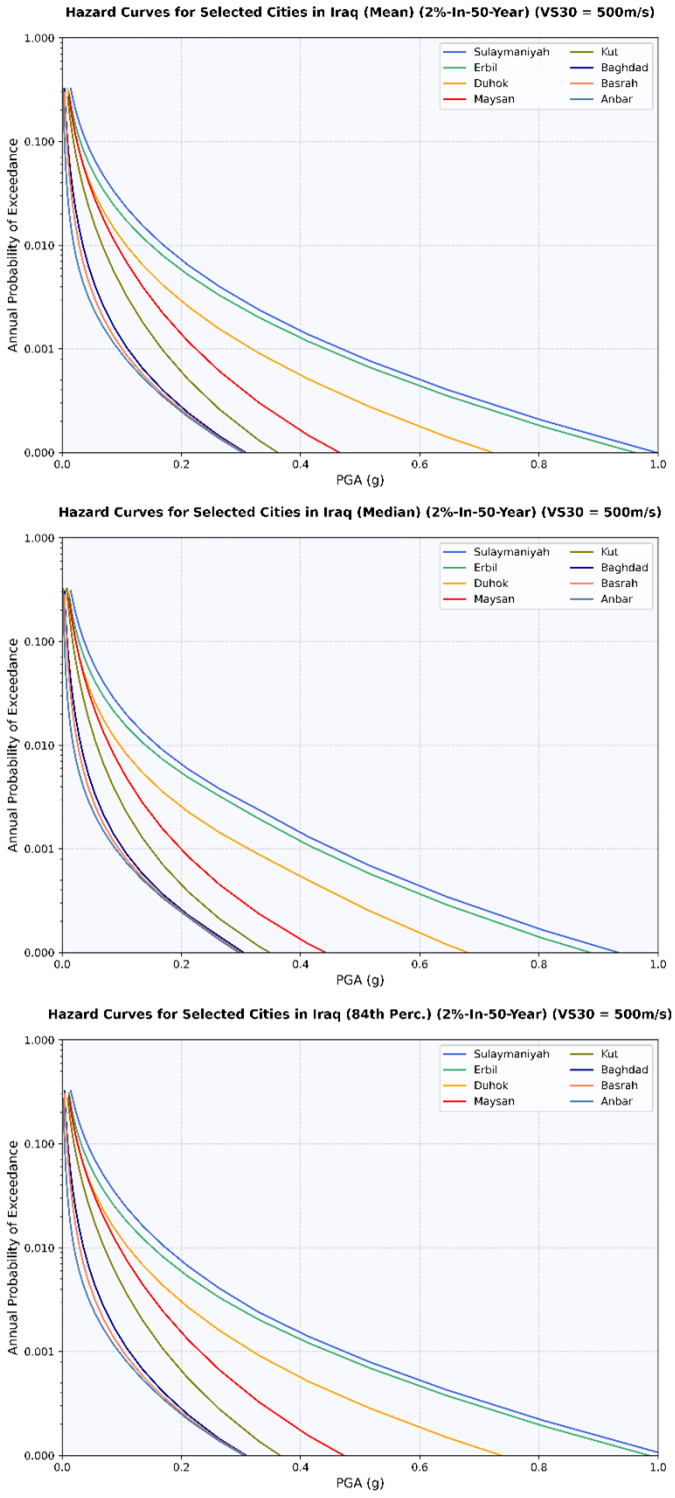

Figure B1: *Mean hazard curves for selected cities in terms of PGA represented by mean, median, and 84th percentile. (Vs30 = 500 m/s)*

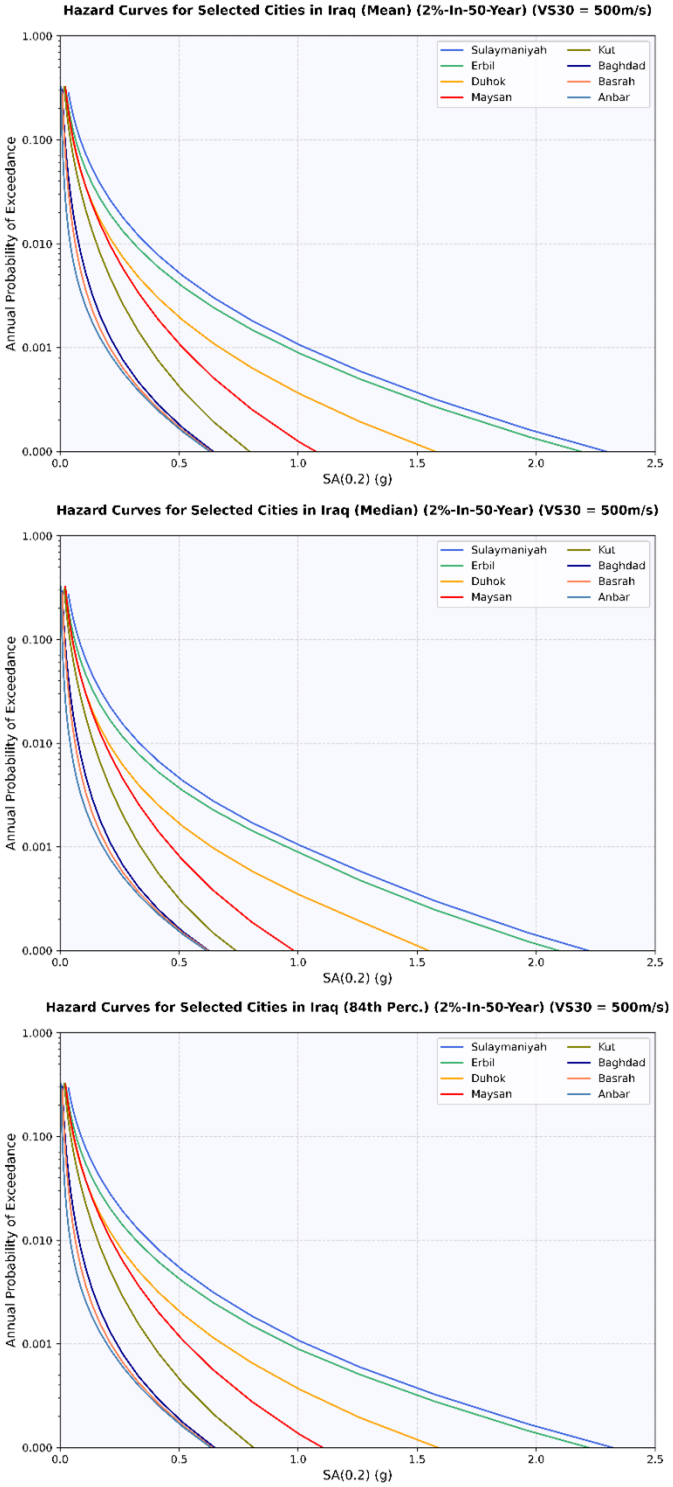

Figure B2: *Hazard curves for selected cities in terms of spectral acceleration (SA) at 0.2s represented by mean, median, and 84th percentile. (Vs30 = 500 m/s)*

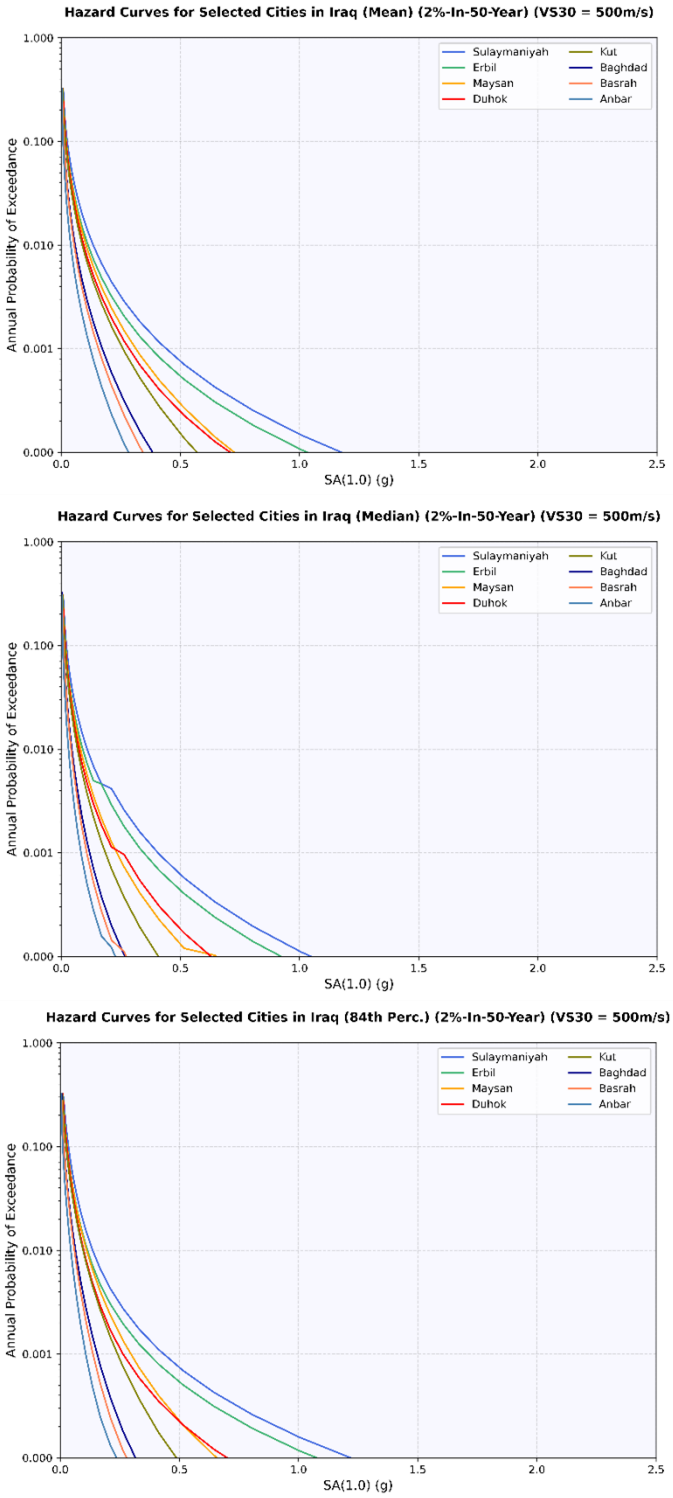

Figure B3: *Hazard curves for selected cities in terms of spectral acceleration (SA) at 1.0s represented by mean, median, and 84th percentile. (Vs30 = 500 m/s)*

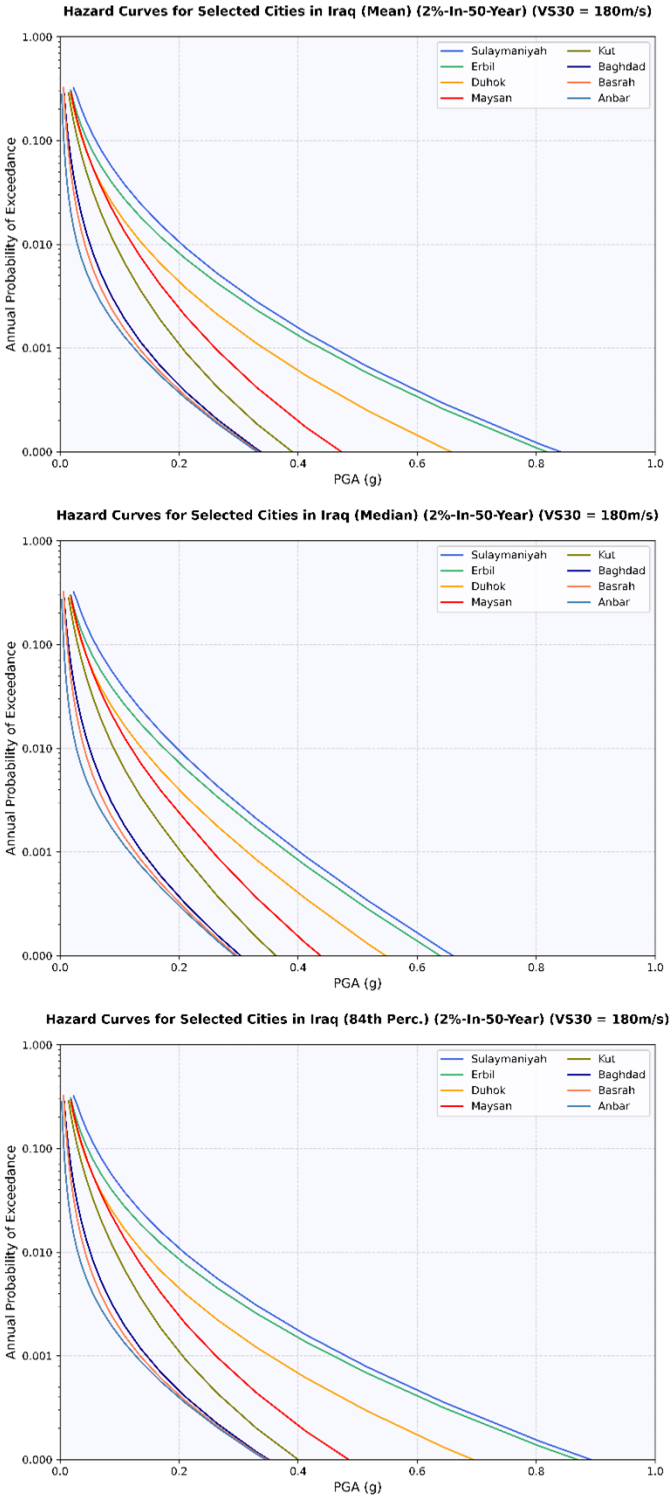

Figure B4: *Mean hazard curves for selected cities in terms of PGA represented by mean, median, and 84th percentile. (Vs30 = 180 m/s)*

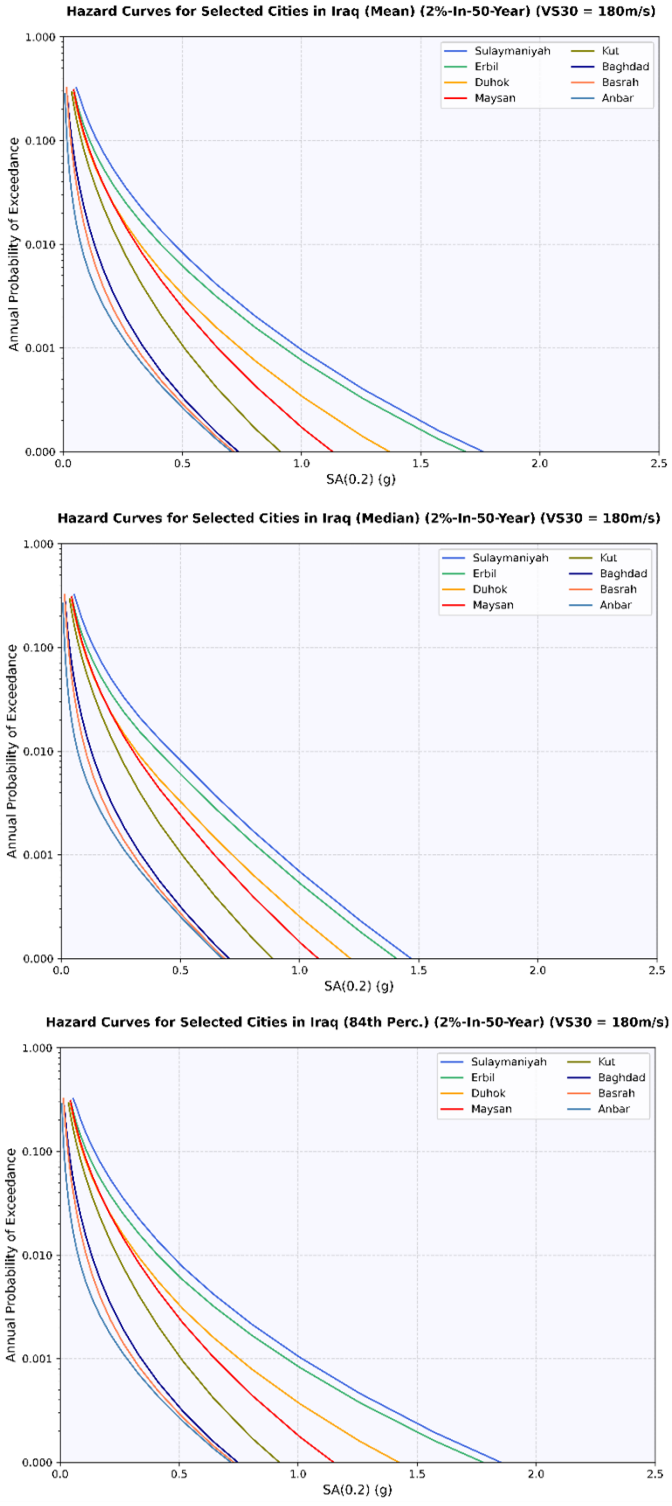

Figure B5: *Hazard curves for selected cities in terms of spectral acceleration (SA) at 0.2s represented by mean, median, and 84th percentile. (Vs30 = 180 m/s)*

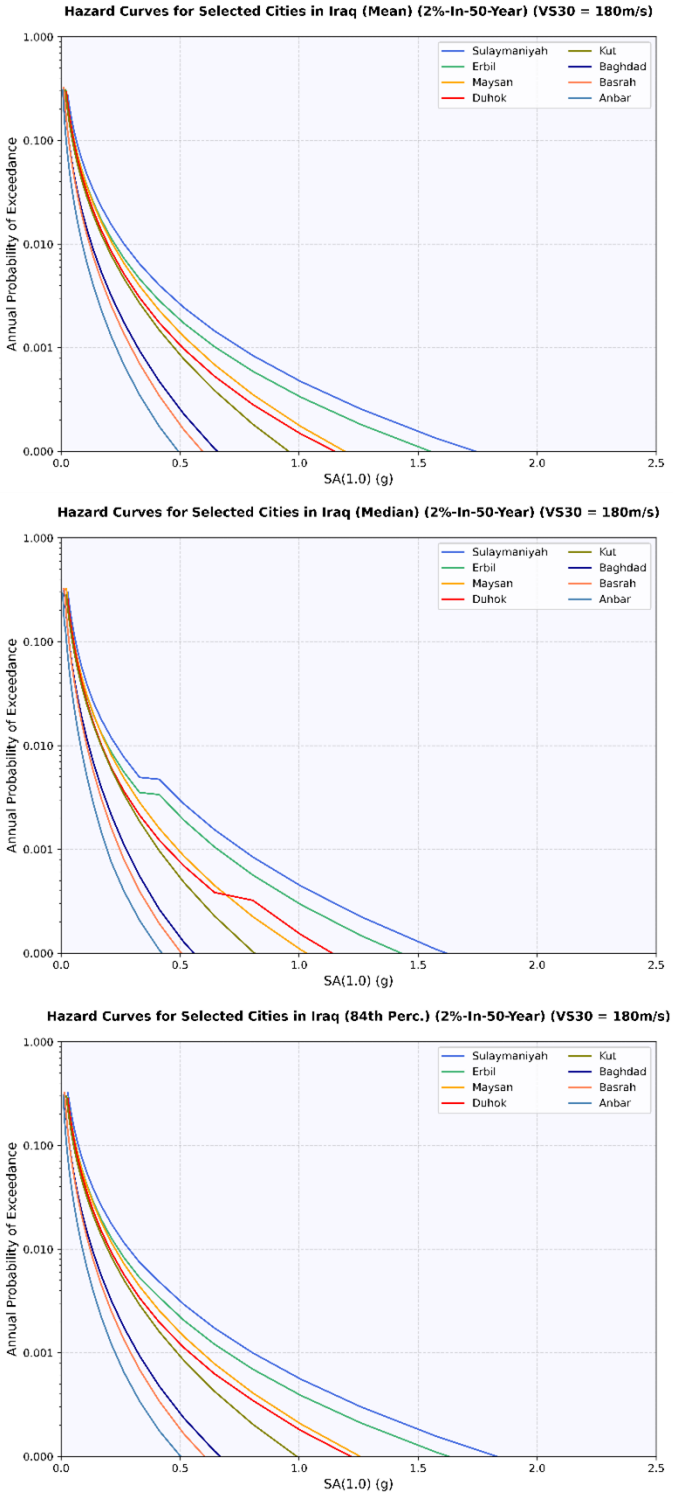

Figure B6: *Hazard curves for selected cities in terms of spectral acceleration (SA) at 1.0s represented by mean, median, and 84th percentile. (Vs30 = 180 m/s)*

Appendix C

Figures C1 through C6 present hazard disaggregations for Erbil, Baghdad, and Basrah for PGA and spectral accelerations at periods of 0.2 sec and 1.0 sec, with a 2% probability of exceedance in 50 years. These hazard deaggregations were calculated for a reference site with Vs30 at 500 m/s and 180 m/s.

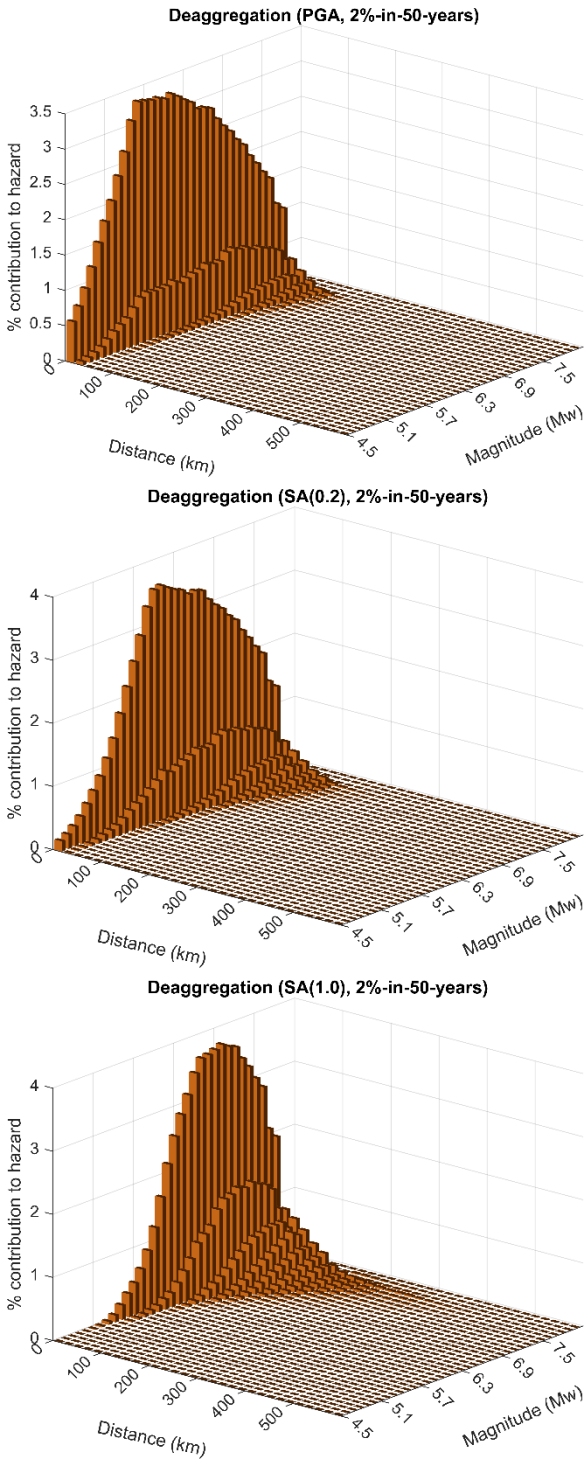

Figure C1: *Hazard deaggregations for Erbil in terms of PGA and spectral accelerations at periods of 0.2 sec and 1.0 sec, with 2% probability of exceedance in 50 years, with reference site of Vs30 of 500 m/s.*

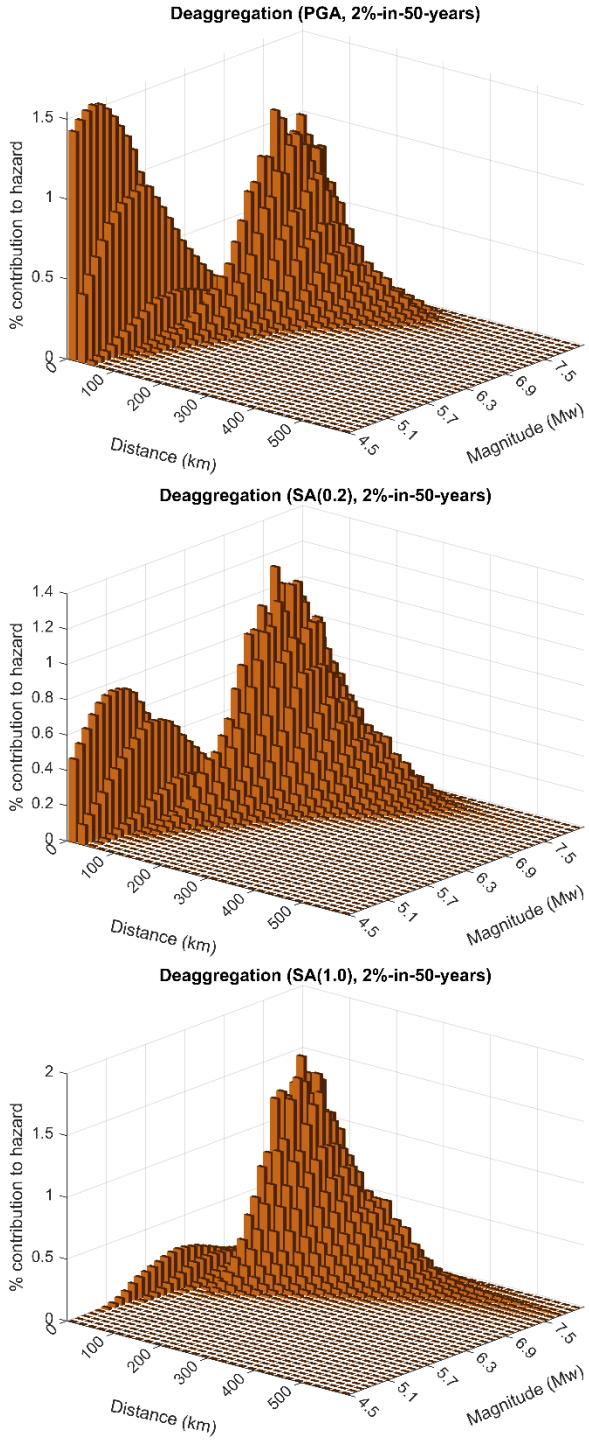

Figure C2: *Hazard deaggregations for Baghdad in terms of PGA and spectral accelerations at periods of 0.2 sec and 1.0 sec, with 2% probability of exceedance in 50 years, with reference site of Vs30 of 500 m/s.*

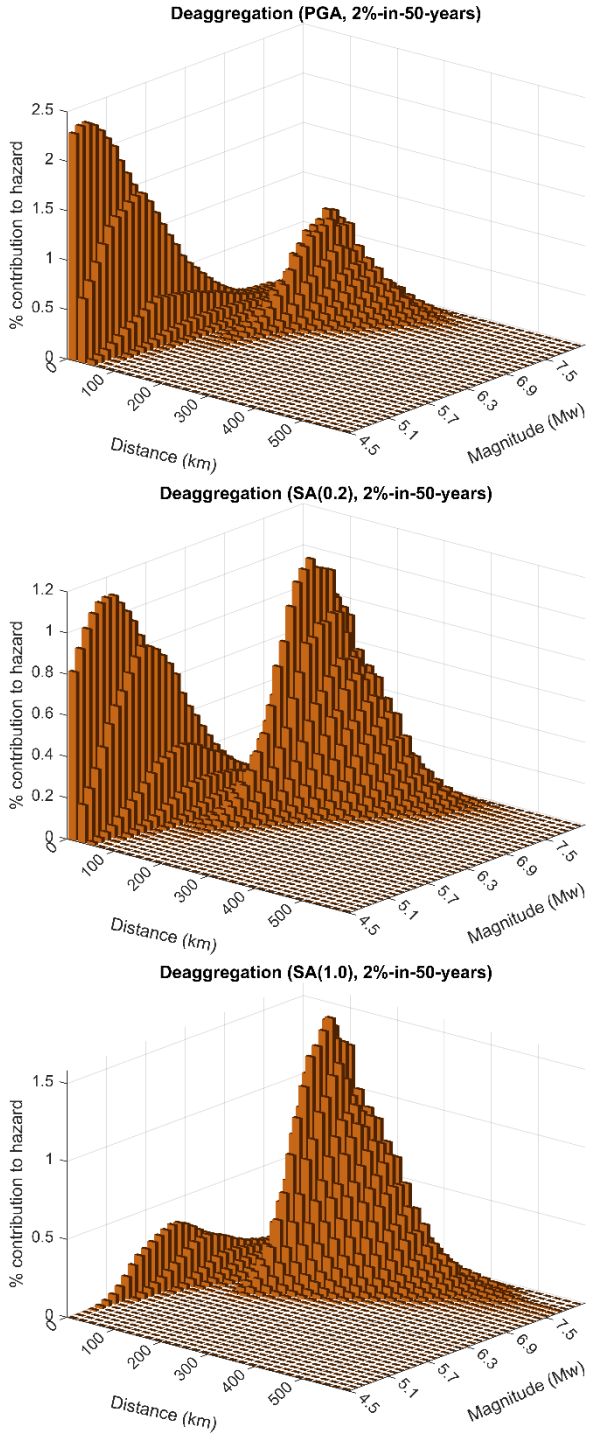

Figure C3: *Hazard deaggregations for Basrah in terms of PGA and spectral accelerations at periods of 0.2 sec and 1.0 sec, with 2% probability of exceedance in 50 years, with reference site of Vs30 of 500 m/s.*

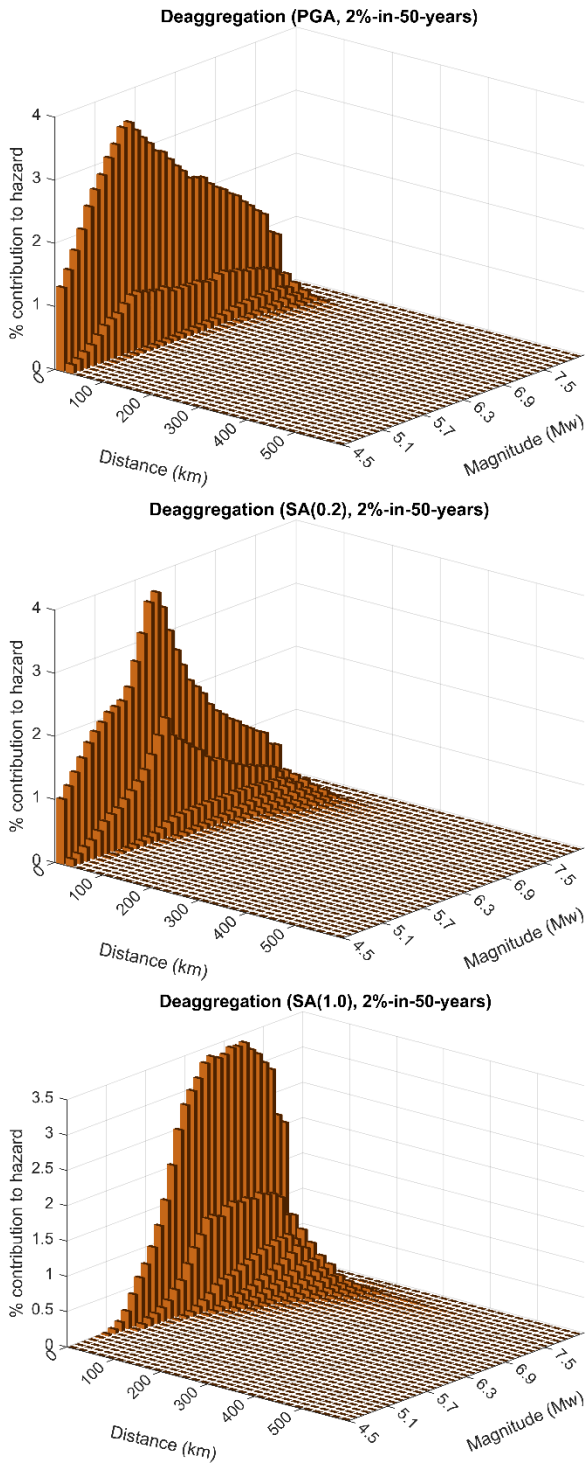

Figure C4: *Hazard deaggregations for Erbil in terms of PGA and spectral accelerations at periods of 0.2 sec and 1.0 sec, with 2% probability of exceedance in 50 years, with reference site of Vs30 of 180 m/s.*

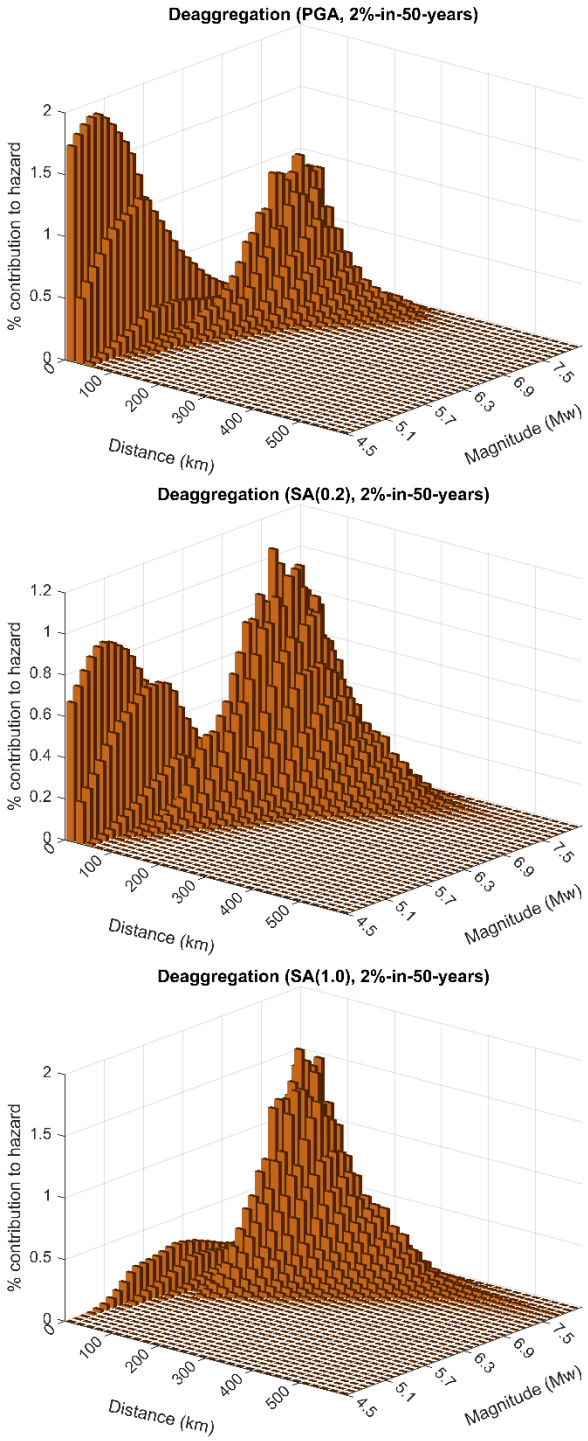

Figure C5: *Hazard deaggregations for Baghdad in terms of PGA and spectral accelerations at periods of 0.2 sec and 1.0 sec, with 2% probability of exceedance in 50 years, with reference site of Vs30 of 180 m/s.*

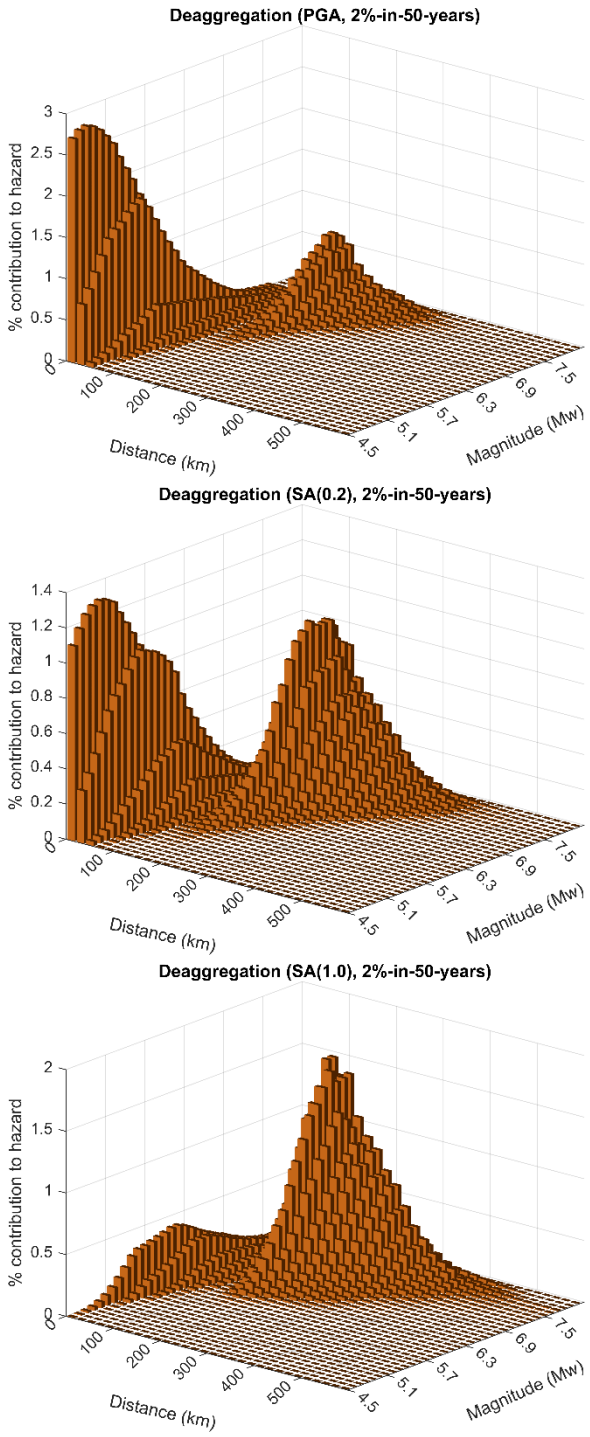

Figure C6: *Hazard deaggregations for Basrah in terms of PGA and spectral accelerations at periods of 0.2 sec and 1.0 sec, with 2% probability of exceedance in 50 years, with reference site of Vs30 of 180 m/s.*